2017

Normal And Epilepsy-Associated Pathologic Function Of The Dentate Gyrus

Christopher Dengler
University of Pennsylvania, christopherdengler@gmail.com

Normal And Epilepsy-Associated Pathologic Function Of The Dentate Gyrus

Abstract
The dentate gyrus plays critical roles both in cognitive processing and in regulating propagation of pathological, synchronous activity through the limbic system. The cellular and circuit mechanisms underlying these diverse functions overlap extensively. At the cellular level, the intrinsic properties of dentate granule cells combine to make these neurons fundamentally reluctant to activate, one of their hallmark traits. At the circuit level, the dentate gyrus is one of the more heavily inhibited regions of the brain, with powerful feedforward and feedback GABAergic inhibition dominating responses to afferent activation. In pathologic states such as epilepsy, disease-associated alterations within the dentate gyrus combine to compromise this circuit's regulatory properties, culminating in a collapse of its normal function. Through the use of dynamic circuit imaging and electrophysiological brain slice recordings, pharmacology, immunohistochemistry, and a pilocarpine model of epilepsy, I characterize the emergence of dentate granule cell firing properties during brain development and then examine how the circuit's normal activation properties become corrupted as epilepsy develops. I find that, in the perinatal brain, dentate granule cells activate in large numbers. As animals mature, these cells become less excitable and activate in extremely sparse populations in a precise, repeatable, frequency-dependent manner. This sparse activation is mediated by local circuit inhibition and not by alterations in afferent innervation of granule cells. Later, in a pilocarpine model of epilepsy, I demonstrate that normally sparse granule cell activation is massively enhanced during both epilepsy development and expression. This augmentation in excitability is mediated primarily by local disinhibition, and the mechanistic cause of this compromised inhibitory function varies over time following epileptogenic injury. My results implicate a reduction in chloride ion extrusion as a mechanism compromising inhibitory function and contributing to granule cell hyperactivation specifically during early epilepsy development. In contrast, we demonstrate that sparse dentate granule cell activation in chronically epileptic mice is rescued by glutamine application, implicating compromised GABA synthesis as a mechanism of disinhibition in chronic epilepsy. We conclude that compromised feedforward inhibition within the local circuit is the predominant mediator of the massive dentate gyrus circuit hyperactivation evident in animals during and following epilepsy development.

Degree Type
Dissertation

Degree Name
Doctor of Philosophy (PhD)

Graduate Group
Neuroscience

First Advisor
Douglas A. Coulter

Keywords
dentate granule cell, dentate gyrus, epilepsy, epileptogenesis

Subject Categories
Neuroscience and Neurobiology

NORMAL AND EPILEPSY-ASSOCIATED PATHOLOGIC FUNCTION OF THE DENTATE GYRUS

Christopher G. Dengler

A DISSERTATION

in

Neuroscience

Presented to the Faculties of the University of Pennsylvania

in

Partial Fulfillment of the Requirements for the

Degree of Doctor of Philosophy

2017

Supervisor of Dissertation

_____

Douglas A. Coulter, PhD
Professor of Pediatrics

Graduate Group Chairperson

_____

Joshua I. Gold, PhD
Professor of Neuroscience

Dissertation Committee:

Diego Contreras, MD, PhD, Professor of Neuroscience
Michael P. Nusbaum, PhD, Professor of Neuroscience
Eric D. Marsh, MD, PhD, Assistant Professor of Neurology
Vijayalakshmi Santhakumar, PhD, MBBS, Associate Prof. of Pharmacology, Physiology, and Neuroscience

NORMAL AND EPILEPSY-ASSOCIATED PATHOLOGIC FUNCTION OF THE DENTATE GYRUS

DEDICATION

This thesis is dedicated to my parents, Gail and Susanne Dengler,

and my wife, Erika Hendel, with love and endless gratitude.

ACKOWLEDGMENT

I would like thank to my mentor, Douglas A. Coulter for his tireless support, advice, and guidance in generating this body of work. Further, I would like to acknowledge all previous and current members of the Coulter Lab for their technical and experimental support, especially Dr. Hajime Takano for lending incomparable support to imaging experiments and analysis, Dr. Cuiyong Yue for aid in physiology experiments, Alicia White and Shareen Nelson for assistance with animal husbandry and epilepsy model implementation, and Dr. Ethan Goldberg for thoughtful discussions and further experimental support. Further thanks go to my current and former thesis committee members, Diego Contreras, Michael Nusbaum, Eric Marsh, Viji Santhakumar, and Gregory Carlson.

ABSTRACT

NORMAL AND EPILEPSY-ASSOCIATED PATHOLOGIC FUNCTION OF THE DENTATE GYRUS.

Christopher G. Dengler

Douglas A. Coulter

The dentate gyrus plays critical roles both in cognitive processing and in regulating propagation of pathological, synchronous activity through the limbic system. The cellular and circuit mechanisms underlying these diverse functions overlap extensively. At the cellular level, the intrinsic properties of dentate granule cells combine to make these neurons fundamentally reluctant to activate, one of their hallmark traits. At the circuit level, the dentate gyrus is one of the more heavily inhibited regions of the brain, with powerful feedforward and feedback GABAergic inhibition dominating responses to afferent activation. In pathologic states such as epilepsy, disease-associated alterations within the dentate gyrus combine to compromise this circuit's regulatory properties, culminating in a collapse of its normal function. Through the use of dynamic circuit imaging and electrophysiological brain slice recordings, pharmacology, immunohistochemistry, and a pilocarpine model of epilepsy, I characterize the emergence of dentate granule cell firing properties during brain development and then examine how the circuit's normal activation properties become corrupted as epilepsy develops. I find that, in the perinatal brain, dentate granule cells activate in large numbers. As animals mature, these cells become less excitable and activate in extremely sparse populations in a precise, repeatable, frequency-dependent manner. This sparse activation is mediated by local circuit inhibition and not by alterations in afferent innervation of granule cells. Later, in a pilocarpine model of epilepsy, I demonstrate that

normally sparse granule cell activation is massively enhanced during both epilepsy development and expression. This augmentation in excitability is mediated primarily by local disinhibition, and the mechanistic cause of this compromised inhibitory function varies over time following epileptogenic injury. My results implicate a reduction in chloride ion extrusion as a mechanism compromising inhibitory function and contributing to granule cell hyperactivation specifically during early epilepsy development. In contrast, we demonstrate that sparse dentate granule cell activation in chronically epileptic mice is rescued by glutamine application, implicating compromised GABA synthesis as a mechanism of disinhibition in chronic epilepsy. We conclude that compromised feedforward inhibition within the local circuit is the predominant mediator of the massive dentate gyrus circuit hyperactivation evident in animals during and following epilepsy development.

TABLE OF CONTENTS

LIST OF ILLUSTRATIONS

AUTHOR CONTRIBUTIONS

Chapter 1 was written by C.G.D., and edited by C.G.D. and D.A.C.

Chapter 2 was originally published as:

Dengler CG, Coulter DA (2016) Normal and epilepsy-associated pathologic function of the dentate gyrus. Prog Brain Res 226:155–178.

It was written by C.G.D. following discussions between C.G.D. and D.A.C., and edited by C.G.D. and D.A.C.

Chapter 3 was originally published as:

Yu EP, Dengler CG, Frausto SF, Putt ME, Yue C, Takano H, Coulter DA (2013) Protracted postnatal development of sparse, specific dentate granule cell activation in the mouse hippocampus. J Neurosci 33:2947–2960.

E.P.Y. and D.A.C. designed research; E.P.Y., C.G.D., S.F.F., C.Y., and H.T. performed research; E.P.Y., C.G.D., M.E.P., and H.T. analyzed data; E.P.Y. and D.A.C. wrote the paper. Specifically, C.G.D. contributed figures 3.3, 3.5, and 3.7 as second author.

Chapter 4 was originally published as:

Dengler CG, Yue C, Takano H, Coulter DA (2017) Massively augmented hippocampal dentate granule cell activation accompanies epilepsy development. Sci Rep 7:42090.

C.G.D. and D.A.C. designed research; C.G.D. and C.Y. performed research; all data and figures generated by CGD with exception of figures 4.8 and 4.9, in which data were collected and initial analysis conducted by C.Y.; C.G.D. and H.T. contributed new analytic tools; C.G.D., C.Y. and H.T. analyzed data; and C.G.D. and D.A.C. wrote the paper.

Chapter 5 was written by C.G.D., and edited by C.G.D. and D.A.C.

CHAPTER 1: Introduction

The research in this dissertation aims to understand the mechanisms by which the principal cells of the dentate gyrus (DG), dentate granule cells (DGCs), are activated by afferent input and how these activation properties may become corrupted as a result of circuit changes occurring during epilepsy development. The DG plays critical roles both in cognitive processing and in regulating propagation of pathological seizure activity in epilepsy. Understanding how DGCs activate within their local circuit is fundamental to understanding how the DG accomplishes its cognitive function of pattern separation, the process whereby one discriminates between similar experiences. Studies have demonstrated that DGCs exhibit firing in extremely small subpopulations during execution of cognitive tasks, consistent with theories that DGCs transform incoming information into a sparse neural code (Jung and McNaughton, 1993; Acsády and Káli, 2007). This sparse DGC activation has also been hypothesized to be particularly important with regard to epilepsy. The DG is the primary gateway regulating cortical input to the hippocampus and a possible contributor to cortical-hippocampal interactions underlying seizures in temporal lobe epilepsy (TLE). The DG acts as a regulated "gate" or "filter," capable of protecting downstream hippocampal areas from runaway excitation and epileptiform activity (Lothman et al., 1992; reviewed in Dengler and Coulter, 2016). In animal models of - and patients with - TLE, the DG undergoes marked circuit perturbations including cell loss, alterations in local inhibitory circuits, axonal and dendritic sprouting, disruptions in ionic homeostasis, and increased/dysregulated neurogenesis. It is unclear how these epilepsy-associated circuit alterations may compromise the network activation properties of the DG and, if

compromised, which circuit changes are responsible. We know little about the mechanisms mediating the sparse network activation properties of the DG and the emergence of this property during brain development. We know even less about how epilepsy development may erode these properties which are critical to normal limbic system function. This dissertation aims to address these gaps in our understanding of this watershed circuit. To provide a general context for our ensuing studies, I begin by introducing relevant background on epilepsy as well as the hippocampus and DG's relevance to both normal and pathological brain function in epilepsy.

Temporal lobe epilepsy and the hippocampus

Epilepsy is defined as the condition of having two or more recurrent, unprovoked seizures in period of longer than 24 hours (I.L.A.E., 1993). With more than 40 clinical variants, epilepsy is estimated to affect over 65 million people worldwide (Ngugi et al., 2010; Thurman et al., 2011). Current estimates suggest that one in 26 people will develop epilepsy in their lifetime (Hesdorffer et al., 2011), yet approximately 1/3 of epileptic patients receiving anticonvulsant medications have inadequate seizure control or experience intolerable side effects of this therapy (Jacobs et al., 2001). In addition to its primary clinical presentation - the occurrence of seizures – epilepsy has many additional consequential impacts on patients and families. Seizures themselves can alter and damage the brain to produce significant cognitive comorbidities (Jokeit and Ebner, 2002) and, further, the sedative and dissociative side-effects of anticonvulsant medications can negatively impact cognitive ability. Beyond pathological changes in the brain function, epilepsy restricts patients' ability to live independently, drive a motorized vehicle, maintain employment, and have children (England et al., 2012). Epilepsy's

prevalence, lack of responsiveness to current therapies, treatment-related side-effects, and its myriad of comorbidities are all critical reasons to study this disorder.

Among all brain regions, the temporal lobe is the most epileptogenic (likely to generate seizures; Tatum, 2012). TLE is a chronic disorder that involves structural damage, dysregulated function and hyperexcitability in temporal lobe structures, including the amygdala, entorhinal cortex, parahippocampal cortex, and most predominately, the hippocampus (Thom et al., 2009; Tatum, 2012). TLE represents the prevalent epilepsy variant in adults and is often associated with a brain injury in a patient's history, such as status epilepticus, traumatic brain injury, central nervous system infection, stroke, and febrile seizures (French et al., 1993; Christensen et al., 2009; Ferguson et al., 2010). As such, TLE is often designated an "acquired epilepsy," meaning that the initial injury may have incited the development of spontaneous recurrent seizures in a previously healthy brain. This process has been termed epileptogenesis and is classically thought to occur in three phases (Goldberg and Coulter, 2013; Maguire, 2016). The first phase of epileptogenesis is the initial precipitating injury, in which some insult to the brain occurs. The second phase is a so-called "latent period" in which the numerous circuit and cellular changes caused by the preceding insult transform a healthy brain into one which can spontaneously generate seizures. This latent period is often characterized as the *epileptogenic* period, a time in which no seizures have yet occurred, despite the brain's increasing propensity for generating pathological discharges. Finally, the third phase is the emergence of epilepsy, a point at which the alterations occurring in the brain during the latent period foment into fully-expressed, chronic epilepsy.

TLE can be effectively modeled by generating a controlled epileptogenic brain insult in an experimental animal, most typically rodents. This injury can take many forms. Among the most common experimental models of epilepsy is one induced by an episode of status epilepticus (a prolonged, unremitting seizure), initiated by either local or systemic administration of convulsant agents such a pilocarpine or kainate (Curia et al., 2008; Ben-Ari, 2010; e.g. this model is implemented in Chapter 4). Pilocarpine is an acetylcholine (ACh) agonist at muscarinic-type ACh receptors, while kainate is a glutamate agonist at ionotropic glutamate receptors. In these models, animals undergo a pharmacologically-induced, prolonged seizure which is then quelled with anticonvulsants. After a short latent period (typically days to weeks), spontaneous, recurrent seizures emerge, and the animal becomes epileptic. During epilepsy development and presentation, alterations occurring in the brain can be assessed experimentally. Other common models of acquired epilepsy include repetitive electrical stimulation (kindling) of temporal lobe structures, physical injury (e.g. fluid percussive injury), as well as early hypoxia-induced ischemic injuries and hyperthermic models of febrile seizures (Bender et al., 2004; Pitkänen et al., 2006; Grone and Baraban, 2015).

After TLE becomes established in patients, it is one of the most intractable epilepsies, with 60-75% of patients experiencing inadequate seizure control with pharmacological treatments (Spencer, 2002). Often, surgical resection of the ictogenic (seizure-initiating) brain region, typically the hippocampus and parahippocampal structures, is the only effective treatment for these uncontrolled epilepsies. Surgical resection eliminates seizures completely in 50-70% of patients, and can significantly reduce seizure frequency in the remainder (reviewed in Spencer, 2002).

Since TLE seizures are often first recorded in the hippocampus (Toyoda et al., 2013), there is a stereotypic pattern of pathology evident in this structure in patients with epilepsy, and because its surgical removal can prevent seizures, the epilepsy-associated alterations to this brain structure have been studied extensively. The changes occurring in the hippocampi of TLE patients and animal models are numerous and share clear patterns of hippocampal damage on several levels. At the gross structural level, hippocampal sclerosis, a combination of structural atrophy and gliosis, is observed in both TLE patients and animal models. (Margerison and Corsellis, 1966; Nadler et al., 1978; Ben-Ari, 1985). At the circuit and cellular levels, there is evidence of numerous epilepsy-associated changes in the hippocampus, among them: synaptic receptor re-organization (Gibbs et al., 1997; Brooks-Kayal et al., 1998; Bernard, 2012; Nadler, 2012), axonal sprouting (Tauck and Nadler, 1985; Zhang et al., 2009; Peng et al., 2013), establishment of pathological recurrent excitatory pathways (Tauck and Nadler, 1985; Buckmaster, 2010), strengthening of existing excitatory pathways (Ang et al., 2006), cell death in a variety of neuronal populations (Margerison and Corsellis, 1966; Sloviter, 1987; Blümcke et al., 2000; Niquet et al., 2012), and aberrant generation of new neurons (Parent et al., 1997; Hattiangady et al., 2004; Parent and Kron, 2012). Collectively, these circuit changes within the hippocampus are thought to transform the hippocampus into a structure capable of generating and propagating seizures. Further, since these same disrupted limbic circuits are important in cognitive processing, these changes are likely to alter normal circuit activation and function within the hippocampus and lead to deficits in hippocampal-dependent cognitive functions (Liu et al., 2003; Kleen et al., 2010).

The dentate gyrus: function and structure

Within the hippocampal formation, the DG has long been implicated as a key structure for seizure initiation and propagation because of several early observations. DGCs are among the few cell types of the hippocampus that survive in significant numbers in epileptic patients (Margerison and Corsellis, 1966), Further, the combined loss of DG inhibitory interneurons and sprouting of recurrent, auto-excitatory mossy fiber synapses in the epileptic DG might allow for pathological circuit activation (Tauck and Nadler, 1985; Sloviter, 1987). Later, many additional aberrant properties of the DG's circuitry were discovered to follow epileptogenic injuries, establishing the ever increasing inquiry into this structure's ability to both generate seizures and/or allow for their propagation (reviewed in detail in Dengler and Coulter, 2016 [*vide infra,* Chapter 2]).

These alterations to the basic DG circuit have received particularly strong attention owing to its position as the gateway to the hippocampus: the site of the first synapse in the canonical trisynaptic loop (**Figure 1.1b**). The DG is situated between the entorhinal cortex and the hippocampus proper (**Figs. 1.1a,b**), where it processes incoming multimodal, entorhinal-cortical spatial information (Sargolini et al., 2006; Fyhn et al., 2008). The DG transforms these cortical inputs into a sparse neural code in a process termed "pattern separation," before relaying its output onto area CA3 via the mossy fiber pathway (Leutgeb et al., 2007; Moser et al., 2008; de Almeida et al., 2009; **Fig 1.1b**). These mossy fiber outputs to CA3 are the second synapse of the trisynaptic circuit. In this location, and owing to its relatively inexcitable activation properties, the DG is poised to restrict incoming inputs from the EC, regulating their propagation onto

downstream CA structures (Coulter and Carlson, 2007; Hsu, 2007; Dengler and Coulter, 2016). The DG's output is then processed locally in area CA3 in a process termed "pattern completion" (Leutgeb and Leutgeb, 2007; Bakker et al., 2008; Neunuebel and Knierim, 2014). This transformed information is then transferred to area CA1 via the Schaffer collaterals in the third synapse of the loop (**Figure 1.1b**). CA1 then further processes this DG-CA3-input and integrates this information together with direct cortical inputs from the temporo-ammonic pathway (Ang et al., 2005; Acsády and Káli, 2007), before relaying the hippocampus's final output back to the subiculum and entorhinal cortex, thus completing the hippocampal loop (**Figure 1.1b**). As a whole, the hippocampal trisynaptic loop structure has been implicated as a key circuit involved in many aspects of spatial and declarative memories (Moser et al., 2008). At same time, this excitatory, interconnected "circular" structure has also raised concerns that pathological excitation may reverberate through the hippocampal loop during seizures (Stringer and Lothman, 1992; Rafiq et al., 1993; Iijima et al., 1996).

Before reviewing the functional roles and properties of the DG and their relevance to both cognitive function and epilepsy in Chapter 2, I will first review the relevant neuroanatomy and cells of the DG circuit. The DG is organized into repeating units called lamellae which are oriented transverse to the long axis of the hippocampus (**Figs. 1.1a,b**). Each lamella of the DG can be divided into three basic areas. The outermost layer of the DG, the molecular layer, contains both the primary excitatory afferent fibers innervating the DG as well as the dendrites of the DG' principle cells, DGCs. The next area of the DG is the granule cell layer, which primarily contains DGC somata. Finally, the hilus (or polymorph layer) harbors a variety of inhibitory interneurons as well excitatory mossy cells (MCs) (**Fig. 1.1c**).

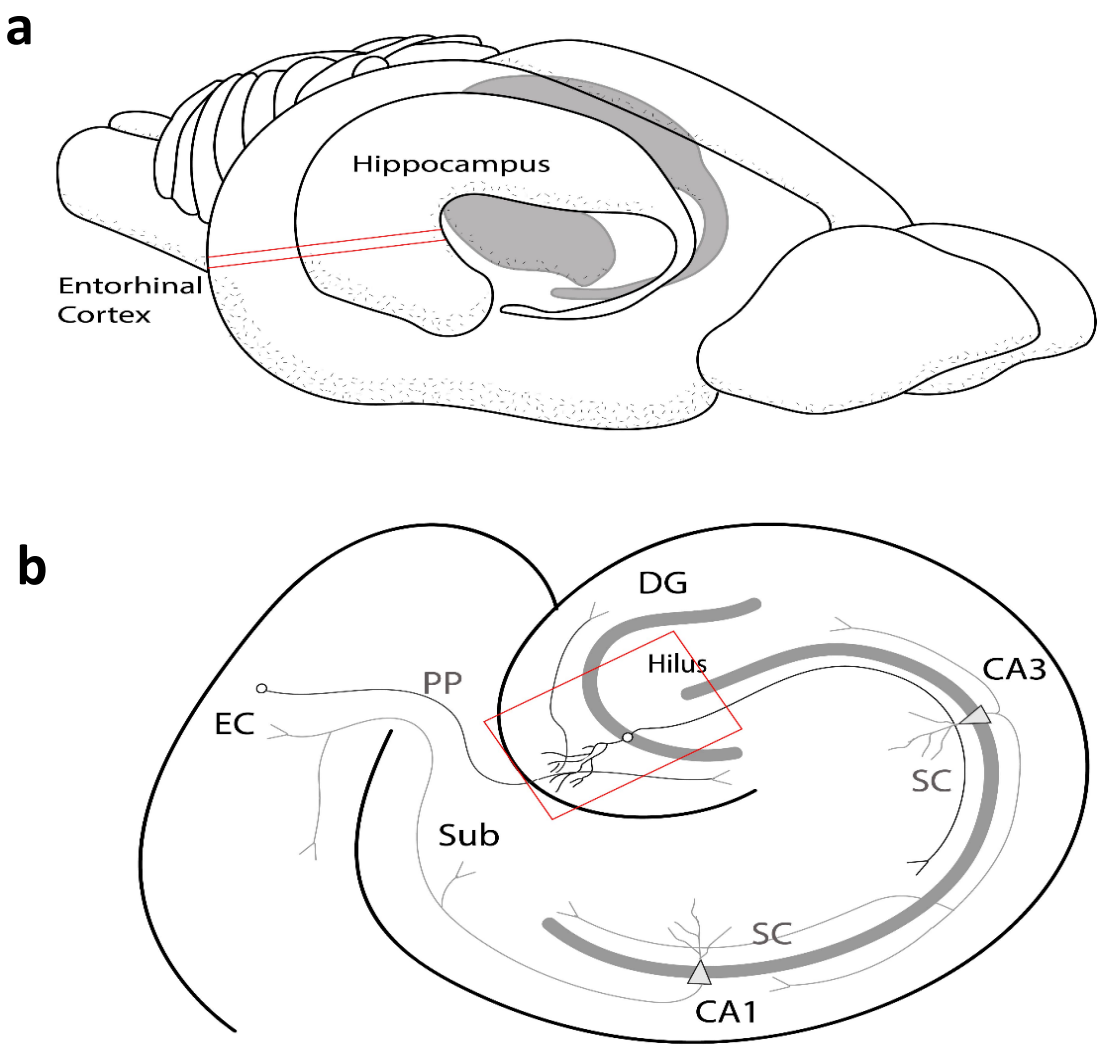

Figure: C. Dengler

Figure 1.1. Basic anatomical position and organization of the DG. (**a**) A sagittal view of the mouse brain highlighting the location of the entorhinal cortex and hippocampus. Red lines indicate the hippocampus' tranverse, lamellar axis. One lamella is shown in (**b**). (**b**) A single hippocampal lamella is illustrated to show the classical "trisynaptic circuit", consisting of the PP axons of entorhinal cortical layer II neurons; mossy fiber (MF) axons of DGCs to CA3; and finally, Schaffer collateral axons (SC) of CA3 to CA1. Red lines indicate area shown in (**c**). (**c**) Schematic illustration of layers in a DG lamella depicting basic connectivity of DG neurons: **Black**, the DG's principle excitatory cells, DGCs; **Grey**, inner molecular layer projecting, excitatory mossy cells; **red**, somatically-targeting inhibitory basket cells with axons in granule cell layer; and **purple**, dendritically-targeting inhibitory hilar interneurons with axonal projections throughout the molecular layer.

The primary excitatory afferent input to the DG is the perforant path (PP) projection. The PP originates from layer II stellate cells of the entorhinal cortex and terminates through excitatory, *en passant* glutamatergic synapses onto DGC dendrites. The PP is composed of two sub-pathways, the lateral and medial perforant paths. The lateral perforant path (LPP) originates in the lateral portion of the entorhinal cortex and projects onto the outer dendrites of DGCs, defining the outer molecular layer, whereas the medial perforant path (MPP) originates in the medial entorhinal cortex and projects onto the middle dendrites of DGCs comprising the middle molecular layer. Additional, minor external inputs to the DG include cholinergic inputs and supramammilary fibers terminating in the inner molecular layer. Finally, the DG receives internal excitatory drive from mossy cells in the hilus, whose axons project onto the hilar neurons and inner molecular layer, synapsing on proximal DGC dendrites. Additionally, the hilus of the DG receives multiple neuromodulatory inputs including cholinergic, noradrenergic and serotonergic fibers from extrahippocampal nuclei. The principle output of the DG is the mossy fiber pathway. This pathway terminates onto excitatory mossy cells and various inhibitory interneurons in the hilus and onto inhibitory interneurons and pyramidal cells in CA3 (See Witter, 1993, for detailed review).

The majority of DGCs comprise a relatively homogenous cell population with two exceptions: adult-born granule cells (abDGCs) and semilunar granule cells. Small numbers of abDGCs are generated in the DG throughout an animal's (and human's) life (Altman and Das, 1965; Eriksson et al., 1998). During their maturation, these neurons display some unique electrophysiological properties, until maturing and become functionally indistinguishable from mature DGCs (van Praag et al., 2002). Semilunar granule cells are a small set of spiny granule cell-like neurons, with slightly pyramidal

morphology present in the inner molecular layer. Their unique plateau potentials enable them to fire continuously during phasic bursts onto their postsynaptic targets which include hilar interneurons and mossy cells (Williams et al., 2007).

The GABAergic neurons of the DG have somata present in all layers of the DG, and different classes of these cells have layer-specific synaptic targets. One of the most common subtypes is the basket cell, a class of inhibitory interneurons typically characterized by fast-spiking membrane behavior and uniformly possessing axonal arbors with exclusively perisomatic-targeting via basket-like plexuses surrounding DGC somata and axon initial segments (Freund and Buzsáki, 1996; **Fig. 1.1b**). Basket cells typically have a pyramidal cell body located at the periphery of the GC layer. These interneurons provide somatic GABA-ergic inhibition to DGCs via both feedforward (afferents from EC; Seress and Pokorny, 1981) and feedback (innervation from DGCs; Ribak and Peterson, 1991) pathways (Freund and Buzsáki, 1996). Basket cells commonly express the calcium-binding protein parvalbumin (Ribak et al., 1990), but can also express other markers such as neuropeptide Y (NPY), cholecystokinin (CCK), and vasoactive-intestinal peptide (VIP), or exhibit no clear expression of known-markers (Gulyás et al., 1991; Acsády et al., 1996).

The second major class of inhibitory interneurons in the DG is the hilar interneurons. These neurons commonly contain the neuropeptides somatostatin and/or neuropeptide Y and their axonal terminals primarily target DGC dendrites in the middle and outer molecular layers (Bakst et al., 1986; Chan-Palay et al., 1986; Köhler et al., 1987; Amaral et al., 1988). These neurons are commonly ascribed to operate in a feedback capacity, receiving the majority of their excitatory input from DGCs (but also from semilunar granule cells and mossy cells), and via their dendritic targeting, they

limit the efficacy of entorhinal cortical afferents onto DGCs (Freund and Buzsáki, 1996; Houser, 2007).

Two less common subtypes of interneurons that are present in the DG are HICAP cells and neurogliaform cells. HICAP cells (hilar interneurons projecting to the commissural/associational pathway) have somata localized in the hilus and axons that innervate the inner molecular layer (Han et al., 1993). Finally, neurogliaform cells have somata located in the molecular layer of the DG with dense local axonal plexuses in the molecular layer and are thought to provide inhibition through "bulk-transmission" of GABA through extrasynaptic receptors (Freund and Buzsáki, 1996; Armstrong et al., 2012).

Owing to the repeating, lamellar structure of the DG and hippocampus, intact, well-connected *ex vivo* brain slices can be prepared by slicing the brain along the transverse axis of the hippocampus. **Figure 1.2** demonstrates this within-slice connectivity via retro-anterograde labeling using the lipophilic dye, DiI, in a standard hippocampal-entorhinal cortical slice. This labeling demonstrates that horizontally oriented hippocampal-entorhinal cortical slices contain PP axons originating in the EC that project onto and around the molecular layer of the DG. These PP path axons are functionally intact and allow for direct afferent stimulation of downstream DG structures. Further, DG efferent connectivity is maintained to both the hilus and CA3. In both of the primary research of chapters of this dissertation (3 and 4), I study functional properties of the DG using these brain slice preparations utilizing both imaging and electrophysiological approaches to better understand circuit function in the DG.

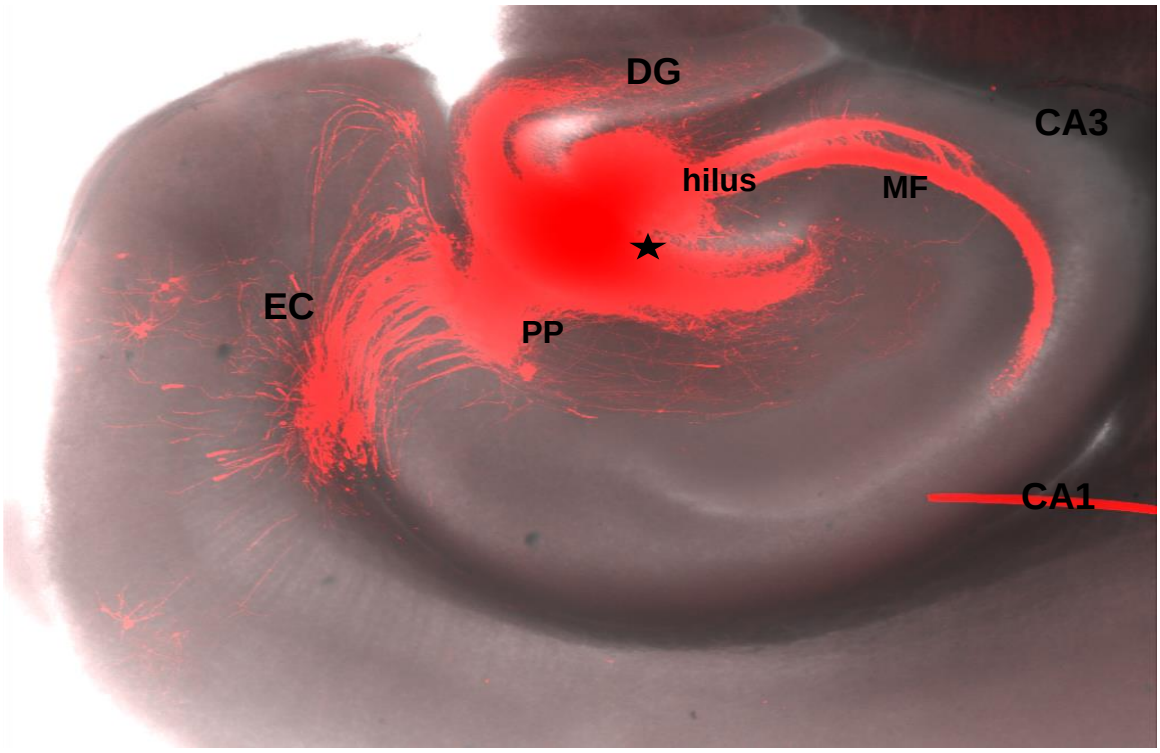

Figure 1.2. Intact EC-DG-Hilar-CA3 excitatory projections in horizontal hippocampal-entorhinal cortex slices. A 350 µm thick, hippocampal-entorhinal cortical brain slice, demonstrating intact projections from the EC to the DG, and from the DG to CA3. Grey, transmitted light micrograph. Red, DiI, a lipophilic fluorescent dye, used to trace cell membranes. ★**,** placement of a small DiI crystal in the DG molecular layer retrogradely traces DG afferent PP fibers originating in the EC, and anterogradely labels DG MF axonal projections to the hilus and CA3.

Objectives and Organization of the Proposed Studies

The two primary aims of this dissertation are to (1) characterize the development of network firing properties in the healthy DG and (2) determine the nature of DGC activation within the DG network in animals with epilepsy. This thesis is, in large part, a compilation of 3 self-contained, published manuscripts, accompanied by additional background, future directions, and final conclusions.

Earlier in the present chapter, I introduced relevant background on epilepsy, the hippocampus, DG neuroanatomy, and the general aims of this thesis as to provide overall context to this dissertation's research.

Chapter 2 provides a detailed literature review of the DG's sparse activation properties, its relevance to cognitive processing, and its secondary role in functioning as a regulated "gate" or "filter" of cortical afferents. Additionally, this chapter discusses many of the epilepsy-associated circuit changes known to occur within the DG and their possible roles in altering this circuits' normal function.

Chapter 3 details the results of a study focused on characterizing the emergence of sparse DGC activation during brain development and how this property accompanies the associated development of an animal's cognitive functions (Aim 1). We demonstrate a protracted, progressive sparsification of DGC responses during brain development, accompanied by increased temporal precision and frequency dependence of activation.

Chapter 4 characterizes the collapse of normal sparse DGC activation in a mouse model of TLE, as well as the mechanisms of this circuit failure (Aim 2). This study reveals that epilepsy emergence is accompanied by massive enhancement of the normally sparse activation of DGCs, mediated by primarily by disinhibition within the

local network, though the mechanistic cause of this compromised inhibitory function varied over time following epileptogenic injury.

Finally, Chapter 5 presents the future directions of this research program and overall implications of this dissertation's body of research.

Chapter 1 Bibliography

Acsády L, Arabadzisz D, Freund TF (1996) Correlated morphological and neurochemical features identify different subsets of vasoactive intestinal polypeptide-immunoreactive interneurons in rat hippocampus. Neuroscience 73:299–315.

Acsády L, Káli S (2007) Models, structure, function: the transformation of cortical signals in the dentate gyrus. Prog Brain Res 163:577–599.

Altman J, Das GD (1965) Autoradiographic and histological evidence of postnatal hippocampal neurogenesis in rats. J Comp Neurol 124:319–335.

Amaral DG, Insausti R, Campbell MJ (1988) Distribution of somatostatin immunoreactivity in the human dentate gyrus. J Neurosci 8:3306–3316.

Ang CW, Carlson GC, Coulter DA (2005) Hippocampal CA1 circuitry dynamically gates direct cortical inputs preferentially at theta frequencies. J Neurosci 25:9567–9580.

Ang CW, Carlson GC, Coulter DA (2006) Massive and specific dysregulation of direct cortical input to the hippocampus in temporal lobe epilepsy. J Neurosci 26:11850–11856.

Armstrong C, Krook-Magnuson E, Soltesz I (2012) Neurogliaform and Ivy Cells: A Major Family of nNOS Expressing GABAergic Neurons. Front Neural Circuits 6:23.

Bakker A, Kirwan CB, Miller M, Stark CEL (2008) Pattern separation in the human hippocampal CA3 and dentate gyrus. Science 319:1640–1642.

Bakst I, Avendano C, Morrison JH, Amaral DG (1986) An experimental analysis of the origins of somatostatin-like immunoreactivity in the dentate gyrus of the rat. J Neurosci 6:1452–1462.

Ben-Ari Y (1985) Limbic seizure and brain damage produced by kainic acid: Mechanisms and relevance to human temporal lobe epilepsy. Neuroscience 14:375–403.

Ben-Ari Y (2010) Kainate and temporal lobe epilepsies: Three decades of progress. Epilepsia 51:40.

Bender RA, Dubé C, Baram TZ (2004) Febrile seizures and mechanisms of epileptogenesis: insights from an animal model. Adv Exp Med Biol 548:213–225.

Bernard C (2012) Alterations in synaptic function in epilepsy.

Blümcke I, Suter B, Behle K, Kuhn R, Schramm J, Elger CE, Wiestler OD (2000) Loss of hilar mossy cells in Ammon's horn sclerosis. Epilepsia 41 Suppl 6:S174-80.

Brooks-Kayal AR, Shumate MD, Jin H, Rikhter TY, Coulter DA (1998) Selective changes in single cell GABA(A) receptor subunit expression and function in temporal lobe epilepsy. Nat Med 4:1166–1172.

Buckmaster PS (2010) Mossy fiber sprouting in the dentate gyrus. Epilepsia 51:39–39.

Chan-Palay V, Köhler C, Haesler U, Lang W, Yasargil G (1986) Distribution of neurons and axons immunoreactive with antisera against neuropeptide Y in the normal

human hippocampus. J Comp Neurol 248:360–375.

Christensen J, Pedersen MG, Pedersen CB, Sidenius P, Olsen J, Vestergaard M (2009) Long-term risk of epilepsy after traumatic brain injury in children and young adults: a population-based cohort study. Lancet (London, England) 373:1105–1110.

Coulter DA, Carlson GC (2007) Functional regulation of the dentate gyrus by GABA-mediated inhibition. Prog Brain Res 163:235–243.

Curia G, Longo D, Biagini G, Jones RSG, Avoli M (2008) The pilocarpine model of temporal lobe epilepsy. J Neurosci Methods 172:143–157.

de Almeida L, Idiart M, Lisman JE (2009) The input-output transformation of the hippocampal granule cells: from grid cells to place fields. J Neurosci 29:7504–7512.

Dengler CG, Coulter DA (2016) Normal and epilepsy-associated pathologic function of the dentate gyrus. Prog Brain Res 226:155–178.

England MJ, Liverman CT, Schultz AM, Strawbridge LM (2012) Epilepsy across the spectrum: Promoting health and understanding. A summary of the Institute of Medicine report. Epilepsy Behav 25:266–276.

Eriksson PS, Perfilieva E, Björk-Eriksson T, Alborn AM, Nordborg C, Peterson DA, Gage FH (1998) Neurogenesis in the adult human hippocampus. Nat Med 4:1313–1317.

Ferguson PL, Smith GM, Wannamaker BB, Thurman DJ, Pickelsimer EE, Selassie AW (2010) A population-based study of risk of epilepsy after hospitalization for traumatic brain injury. Epilepsia 51:891–898.

French JA, Williamson PD, Thadani VM, Darcey TM, Mattson RH, Spencer SS, Spencer DD (1993) Characteristics of medial temporal lobe epilepsy: I. Results of history and physical examination. Ann Neurol 34:774–780.

Freund TF, Buzsáki G (1996) Interneurons of the hippocampus. Hippocampus 6:347–470.

Fyhn M, Hafting T, Witter MP, Moser EI, Moser M-B (2008) Grid cells in mice. Hippocampus 18:1230–1238.

Gibbs JW, Shumate MD, Coulter DA (1997) Differential epilepsy-associated alterations in postsynaptic GABA(A) receptor function in dentate granule and CA1 neurons. J Neurophysiol 77:1924–1938.

Goldberg EM, Coulter DA (2013) Mechanisms of epileptogenesis: a convergence on neural circuit dysfunction. Nat Rev Neurosci 14:337–349.

Grone BP, Baraban SC (2015) Animal models in epilepsy research: legacies and new directions. Nat Neurosci 18:339–343.

Gulyás AI, Tóth K, Dános P, Freund TF (1991) Subpopulations of GABAergic neurons containing parvalbumin, calbindin D28k, and cholecystokinin in the rat hippocampus. J Comp Neurol 312:371–378.

Han ZS, Buhl EH, Lörinczi Z, Somogyi P (1993) A high degree of spatial selectivity in the axonal and dendritic domains of physiologically identified local-circuit neurons in

the dentate gyrus of the rat hippocampus. Eur J Neurosci 5:395–410.

Hattiangady B, Rao MS, Shetty AK (2004) Chronic temporal lobe epilepsy is associated with severely declined dentate neurogenesis in the adult hippocampus. Neurobiol Dis 17:473–490.

Hesdorffer DC, Logroscino G, Benn EKT, Katri N, Cascino G, Hauser WA (2011) Estimating risk for developing epilepsy. Neurology 76:23–27.

Houser CR (2007) Interneurons of the dentate gyrus: an overview of cell types, terminal fields and neurochemical identity. Prog Brain Res 163:217–232.

Hsu D (2007) The dentate gyrus as a filter or gate: a look back and a look ahead. Prog Brain Res 163:601–613.

I.L.A.E. (1993) Guidelines for epidemiologic studies on epilepsy. Commission on Epidemiology and Prognosis, International League Against Epilepsy. Epilepsia 34:592–596.

Iijima T, Witter MP, Ichikawa M, Tominaga T, Kajiwara R, Matsumoto G (1996) Entorhinal-Hippocampal Interactions Revealed by Real-Time Imaging. Science (80-) 272:1176–1179.

Jacobs MP, Fischbach GD, Davis MR, Dichter MA, Dingledine R, Lowenstein DH, Morrell MJ, Noebels JL, Rogawski MA, Spencer SS, Theodore WH (2001) Future directions for epilepsy research. Neurology 57:1536–1542.

Jokeit H, Ebner A (2002) Effects of chronic epilepsy on intellectual functions. Prog Brain Res 135:455–463.

Jung MW, McNaughton BL (1993) Spatial selectivity of unit activity in the hippocampal granular layer. Hippocampus 3:165–182.

Kleen JK, Scott RC, Holmes GL, Lenck-Santini PP (2010) Hippocampal interictal spikes disrupt cognition in rats. Ann Neurol 67:250–257.

Köhler C, Eriksson LG, Davies S, Chan-Palay V (1987) Co-localization of neuropeptide tyrosine and somatostatin immunoreactivity in neurons of individual subfields of the rat hippocampal region. Neurosci Lett 78:1–6.

Leutgeb JK, Leutgeb S, Moser M-B, Moser EI (2007) Pattern separation in the dentate gyrus and CA3 of the hippocampus. Science 315:961–966.

Leutgeb S, Leutgeb JK (2007) Pattern separation, pattern completion, and new neuronal codes within a continuous CA3 map. Learn Mem 14:745–757.

Liu X, Muller RU, Huang L-T, Kubie JL, Rotenberg A, Rivard B, Cilio MR, Holmes GL (2003) Seizure-induced changes in place cell physiology: relationship to spatial memory. J Neurosci 23:11505–11515.

Lothman EW, Stringer JL, Bertram EH (1992) The dentate gyrus as a control point for seizures in the hippocampus and beyond. Epilepsy Res Suppl 7:301–313.

Maguire J (2016) Epileptogenesis: More than just the latent period. Epilepsy Curr 16:31–33.

Margerison JH, Corsellis JAN (1966) Epilepsy and the temporal lobes: A clinical, electroencephalographic and neuropathological study of the brain in epilepsy, with particular reference to the temporal lobes. Brain 89:499–530.

Moser EI, Kropff E, Moser M-B (2008) Place cells, grid cells, and the brain's spatial representation system. Annu Rev Neurosci 31:69–89.

Nadler J (2012) Plasticity of Glutamate Synaptic Mechanisms. In Jasper's Basic Mechanisms of the Epilepsies, 4th edition pp 1–17.

Nadler JV, Perry BW, Cotman CW (1978) Intraventricular kainic acid preferentially destroys hippocampal pyramidal cells. Nature 271:676–677.

Neunuebel JP, Knierim JJ (2014) CA3 retrieves coherent representations from degraded input: Direct evidence for CA3 pattern completion and dentate gyrus pattern separation. Neuron 81:416–427.

Ngugi AK, Bottomley C, Kleinschmidt I, Sander JW, Newton CR (2010) Estimation of the burden of active and life-time epilepsy: A meta-analytic approach. Epilepsia 51:883–890.

Niquet J, Lopez-Meraz M-L, Wasterlain CG (2012) Programmed Necrosis After Status Epilepticus.

Parent JM, Kron MM (2012) Neurogenesis and Epilepsy. In Jasper's Basic Mechanisms of the Epilepsies, 4th edition.

Parent JM, Yu TW, Leibowitz RT, Geschwind DH, Sloviter RS, Lowenstein DH (1997) Dentate granule cell neurogenesis is increased by seizures and contributes to aberrant network reorganization in the adult rat hippocampus. J Neurosci 17:3727–3738.

Peng Z, Zhang N, Wei W, Huang CS, Cetina Y, Otis TS, Houser CR (2013) A reorganized GABAergic circuit in a model of epilepsy: evidence from optogenetic labeling and stimulation of somatostatin interneurons. J Neurosci 33:14392–14405.

Pitkänen A, Schwartzkroin P, Moshe SL (2006) Models of Seizures and Epilepsy. Elsevier Academic Press.

Rafiq A, DeLorenzo RJ, Coulter DA (1993) Generation and propagation of epileptiform discharges in a combined entorhinal cortex/hippocampal slice. J Neurophysiol 70:1962–1974.

Ribak CE, Nitsch R, Seress L (1990) Proportion of parvalbumin-positive basket cells in the GABAergic innervation of pyramidal and granule cells of the rat hippocampal formation. J Comp Neurol 300:449–461.

Ribak CE, Peterson GM (1991) Intragranular mossy fibers in rats and gerbils form synapses with the somata and proximal dendrites of basket cells in the dentate gyrus. Hippocampus 1:355–364.

Sargolini F, Fyhn M, Hafting T, McNaughton BL, Witter MP, Moser M-B, Moser EI (2006) Conjunctive representation of position, direction, and velocity in entorhinal cortex. Science 312:758–762.

Seress L, Pokorny J (1981) Structure of the granular layer of the rat dentate gyrus. A light microscopic and Golgi study. J Anat 133:181–195.

Sloviter RS (1987) Decreased hippocampal inhibition and a selective loss of interneurons in experimental epilepsy. Science 235:73–76.

Spencer SS (2002) When should temporal-lobe epilepsy be treated surgically? Lancet Neurol 1:375–382.

Stringer JL, Lothman EW (1992) Reverberatory seizure discharges in hippocampal-parahippocampal circuits. Exp Neurol 116:198–203.

Tatum WO (2012) Mesial temporal lobe epilepsy. J Clin Neurophysiol 29:356–365.

Tauck DL, Nadler J V (1985) Evidence of functional mossy fiber sprouting in hippocampal formation of kainic acid-treated rats. J Neurosci 5:1016–1022.

Thom M, Eriksson S, Martinian L, Caboclo LO, McEvoy AW, Duncan JS, Sisodiya SM (2009) Temporal Lobe Sclerosis Associated With Hippocampal Sclerosis in Temporal Lobe Epilepsy: Neuropathological Features. J Neuropathol Exp Neurol 68:928–938.

Thurman DJ et al. (2011) Standards for epidemiologic studies and surveillance of epilepsy. Epilepsia 52:2–26.

Toyoda I, Bower MR, Leyva F, Buckmaster PS (2013) Early activation of ventral hippocampus and subiculum during spontaneous seizures in a rat model of temporal lobe epilepsy. J Neurosci 33:11100–11115.

van Praag H, Schinder AF, Christie BR, Toni N, Palmer TD, Gage FH (2002) Functional neurogenesis in the adult hippocampus. Nature 415:1030–1034.

Witter MP (1993) Organization of the entorhinal-hippocampal system: a review of current anatomical data. Hippocampus 3:33–44.

Zhang W, Yamawaki R, Wen X, Uhl J, Diaz J, Prince DA, Buckmaster PS (2009) Surviving hilar somatostatin interneurons enlarge, sprout axons, and form new synapses with granule cells in a mouse model of temporal lobe epilepsy. J Neurosci 29:14247–14256.

CHAPTER 2: Normal and epilepsy-associated pathologic function of the dentate gyrus.

Abstract

The dentate gyrus plays critical roles both in cognitive processing and in the regulation of the induction and propagation of pathological activity. The cellular and circuit mechanisms underlying these diverse functions overlap extensively. At the cellular level, the intrinsic properties of dentate granule cells combine to endow these neurons with a fundamental reluctance to activate, one of their hallmark traits. At the circuit level, the dentate gyrus constitutes one of the more heavily inhibited regions of the brain, with strong, fast feedforward and feedback GABAergic inhibition dominating responses to afferent activation. In pathologic states such as epilepsy, a number of alterations within the dentate gyrus combine to compromise the regulatory properties of this circuit, culminating in a collapse of its normal function. This epilepsy-associated transformation in the fundamental properties of this critical regulatory hippocampal circuit may contribute both to seizure propensity, and cognitive and emotional comorbidities characteristic of this disease state.

Introduction

Situated as the initial component of the canonical trisynaptic circuit, the dentate gyrus (DG) is a critical entry point to the hippocampus, functioning as a key regulator of cortical input to the limbic system. The DG is involved in the performance of hippocampal-dependent tasks and is postulated to accomplish these cognitive functions through a transformation of highly active and multimodal afferent cortical inputs into a sparse neural code in which very few of its principal cells activate. In this chapter, we will

discuss how the sparse, selective activation properties of the DG's principal cells, dentate granule cells (DGCs), are critical to hippocampal cognitive function and how this characteristic firing property plays a key role in the regulation of seizure activity in diseases such as epilepsy. Finally, we will consider mechanisms that may erode appropriate DG circuit activation and play a pivotal role in epileptogenesis, seizure propensity in epilepsy, as well as the cognitive comorbidities associated with the disease.

In vivo recording studies have demonstrated that DGCs exhibit spatially selective firing in extremely small populations (Jung and McNaughton, 1993a; Chawla et al., 2005). This characteristic sparse activation is thought to enable DGCs to participate in the execution of cognitive functions such as pattern separation and novelty detection (Leutgeb et al., 2007). The propensity for DGCs to generate action potentials (APs) is normally tightly constrained by a combination of cell-intrinsic properties and powerful local inhibitory control, culminating in a population of neurons that are extremely reluctant to activate. However, when DGCs do activate, they exert strong excitatory influence on their downstream targets. A secondary consequence of the DG's low excitability is its ability to restrict relay of pathological, synchronous cortical activity into the hippocampus and regulate seizure activity in diseases such as epilepsy: a phenomenon termed "dentate gating" (Lothman et al., 1992; Stringer and Lothman, 1992). However, if this regulatory ability becomes compromised, the DG's powerful excitatory influence on its downstream targets in the hippocampus can allow it to relay and amplify synchronous pathological activity through the limbic system, potentially fomenting seizure activity.

These characteristic DG circuit properties are significantly disrupted both in humans with epilepsy and in animal models of the disorder. A large aggregation of cellular and circuit alterations occurs in the DG during epilepsy development, including

sprouting of pathologic, recurrent excitatory networks, molecular and cellular alterations of local inhibitory circuits, aberrant neurogenesis, astrocytic gliosis, and changes in the intrinsic properties of DGCs. These pathology-associated alterations have generated a prevalent hypothesis that the DG's normal gating function is compromised during epilepsy and its development and contributes to increased seizure propensity. However, this DG gate failure hypothesis has yet to receive adequate experimental support, and if found to exist, the exact mechanisms mediating such a circuit collapse are likely mechanistically complex.

Activity in the DG is sparse

Among the most unusual properties of the DG is the uniquely low level of neuronal activity among its principal cell population. Assays measuring DGC activity over the last several decades have consistently described DGC activation as unusually low compared to many other brain areas. *In vivo* unit recordings during spatial navigation tasks have demonstrated exceedingly low levels of DGC activity; the vast majority of recorded DGCs display extremely low mean firing rates (typically <0.5 Hz) and activate only in tightly restricted spatial and directional receptive fields (Jung and McNaughton, 1993a; Leutgeb et al., 2007; Neunuebel and Knierim, 2012). Moreover, studies examining neuronal expression of activity-dependent immediate-early genes such as c-Fos, Zif286, and Arc as surrogate measures of DGC AP firing have found exceptionally sparse labeling in DGCs, with only 2–5% of DGCs expressing these genes, even after exposure to multiple environments or spatial cognitive tasks (Chawla et al., 2005; Tashiro et al., 2007; Alme et al., 2010). In comparison, similar spatial navigation sessions activate immediate-early gene expression in 40% of hippocampal pyramidal

cells in downstream CA subfields (Guzowski et al., 1999), highlighting the comparative paucity of DGC activation.

The extremely sparse activation of DGCs is particularly puzzling given the anatomy of their primary afferents from the entorhinal cortex (EC). DGCs receive massively convergent and divergent inputs from the medial and lateral entorhinal cortices. Singly-labeled EC stellate cells projecting to the DG can project to as much as 1/3 of the rodent DG, making en passant synapses with DGCs throughout this extensive axonal arbor (Tamamaki and Nojyo, 1993). Conversely, retrograde tracing studies have shown that discrete regions of the DG can receive inputs from substantial portions of the EC, with a single DGC receiving inputs from 3600 to 5600 neurons widely distributed across the EC (Patton and McNaughton, 1995; van Groen et al., 2003). In addition to the massive convergence and divergence of DG afferents, the originating EC stellate cells of this pathway, particularly "grid cells" in the medial EC, are promiscuously active. These neurons exhibit large-scale activation and demonstrate tessellated grid-like receptive fields across spatial environments (Fyhn et al., 2004, 2007). Given the repeating nature of grid cell activity throughout spatial environments, it appears that a significant portion of DG afferents are almost always active, given that the vertices of grid cells receptive fields comprise approximately 20% of the entire environment (Lisman, 2011). Thus, the convergence, divergence, and nearly continuous activity of the EC perforant path projection provide substantial excitatory input to the DG.

Given this robust and constant excitatory drive impinging onto DGCs from the EC, why are so few of these cells active during behavioral tasks? It is likely that cell-intrinsic biophysical properties of DGCs contribute in part to their relative inexcitability. DGCs exhibit hyperpolarized membrane potentials compared to most hippocampal neurons, typically resting near -85 to -90 mV, and their high membrane resistance

endows them with a long time constant for integrating synaptic inputs. Further, they lack regenerative calcium conductances to permit phasic or "burst mode" firing and they exhibit remarkable spike frequency adaptation during sustained depolarizations (Fricke and Prince, 1984; Spruston and Johnston, 1992; Staley et al., 1992). Finally, DGC dendrites display significant attenuation of synaptic input owing to the lack of active conductances that would allow dendritic spiking or input amplification (Krueppel et al., 2011). This combination of properties endows DGCs with an innate reluctance to fire APs.

In addition to these relatively hypoexcitable cell-intrinsic properties, DGCs reside in a strongly inhibitory local network, which provides rich feedforward, feedback, and tonic inhibitory input. Feedforward inhibitory drive onto DGCs is particularly strong due to a number of factors. First, several classes of feedforward inhibitory interneurons, including both somatically targeting fast-spiking interneurons on the granule cell layer's periphery as well as dendritically targeting hilar interneurons, are far more easily recruited by perforant path activation than are DGCs (Scharfman, 1991; Ewell and Jones, 2010). Second, the fast-spiking basket cell interneurons of the DG are particularly specialized to integrate afferent inputs, generate APs, and powerfully inhibit DGCs upon perforant path activation with extraordinary rapidity. Among the many specializations of these basket cells are high K^+–Na^+ conductance ratios in their dendrites which allow for rapid and temporally precise integration and activation (Hu et al., 2010), nonuniform cable properties that accelerate the time course of fast somatic synaptic potentials and elevate the efficacy of slower distal inputs (Nörenberg et al., 2010), and highly efficient calcium-buffering abilities that allow them to rapidly and repeatedly couple synchronous transmitter release with AP firing (Aponte et al., 2008; see Hu et al., 2014; for review of fast-spiking interneurons). This fast, strong feedforward inhibition would function to

constrain DGC firing, and limit firing rates of DGCs when spiking occurs, because this inhibitory input primarily targets DGC somata and axon initial segments, the cellular domains of synaptic integration of excitatory and inhibitory inputs.

Third, feedback inhibition in the DG also appears particularly specialized. DGC axons are normally not present in the molecular layer or granule cell layer, but are instead restricted exclusively to the hilus (Claiborne et al., 1986), where 50% of their target cell population is composed of GABAergic interneurons (Houser and Esclapez, 1994; Houser, 2007), suggesting that many of the DGCs' postsynaptic targets may be inhibitory neurons. DGCs are unique among cortical principal cells in that they are endowed with a repertoire of differing synaptic terminal types in their axons. These axons give rise to 7–12 mossy fiber boutons which synapse with excitatory hilar mossy cells and onto CA3 pyramidal cells, but they have a far larger number (100–150) of smaller terminals, including filopodial extensions and en passant synapses, which primarily target interneurons (Acsády et al., 1998). Due to this target selectivity, the vast majority of DGCs' postsynaptic targets may be inhibitory interneurons. These targets include both hilar feedback interneurons (a majority of which are somatostatin positive) that provide both dendritic feedback inhibition onto DGCs, which limits the strength of cortical afferent inputs, as well as fast-spiking interneurons with somatically targeted inhibition (typically also performing feedforward functions). This biases synaptic integration toward restriction of DGC activation (Freund and Buzsáki, 1996). This feedback inhibition is hypothesized to contribute to making the DG a competitive network, or a "winner-take-all" scheme, in which the activation of a sparse population of DGCs effectively silences the remaining majority of the population (de Almeida et al., 2009a, 2009b; Rolls, 2010).

Given the high levels of activity of its upstream cortical afferents in relation to the surprisingly low activity levels of its principal cells, the information transformation within the DG has been described as a "sparsification" operation or as a form of "sparse coding" in which the DG's output becomes a more sparse representation of its incoming neuronal activity pattern, both in terms of number of DGCs activating, as well as their limited firing rates (O'Reilly and McClelland, 1994; Treves and Rolls, 1994; Acsády and Káli, 2007). The sheer paucity of DGC activation raises an important question with regard to cognitive processing. If so few DGCs are active, how can their extremely sparse activity contribute in any significant way toward neural processing of hippocampal-dependent cognitive tasks? In short, the DG could only effectively transmit information through an amplifying mechanism by which DGCs could strongly excite their downstream targets in the hilus, and perhaps more critically, the pyramidal cells of CA3, without relying on synaptic convergence (since DGCs only target a few CA3 pyramidal cells). Without such a mechanism, the sparse coding in the DG would be a synaptic "dead end" and little, if any, information content could be relayed to downstream hippocampal structures. *In vivo* recordings have shown that single DGCs are indeed capable of reliably activating CA3 pyramidal cells (Henze et al., 2002). Unique properties of DGC axon terminals appear to be specialized to achieve this end. Mossy fiber boutons synapse with excitatory hilar mossy cells and CA3 pyramidal cells. These synapses are unique in the mammalian brain in that they are exceptionally large, contain multiple release sites, and display extraordinarily robust frequency facilitation, even at very low frequencies (Salin et al., 1996). Furthermore, even though the majority of DGCs' synaptic targets are feedback (onto DGCs) and feedforward (onto CA3) inhibitory interneurons, these connections are mediated by filopodial synapses, which, in contrast to mossy fiber boutons, exhibit rapid depression upon repetitive activation (Mori et al., 2004). These

specialized synaptic properties allow DGCs to act as conditional “detonators” (McNaughton and Morris, 1987) of their postsynaptic CA3 targets during periods of elevated firing rates.

What functions are served by sparsely activating DGCs?

What are the implications of a sparsely coding network of cells that rarely activate, yet when they do, exert massive excitatory influence on their postsynaptic targets? The answer varies depending on whether one is considering the DG’s role in cognition and memory, or epilepsy. The DG’s position at the entrance to the hippocampus combined with the sparse activation of DGCs led to the theory that DG circuitry transforms promiscuous and highly active cortical input into a sparse neural code suitable for representing novel aspects of episodic memories (Treves and Rolls, 1994; Treves et al., 2008). This DG-mediated transformation is critical to many aspects of hippocampal-dependent neural processing, most notably pattern separation and pattern completion, which are fundamental components of episodic memory encoding (Leutgeb et al., 2007; McHugh et al., 2007; Nakashiba et al., 2012; Neunuebel and Knierim, 2014). Behaviorally, pattern separation is the ability to discriminate subtle differences between similar episodes (e.g. “where one parked one’s car today is not necessarily the same place as yesterday”; O’Reilly and McClelland, 1994). From a computational perspective, this translates to the "process of transforming similar inputs into more dissimilar outputs" (Piatti et al., 2013), thereby detecting novelty and isolating salient differences between inputs. Computational models suggest that the DG could separate similar patterns through the output of different, small subsets of DGCs with distinct DGC ensembles activating to each unique stimulus (O’Reilly and McClelland, 1994; de Almeida et al., 2009b). However, tetrode recording and immediate-early gene

reporter studies have both reported that the same sparse population of DGCs may activate in multiple environments (Leutgeb et al., 2007; Alme et al., 2010) and that the rest of the population may remain essentially dormant during a given behavioral epoch. This conflicts with the expectation of sparse firing of multiple, distinct DGC ensembles in different environments (Jung and McNaughton, 1993b; Chawla et al., 2005) predicted by computational models (O'Reilly and McClelland, 1994; de Almeida et al., 2009b). In this case, rate coding within the active population of cells could instead differentiate inputs. Other models hypothesize that newborn and mature DGC's contribute differentially to the active population of DGCs involved in pattern separation (Aimone et al., 2011; Lisman, 2011; see Piatti et al., 2013 for review of neurogenesis and sparse coding). It is not yet known which of these coding schemes is utilized by the DG in execution of DG-dependent tasks such as pattern separation. What remains abundantly clear, however, is that information coding is achieved through sparse activation of principal cells within the DG and that this is critical to normal execution of DG-dependent cognitive function.

Dentate gating: a secondary consequence of the DG's sparse code

A secondary consequence of the DG's sparse activation and low excitability has received considerable attention with regard to epilepsy: the DG is capable of preventing and restricting the relay of pathological, synchronous activity in the EC into the hippocampus and limbic system, regulating seizure activity in diseases such as epilepsy. This phenomenon has been termed "dentate gating" (Heinemann et al., 1992; Lothman et al., 1991). The term, "dentate gating," and others, such as "the dentate gate," "gatekeeper," "regulatory checkpoint," "critical checkpoint," and "filter function," have all been used extensively by epilepsy researchers to describe the phenomena in which the dentate effectively limits (or sometimes fails to limit) cortical input from entering the

hippocampus proper. These terms do not semantically imply that this behavior is the function of the DG, but rather a role that emerges as a consequence of the DG's transformation of cortical inputs into a sparse, neural code during execution of its cognitive functions.

Some of the first evidence suggesting a "gatekeeper" role for the DG appeared in early *in vivo* field recordings from the DG molecular layer in rabbits during electrical stimulation of the EC and perforant path. In these studies, the DG was capable of filtering out higher frequency inputs (>10 Hz) via EPSP habituation due to large, slow post-stimulus IPSPs as long as the stimulus train was brief; higher frequency stimulation for longer durations (several seconds) appeared to break this filter down and facilitate DG EPSPs (Andersen et al., 1966). Later, Collins et al., (1983) more directly demonstrated the DG's role in regulating seizure propagation in behaving rats. Seizure-like activity was initiated in the EC by focal application of chemoconvulsants, and then activation of hippocampal structures was measured post hoc using a metabolic deoxyglucose autoradiography assay in sectioned hippocampal slices. When convulsant injection failed to induce epileptic activity, 10 or fewer spike events were observed per minute in the EC and there were no apparent changes in deoxyglucose autoradiography or behavior. When mild convulsive activity was initiated (10–30 interictal spikes per minute), animals exhibited slight to no signs of behavioral seizures, which included intermittent staring and sniffing. In these animals, deoxyglucose uptake was restricted to the EC and DG molecular layer and there was no indication of propagation of seizure activity into the DG granule cell layer or CA fields of the hippocampus proper. However, when greater than 40 interictal spikes per minute were induced (by either convulsants alone or in combination with electrical stimulation), animals displayed clear behavioral seizures, including shaking, sniffing, head nodding, and freezing. In these animals,

metabolic changes were observed to spread through the EC, the DG, and beyond into CA3, CA1, and other extrahippocampal structures in both the ipsilateral and contralateral hemispheres. Since enhanced deoxyglucose uptake was initially restricted to only the DG molecular layer in mild to moderate convulsive states, and only propagated beyond the DG through the entire hippocampus and beyond after strong convulsive states, the authors concluded that this sequential metabolic activation suggests that "the [DG] acts as a restrictive gateway for seizure spread from EC to the rest of the limbic system."

Stringer and Lothman further developed this gating theory by introducing a concept termed "maximal dentate activation" (MDA; Stringer et al., 1989; Lothman et al., 1992). In these studies, either the perforant path or CA3 was electrically stimulated in urethane-anesthetized rats. MDA was defined as the state in which stimulation elicited a saturating response in the DG. Stimulation frequencies between 10 and 40 Hz most easily elicited MDA, and once MDA occurred, electrical recordings revealed a marked, negative DC shift indicating depolarization of DGCs. This was accompanied by a rapid and substantial elevation of extracellular K+ concentrations (6–8 mM increase) and the emergence of large-amplitude DGC population spikes and bursting. Stimuli above the MDA threshold also elicited prominent after-discharges as well as synchronous epileptiform discharges in CA3, CA1, subiculum, and the EC. When stimulation was applied to the angular bundle of the perforant path, MDA occurred first in the DG, before subsequent propagation to CA1, ruling out the possibility of direct EC activation of the temporoammonic pathway to CA1 being responsible for CA1's activation. Moreover, when the DGCs were selectively lesioned with colchicine, stimulation that would normally generate MDA failed to elicit it, and there was no concomitant activation of CA1. These results showed clearly that maximal activation of the DG, even unilaterally,

can both initiate and sustain seizure activity throughout the hippocampus and extrahippocampal structures bilaterally. In total, these results indicated that when the DG fails to filter and control cortical excitatory inputs as a gatekeeper or regulatory checkpoint, it acts instead as an ictal amplifier or promoter of seizure activity (further reviewed in Heinemann et al., 1992). This duplicitous role of the DG as both a filter and amplifier likely emerges from a combination of DGCs' reluctance to fire, the rich inhibitory network they reside in, and the unique properties of the large mossy fiber boutons of their axons endowing with them the ability to "detonate" area CA3 when upon DGC activation.

Recent studies have further supported the DG's role as a gatekeeper. Among the most visually demonstrative of these are studies utilizing dynamic imaging techniques. In particular, use of voltage-sensitive dyes, when combined with state-of-the-art cameras, can resolve propagation of synaptic potentials through multiple sites within a brain slice, at an extremely high temporal resolution. Voltage-sensitive dye imaging can therefore facilitate recording of synaptic integration and propagation of activity across multiple circuits. Specifically within hippocampal and parahippocampal structures, this technique allows simultaneous monitoring of afferent activation of the DG via the EC, processing within the DG, and propagation of DG signals to efferent structures in CA3 and CA1.

One early voltage-sensitive dye imaging study strikingly illustrated the gating dynamics of the DG (Iijima et al., 1996). In this study, rat entorhinal cortical–hippocampal slices were perfused with low concentrations of GABA-A receptor antagonists, the EC was stimulated, and activation of the slices imaged. This study demonstrated that the disinhibited DG more easily allowed cortical activity to enter the hippocampus and activate the entire hippocampal loop, later reentering the EC. Further

experiments in the absence of inhibitory blockade showed that repetitive stimulation of the EC would initially activate only cortical areas. Each successive stimulus would increase sustained activity in the EC, and only after multiple successive stimuli would the DG "gate" collapse, allowing activity to penetrate through DG and enter the hippocampus proper. This study clearly demonstrated that activation of the EC is usually restricted by the DG, but that successive stimulation could, within a short time frame, erode gating and elicit propagation activity into the hippocampus.

We (Ang et al., 2006; Yu et al., 2013; **Fig. 2.1**) have further utilized voltage-sensitive dye imaging techniques to monitor activation of the DG and downstream structures in control and epileptic animals, in response to stimulation of the perforant path. Our recordings clearly illustrate the "gatekeeper" function of the DG (**Fig. 2.2A–C**), as well as the important finding that activation of GABA-A receptors on DGCs is required for this filtering of EC inputs. Even modest levels of disinhibition (pharmacologic block of 20–25% of IPSC amplitudes with picrotoxin) resulted in DG gating collapse and activation of downstream CA3 (**Fig. 2.1D–F**).

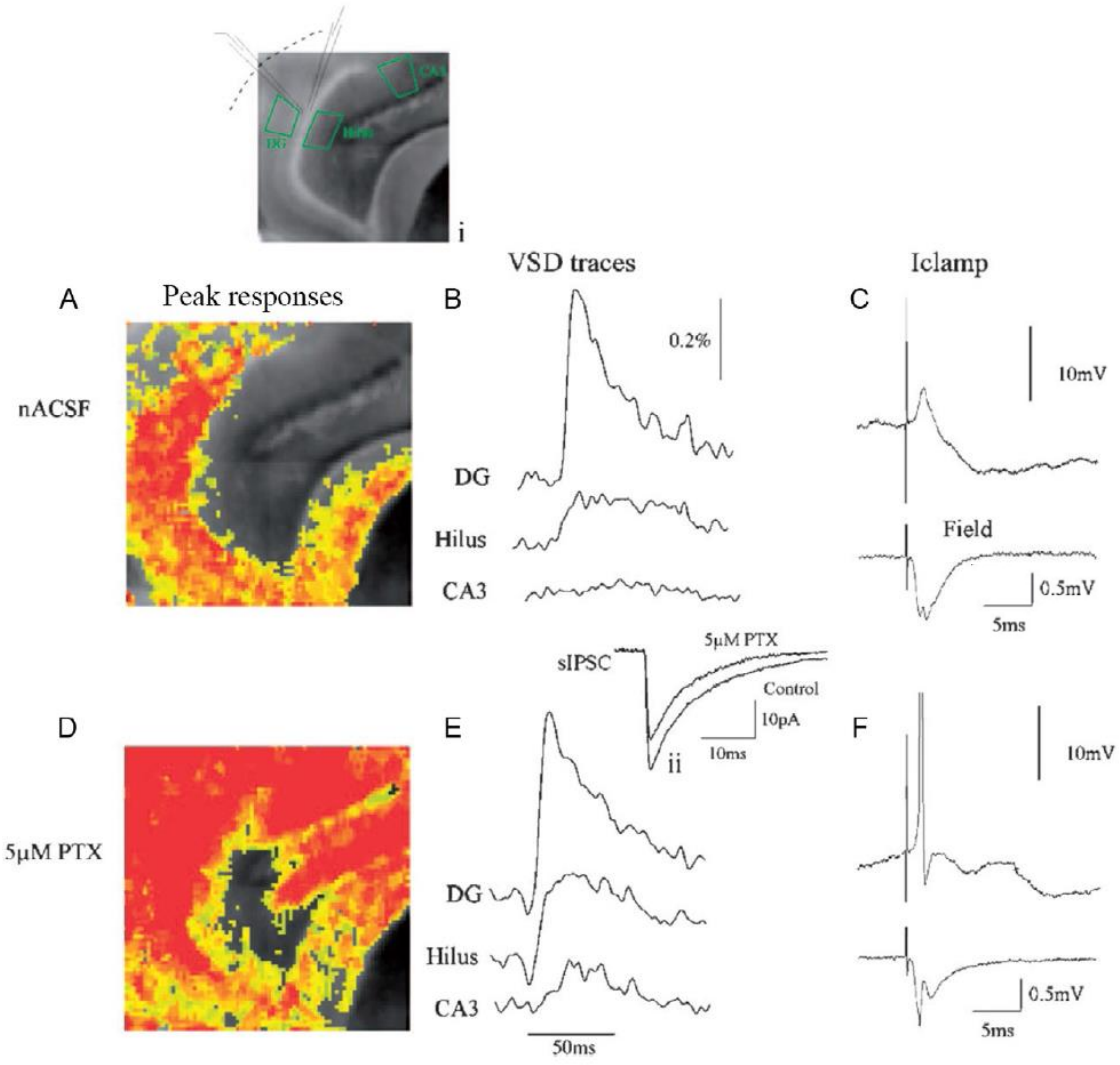
i
VSD traces
Iclamp
A
Peak responses
B
C
nACSF
0.2%
10mV
DG
Hilus
CA3
Field
0.5mV
5ms
5μM PTX
sIPSC
Control
10pA
10ms
ii
D
E
F
5μM PTX
10mV
DG
Hilus
CA3
0.5mV
5ms
50ms

Figure 2.1. "Gatekeeper" function of the DG is maintained by GABAergic inhibition. Simultaneous voltage sensitive dye (A) snapshot taken at the peak of the response. A grayscale image of the slice, with patch and field potential recording electrode location is depicted in the inset above (A). (B) trace illustrating the VSD response over time, (C) patch clamp (top) and field potential recording (bottom) of DG response to perforant path activation in control ACSF. (A) Note robust activation of dentate gyrus molecular layer (red color in A, corresponding to a 10–15 mV EPSP in (B), which does not result in activation of downstream structures (note lack of response in area CA3 in (A) and (B)). This lack of CA3 activation is because DGCs do not fire APs in response to perforant path activation under these conditions. This is evident in both the patch (C, top trace, the neuron depolarized to Vm of -50 mV) and field potential recording (C, bottom trace), due to powerful feedforward inhibition activated by perforant path stimulation (C, note large IPSP in patch recording) The importance of inhibition in mediating this "gatekeeper" function is illustrated in responses in (D), (E), and (F), following perfusion with 5 mM picrotoxin, a noncompetitive GABA-A receptor antagonist. This concentration blocks 20–25% of inhibition (see inset [located above (E)] depicting an averaged spontaneous IPSC [sIPSC] before and after perfusion with 5 mM picrotoxin). During 25% GABAergic blockade, perforant path activation resulted in powerful activation of both the DG and downstream structures (CA3 and hilus; D, E). It also triggered AP firing in DGCs (see patch and field potential recordings in (F), both of which exhibit AP firing). From Coulter, D.A., Carlson, G.C., 2007. Functional regulation of the dentate gyrus by GABA-mediated inhibition. Prog. Brain Res. 163, 235–243.

In Yu et al. (2013), we further demonstrated the emergence of this gating function during postnatal development using a novel, combined dynamic imaging approach capable of resolving sequentially both synaptic potentials (voltage-sensitive dye imaging) and AP firing (multicellular calcium imaging in large populations of DGCs) in response to perforant path afferent activation in mouse hippocampal–entorhinal cortical slices. During postnatal development, DG gating function was expressed only as animals matured. Neonatal animals (P6) showed robust activation of both the DG and CA3 upon perforant path activation, whereas older animals (P22, P60) displayed robust gating in which the DG showed marked depolarization, but activation did not propagate into area CA3 (**Fig. 2.2**). Development of this gating property was primarily mediated by changes in local circuit inhibition, as inhibitory blockade (with picrotoxin) normalized responses at all developmental time points. During development, GABA responses are often depolarizing and excitatory, due to differential expression of the chloride accumulator, NKCC1, and chloride extruder, KCC2, which invert their relative expression levels during development to produce hyperpolarizing or shunting inhibitory currents at GABAergic synapses in adulthood (Liu et al., 1996; Hollrigel et al., 1998). These changes as well as further inhibitory synaptic innervation of DGCs and electrophysiological maturation of DGCs with development likely combine to establish the gating function of the DG.

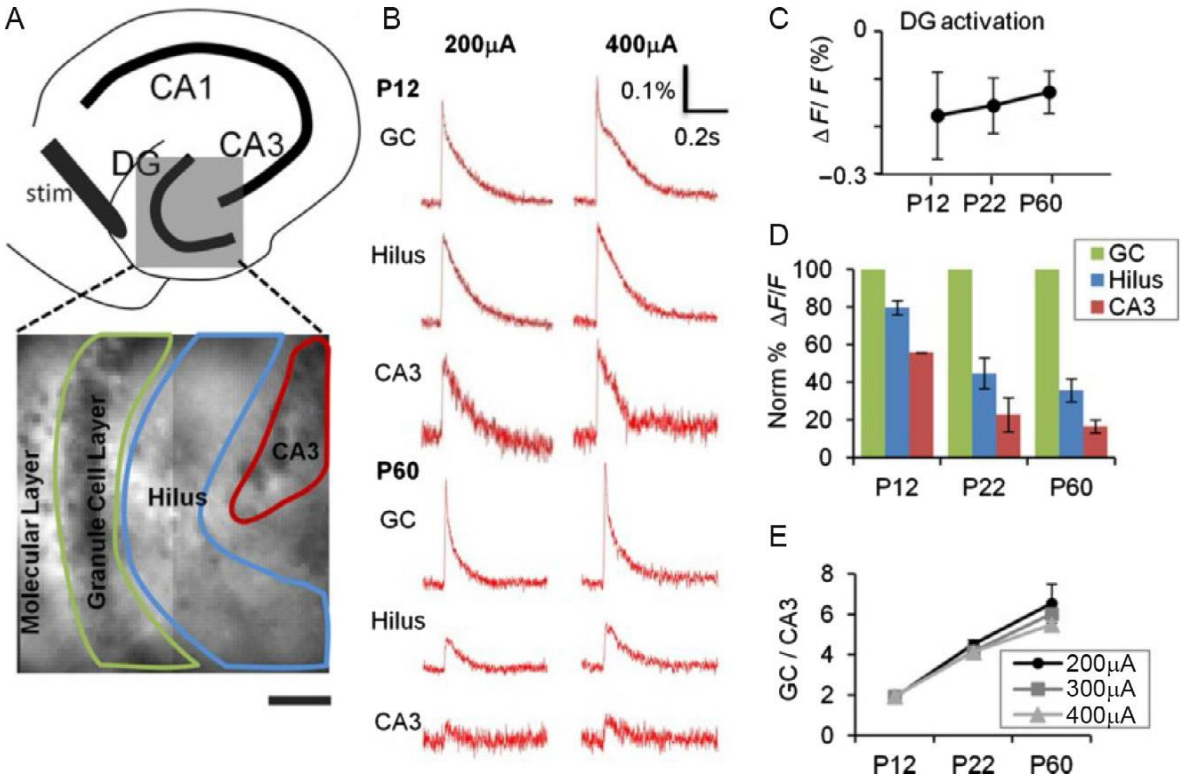
A
CA1
DG
CA3
stim
Molecular Layer
Granule Cell Layer
Hilus
CA3
B
200μA
400μA
P12
0.1%
0.2s
GC
Hilus
CA3
P60
GC
Hilus
CA3
C
DG activation
ΔF/ F (%)
0
−0.3
P12 P22 P60
D
Norm % ΔF/F
100
80
60
40
20
0
GC
Hilus
CA3
P12 P22 P60
E
GC / CA3
8
6
4
2
0
200μA
300μA
400μA
P12 P22 P60

Figure 2.2. Postnatal development of DG gating behavior. (A) Top: A schematic illustration depicting subregions of the hippocampus. Bottom: The DG (gray box) is expanded in a VSD image with an overlay of the region of interest (ROI) delineating subregions used to measure DG responses elicited by perforant path stimulation. (B) VSDI time-resolved fluorescence plots for the subregions depicted in (A) for P12 (top) and P60 (bottom) animals. PP stimulation elicited comparable depolarizations in the DGC, hilus, and CA3 at P12, but little depolarization of hilus and CA3 at P60, despite robust responses in DGC. (C) DG response amplitude (DF/F) is comparable at all developmental ages (elicited by a 400 mA PP stimulus). (D) P12, P22, and P60 mice (n=8 slices in 3 animals, n=7 of 2 animals, and n=6 of 2 animals, respectively) show progressively less propagation of synaptic responses through DGC (green, light gray in the print version) to hilus (blue, dark gray in the print version) and CA3 (red, gray in the print version). All data points are normalized to DGC layer response at 400 mA, which is equivalent across groups (see C). (E) Plots of DG gating function, the ratio of DGC to CA3 activation intensity, depict the significant increase in the DG gating property as postnatal development progresses, at several stimulus intensities 200 mA (circle), 300 mA (square), and 400 mA (triangle). p=0.001 for the animal age factor affecting gating (two-way ANOVA). p=0.16 for stimulus intensity affecting gating (two-way ANOVA). From Yu, E.P., Dengler, C.G., Frausto, S.F., Putt, M.E., Yue, C., Takano, H., Coulter, D.A., 2013. Protracted postnatal development of sparse, specific dentate granule cell activation in the mouse hippocampus. J. Neurosci. 33, 2947–2960.

The sequential imaging approach in this study allowed us not only to resolve the spatiotemporal properties of afferent activation in the DG and downstream structures using voltage-sensitive dye imaging but also to resolve cellular activation in large numbers of DGCs with single-cell resolution using multicellular calcium imaging. This technique can transduce AP firing in individual neurons into changes in fluorescence intensity through the use of calcium-chelating dyes, or genetically encoded calcium indicators. Using this imaging approach, we found that the population activity of DGCs displayed a progressive sparsification with postnatal development (**Fig. 2.3**) and that differences in proportional activation of DGCs were also normalized by inhibitory blockade, further demonstrating the critical role of inhibition in restricting DGC activation. An interesting side note of the study was that dentate gating and sparse firing of DGCs develop synchronously with the protracted representation of space within the hippocampus and EC, which become evident 3.5–4 weeks after birth (Langston et al., 2010) as well as with competency in hippocampal-dependent spatial memory tasks (Schenk, 1985; Rudy et al., 1987; Ainge and Langston, 2012). Given that appropriate neuronal activity within the DG is likely critical to completion of these tasks, the delays in development of adult levels of DG filtering and sparse DGC activation may contribute to the delayed development of both neuronal representations of space and competence in spatial memory tasks.

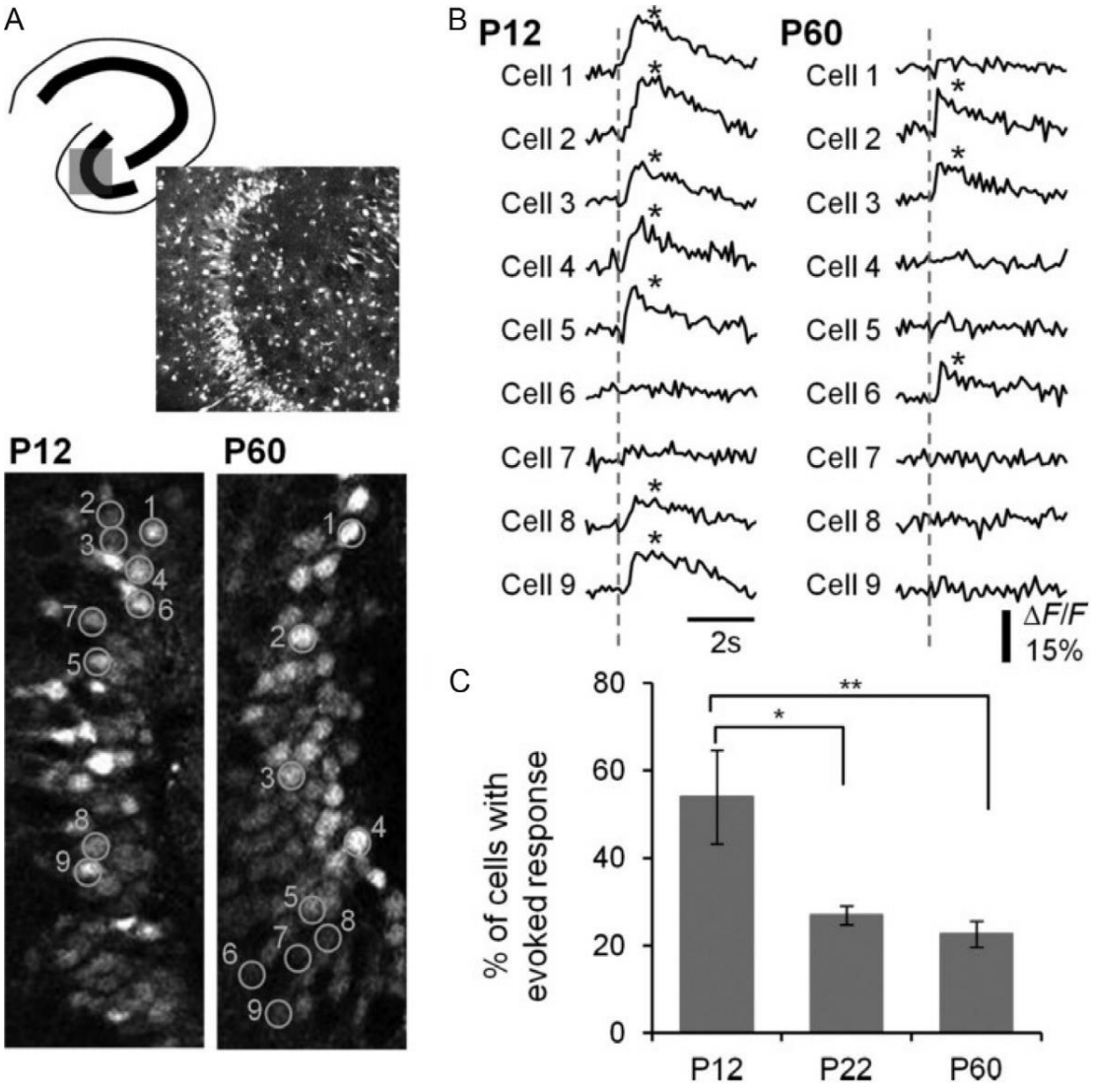
A
P12
P60
B
P12
P60
Cell 1
Cell 2
Cell 3
Cell 4
Cell 5
Cell 6
Cell 7
Cell 8
Cell 9
2s
ΔF/F
15%
C
% of cells with evoked response
80
60
40
20
0
**
*
P12
P22
P60

Figure 2.3. Decreased DGC activation during postnatal development. ***A***, Top, Schematic of a hippocampal slice depicting the imaged area in the DG and a Fura2-loaded DG of a P12 mouse (370μmx370μm). Bottom, Image of P12 and P60 DGCs, with ROI created on a random sample of cells (orange) (90 μm x 200 μm). Numbers denote cell identification with time-resolved fluorescence responses depicted in ***B***. ***B***, Representative traces of time-resolved calcium imaging responses for the ROI in the P12 and P60 images in ***A***. The dotted line indicates the time when PP stimulation (400 μA) occurred. An asterisk indicates detection of a calcium transient. ***C***, Plot of the percentage DGC activation by PP stimulation for P12, P22, and P60 animals. Note the decrease in cell activation with postnatal development. $P < 0.0001$ for the animal age factor (ANOVA). *$p = 0.05$, significant differences between P12 and P22 (Tukey's multiple-comparison *post hoc* testing). **$p = 0.01$, significant differences between P12 and P60 groups (Tukey's multiple-comparison *post hoc* testing). P12: $n = 322$ PTX-active cells in 10 imaged regions; P22: $n = 198$ in 10 imaged regions; P60: $n = 239$ of 12 imaged regions.

Recent studies have used optogenetic techniques to modulate dentate gating function directly in a mouse model of temporal lobe epilepsy. In Krook-Magnuson et al. (2015), investigators used a closed-loop system to detect seizures and selectively modulate the activity of DGCs by triggering either optical activation of these neurons with channelrhodopsin or inhibition with halorhodopsin. They found that optogenetic hyperpolarization of DGCs efficiently stopped spontaneous seizures (gate restoration). In contrast, optogenetic activation of DGCs exacerbated spontaneous seizures. Additionally, this study revealed that optogenetic activation of DGCs in healthy, nonepileptic animals elicits acute seizures and that the intensity and duration of these seizures increase with repeated DGC photostimulation. These results clearly support the concept that the DG is a critical node within the hippocampus and provides direct *in vivo* evidence consistent with the dentate "gate" hypothesis. Additional experiments have elaborated on this finding and demonstrated that optogenetic activation of DG inhibitory interneurons can immediately stop the spread of seizures in the hippocampus and EC, further highlighting the important role of inhibition within dentate circuitry in regulating cortical inputs (Lu et al., 2016).

The studies mentioned above all demonstrate ways in which the DG is a critical node within the hippocampal circuit, both for restricting entrance of EC activity into the hippocampus and, when sufficiently hyperactivated, allowing propagation of pathological activity to reverberate through the hippocampus. Given that the DG functions as a key node within the limbic system, a critical question is whether the DG's gating function is compromised during epilepsy development and expression in both animal models and humans with epilepsy. Several lines of evidence have suggested that this may be the case. In one such study, Behr et al. (1998) demonstrated enhanced propagation of epileptiform activity through the DG in a rat kindling model of epilepsy.

In this study, investigators prepared hippocampal–EC slices from control and kindled animals, evoked isolated epileptiform activity in the EC via local perfusion of GABA antagonists and high K+, and recorded activation of downstream DG and CA3 extracellularly. Slices from kindled animals displayed markedly enhanced propagation of EC bursting activity through the DG. Another study by Patrylo et al. (1999) showed a similar pattern of abnormal DG responses in a systemic kainate model of epilepsy in rats. In this investigation, slices from kainate-treated rats (both acutely 2–4 days following kainate administration, as well as from chronically epileptic rats >3 months after kainate treatment) showed multiple population spikes following perforant path stimulation, while control slices consistently produced only a single spike in response to the same stimulus. An additional investigation in this kainate-induced epilepsy model also showed that slices from epileptic rats would produce epileptiform bursts when stimulated repetitively at 5–10 Hz (in the range of hippocampal theta rhythms), while the same stimulation elicited only single spikes in control slices (Shao and Dudek, 2011). Further, in a slice voltage-sensitive dye imaging study in our laboratory (Pathak et al., 2007), we showed that in a rat pilocarpine status-epilepticus model, DG throughput onto downstream structures was also dysregulated for several days following status epilepticus. In this study (**Fig. 2.1**), control slices exhibited little downstream CA3 activation following perforant path stimulation. However, immediately following status epilepticus (and until 2 weeks post-SE), perforant path stimulation reliably activated CA3 showing a collapse of normal DG gating function. Interestingly, in this model normal gating function appeared to be restored to control levels in chronically epileptic animals. This caveat aside, these studies collectively show that the DG's gatekeeper function can be corrupted in multiple models of epilepsy, including kindling, as well as kainate- and pilocarpine-induced status-epilepticus models. Further, these data are

congruent with a number of electrophysiological studies demonstrating varying degrees of DGC hyperexcitability in hippocampal slices prepared from tissue resected from patients with intractable temporal lobe epilepsy (Masukawa et al., 1989, 1996; Williamson, 1994; Isokawa and Fried, 1996).

Which mechanisms contribute to the DG gate breakdown in epilepsy?

Failure of dentate gating and its hypothesized relationship to both icto- and epileptogenesis encouraged many studies detailed earlier. The common theme described in these investigations is that the DG is normally resistant to allowing EC activity to propagate to downstream structures of the hippocampus proper. In epilepsy, the gatekeeping function of the DG is compromised, allowing relay of cortical activity from the EC into the hippocampus, and propagation in a reverberatory cycle back to EC (Lothman et al., 1992). This hypothesis has prompted numerous studies to characterize cellular and circuit alterations in DG circuitry which may contribute to failure of the DG's gatekeeper function.

Among the earliest discovered and most striking of these alterations, and a classic hallmark of temporal lobe epilepsy, is the de novo sprouting of recurrent mossy fiber synapses. First described by Tauck and Nadler (1985), mossy fiber sprouting is the generation of aberrant mossy fiber collaterals which form recurrent, excitatory synapses from DGCs to other DGCs via synapses located in the inner third of the molecular layer. This phenomenon, which is thought to be a form of reactive plasticity in response to death of many of the DGC population's synaptic targets, is particularly well described in the DG in both human epilepsies and in animal models of injury-induced epilepsy (Tauck and Nadler, 1985; de Lanerolle et al., 1989; Sutula et al., 1989; Houser et al., 1990). It is also hypothesized to contribute to DG hyperexcitability in epilepsy. Initial

electrophysiological experiments involved electrical antidromic stimulation of the hilus (to activate mossy fibers directly) and demonstrated the role of mossy fiber sprouting in elevating DGC excitability (Tauck and Nadler, 1985; Cronin et al., 1992), but these approaches were indirect because such stimulation might also activate other afferent fibers or excitatory mossy cells. Later, however, direct evidence showing monosynaptic excitatory transmission between DGCs following mossy fiber sprouting was obtained through paired whole-cell recordings (Scharfman et al., 2003b). In this study, the amplitudes of the EPSPs between DGCs were small, and the percentage of paired connections was relatively low, suggesting that the mossy fiber recurrent excitatory network would be relatively weak at promoting hyperexcitability in the DG. Supporting this conclusion, use of rapamycin to suppress mossy fiber sprouting in a pilocarpine model of temporal lobe epilepsy did not reduce seizure frequency (Heng et al., 2013). However, in slices prepared from chronically epileptic rats, these aberrant kainate receptors present at these sprouted synapses were capable of generating abnormal, sustained, and rhythmic firing among DGCs that could not be generated in control slices (Artinian et al., 2011), suggesting that even if mossy fiber sprouting does not alter seizure propensity, it may still subtly alter excitability in the DG. Thus, the overall importance of mossy fiber sprouting and its contributions to DGC excitability in epilepsy is unclear. Interestingly, further work has shown that currents mediated through these aberrant kainate receptor-containing mossy fiber synapses can be selectively blocked using pharmacologic agents (Pinheiro et al., 2013); such tools may provide great utility in further clarifying this issue.

While increased recurrent excitatory drive may play a role in breakdown of the dentate gate, reduced inhibition of DGCs could also play a role in this process. GABAergic inhibition is a critical mediator of DG gating (**Fig. 2.1**), and compromised

filter function of the DG is a major contributor to seizure propagation in models of epilepsy. One could easily hypothesize that the DG in these models undergoes disinhibition. However, in both kindling and post-status-epilepticus models of temporal lobe epilepsy, numerous studies have shown a surprising upregulation of GABA-A receptor expression, both synaptically (Buhl et al., 1996; Cohen et al., 2003; Nusser et al., 1998; Otis et al., 1994) and in whole-cell recordings (Brooks-Kayal et al., 1998; Gibbs et al., 1997; Leroy et al., 2004; Mtchedlishvili et al., 2001) from chronically epileptic rats. Some studies do, nevertheless, describe a transient decrease in GABAergic currents onto DGCs immediately following epileptogenic injuries that persists for weeks following initial injury, but this reduction recovers toward or beyond control levels over time (Cohen et al., 2003; Thind et al., 2010). However, in a recent study in a mouse model of temporal lobe epilepsy, phasic GABAergic inhibition was reduced, likely as a result of relocalization of γ2 GABA receptor-containing subunits away from the center of synaptic contacts (Zhang et al., 2007). While this result in mice differs from many of the results earlier (all conducted in rats), it may, in fact, highlight an important species difference between rat and mouse models of temporal lobe epilepsy.

While the amplitude of GABAergic inhibitory currents in DGCs may be increased in many chronically epileptic animals, several studies have demonstrated that inhibitory connectivity within the DG is compromised in epileptic animals following epileptogenic injuries and remain low in chronically epileptic animals (Kobayashi and Buckmaster, 2003; Shao and Dudek, 2005; Sun et al., 2007). This decreased inhibitory synaptic connectivity is often presumed to be caused by a loss of hilar somatostatin-positive interneurons following epileptogenic insults (Sloviter, 1987). Further experiments have also demonstrated that deficits in inhibitory basket cell circuit function may also contribute to reduced inhibitory efficacy as a result of less excitatory synaptic drive onto

basket cells, diminished pools of readily releasable vesicles, and frequent synaptic transmission failure between basket cells to DGCs (Zhang and Buckmaster, 2009).

While results implicating alterations in phasic DG disinhibition have been mixed, studies have shown that tonic inhibition within the DG is compromised as a result of epileptogenic injuries and epilepsy development. Tonic inhibition in the DG is typically mediated by δ subunit-containing GABA-A receptors, which are located primarily at nonsynaptic sites on DGCs. These receptors play a critical role in mediating controlled DG excitability by responding to GABA spillover from GABAergic synapses because of their perisynaptic localization (Wei et al., 2003), as well as their high affinity for GABA and their relatively slow desensitization rates (Saxena and Macdonald, 1994; Haas and Macdonald, 1999; Mtchedlishvili and Kapur, 2006). It is also likely that these receptors can be activated by neurogliaform interneurons in the DG's molecular layer, which have dense local axonal plexuses that are thought to provide inhibition largely through "bulk transmission" of GABA through activation of extrasynaptic receptors by release of a local "cloud" of GABA (Armstrong et al., 2011, 2012). In models of temporal lobe epilepsy, studies have demonstrated a reduction of these extrasynaptic, tonic GABA-A receptors with a corresponding downregulation in expression of δ subunits (Peng et al., 2004; Zhang et al., 2007). As of now, the role of this reduction in tonic inhibition onto DGCs with regard to DG excitability and gating in epileptic animals is unknown. It is possible that repetitive activation of EC afferents, like those occurring during seizure initiation, will elevate extrasynaptic GABA concentrations and enhance tonic current in normal animals (helping to suppress ictal propagation), and loss of these receptors will compromise this check on excitability in animals with epilepsy.

However, the efficacy of ionotropic GABAergic synapses depends not only on the pre- and postsynaptic function of synaptic machinery or number of inhibitory synaptic

inputs onto DGCs but also on the driving force of chloride ions across the neuronal membrane at these synapses. The chloride reversal potential is a potent determinant of ionotropic GABAergic inhibition. Typically, E_{GABA} is ~-70 to -80 mV in adult DGCs under normal conditions. However, immediately following status epilepticus, this reversal potential shifts to markedly less hyperpolarized levels (~-55 to -60 mV), which greatly diminishes inhibitory efficacy. During this time period, DGC excitability is markedly enhanced via reduced inhibitory influence in DGC synaptic integration and further, the DG's gating ability is consequently compromised (Pathak et al., 2007). This transient depolarizing shift in E_{GABA} manifests as a result of reduced expression of the chloride-extruding potassium/chloride cotransporter, KCC2, which normally functions to maintain E_{GABA} at hyperpolarized levels. Interestingly, this phenomenon of reduced KCC2 expression in animals immediately following status epilepticus closely mirrors the developing brain in which the response to GABA is also depolarizing. During development, the expression of the chloride extruder, KCC2, is low and the chloride accumulator, NKCC1, is relatively high before the "GABA switch" (around the second postnatal week), which involves reversed relative expression of these chloride transporters, and decreased DG gating efficacy (Ben-Ari, 2002; Owens and Kriegstein, 2002; Yu et al., 2013; **Figs. 2.2 and 2.3**). Interestingly, in Pathak et al. (2007), chloride reversal potentials return to near control levels as animals become chronically epileptic, and DG excitability appears to return to normal levels. However, even though transient, the failure of the DG gate immediately following epileptogenic injury may have critical implications in epileptogenesis, since the likelihood of synchronous, epileptiform activity reaching downstream structures is greatly enhanced. Bursting activity in the DG can potentially damage neurons in the hilus, and areas CA3 and CA1, leading to further neuronal loss, aberrant plasticity, and hippocampal sclerosis, in the period following the

initial epileptogenic injury, thus furthering the initial insult and potentially promoting further epileptogenesis.

While GABAergic disinhibition and altered chloride regulation are potential mechanisms for enhancing DG excitability in epilepsy and its development, another possible contributor to aberrant DG circuit activation is astrocytic gliosis. Reactive astrocytosis is a prominent pathology in both human (Eid et al., 2004) and animal models of epilepsy (Xu et al., 2011; do Nascimento et al., 2012; Estrada et al., 2012). Studies from our laboratory have demonstrated that astrocytic gliosis can reduce the efficacy of inhibitory neurotransmission onto hippocampal principal cells via downregulation of glutamine synthetase. Loss of glutamine starves inhibitory synapses of necessary local precursors to regenerate GABA and results in disinhibition (Ortinski et al., 2010; Coulter and Eid, 2012). While it is currently known that astrogliosis is present in the hippocampus, and specifically, in the DG of patients with temporal lobe epilepsy and in animal models of the disease, the exact contributions of this pathology in altering circuit function within the DG are currently unknown. However, in one recent study, Dhaher et al. (2015) pharmacologically mimicked the glutamine synthetase-reducing effects of astrogliosis, by infusing the glutamine synthetase inhibitor, methionine sulfoximine into different hippocampal substructures, including the angular bundle of the perforant path, deep layers of the EC, the DG, CA1, subiculum, and the lateral ventricle and monitored animals for seizures via video and EEG recordings. Among all tested structures, methionine sulfoximine infusion into the DG produced the highest number of seizures over the recording period, highlighting both the importance of the DG in seizure generation, and its potential susceptibility for gliosis-mediated disinhibition in epilepsy.

Yet another circuit alteration in the epileptogenic DG is aberrant neurogenesis. The DG is a unique brain structure in that it continuously generates new, functional neurons throughout life (van Praag et al., 2002). These newly generated DGCs have electrophysiological properties distinct from their mature counterparts and some studies suggest that these newborn cells may be activated preferentially compared to mature DGCs (Alme et al., 2010; Marín-Burgin et al., 2012). However, following SE, there is a marked increase in neurogenesis of DGCs, many of which integrate aberrantly into the local DG network (Parent et al., 1997; Parent, 2007; Kron et al., 2010). Several studies have posited both pathophysiological and compensatory roles for these aberrantly integrated neurons following epileptogenic injuries. Transgenic ablation of DGC neurogenesis prior to the inciting injury has recently been demonstrated to decrease epilepsy severity (Cho et al., 2015). Many DGCs born following epileptogenic injuries migrate to ectopic locations within the hilus and integrate abnormally into hippocampal circuitry (Scharfman et al., 2003a). The accumulation of these ectopic, but not normotopic, adult-born DGCs correlates with epilepsy severity (Hester and Danzer, 2013) as normotopic adult-born DGCs in epileptic animals do not exhibit aberrant excitability (Jakubs et al., 2006). While these studies have shown that these newly generated DGC (whether normotopic or ectopic) can play both pathologic and apparently compensatory roles, it is currently unclear how these newborn neurons participate in aggregate DG function, or the degree to which they compromise activation and output of the DG.

Conclusions

The DG is a structure characterized by the sparse activity of its principal neurons, DGCs. This low excitability is important in the cognitive function of the hippocampus and results predominantly from the high degree of inhibitory synaptic regulation, as well as intrinsic properties of DGCs themselves. This sparse activation serves an additional role in the context of epilepsy, where the DG's inherent ability to restrict pathological activation of the hippocampus and limbic system is of critical importance. A combination of circuit changes occurs in the DG during epilepsy development and expression, including mossy fiber sprouting, alterations to inhibitory circuits and their function, transmembrane chloride regulation, astrogliosis, aberrant neurogenesis, and alterations to the intrinsic properties of DGCs themselves. These epilepsy-associated modifications to the DG circuit may, to varying degrees, compromise the DG's ability to fulfill its regulatory gatekeeper role. Given the abundance of alterations, the mechanisms mediating this circuit collapse are likely not mutually exclusive, but instead mechanistically complex. Given that the DG functions as both a sparsifying transformer of cortical information in spatial cognitive processes and a regulator of cortical hyperactivity, inappropriate or pathological excitability within this watershed circuit may contribute to seizure propagation, both primary and secondary epileptogenic processes, as well as the many cognitive comorbidities associated with epilepsy. Understanding how epilepsy development alters the basic circuit properties of hippocampal structures may be important not only in targeting new therapies for seizure amelioration but also in developing new treatments to reduce comorbidities accompanying epilepsy.

Chapter 2 Bibliography

Acsády L, Káli S (2007) Models, structure, function: the transformation of cortical signals in the dentate gyrus. Prog Brain Res 163:577–599.

Acsády L, Kamondi A, Sík A, Freund T, Buzsáki G (1998) GABAergic cells are the major postsynaptic targets of mossy fibers in the rat hippocampus. J Neurosci 18:3386–3403.

Aimone JB, Deng W, Gage FH (2011) Resolving New Memories: A Critical Look at the Dentate Gyrus, Adult Neurogenesis, and Pattern Separation. Neuron 70:589–596.

Ainge JA, Langston RF (2012) Ontogeny of neural circuits underlying spatial memory in the rat. Front Neural Circuits 6:8.

Alme CB, Buzzetti RA, Marrone DF, Leutgeb JK, Chawla MK, Schaner MJ, Bohanick JD, Khoboko T, Leutgeb S, Moser EI, Moser M-B, McNaughton BL, Barnes CA (2010) Hippocampal granule cells opt for early retirement. Hippocampus 20:1109–1123.

Andersen P, Holmqvist B, Voorhoeve PE (1966) Entorhinal activation of dentate granule cells. Acta Physiol Scand 66:448–460.

Ang CW, Carlson GC, Coulter DA (2006) Massive and specific dysregulation of direct cortical input to the hippocampus in temporal lobe epilepsy. J Neurosci 26:11850–11856.

Aponte Y, Bischofberger J, Jonas P (2008) Efficient Ca2+ buffering in fast-spiking basket cells of rat hippocampus. J Physiol 586:2061–2075.

Armstrong C, Krook-Magnuson E, Soltesz I (2012) Neurogliaform and Ivy Cells: A Major Family of nNOS Expressing GABAergic Neurons. Front Neural Circuits 6:23.

Armstrong C, Szabadics J, Tamás G, Soltesz I (2011) Neurogliaform cells in the molecular layer of the dentate gyrus as feed-forward γ-aminobutyric acidergic modulators of entorhinal-hippocampal interplay. J Comp Neurol 519:1476–1491.

Artinian J, Peret A, Marti G, Epsztein J, Crépel V (2011) Synaptic kainate receptors in interplay with INaP shift the sparse firing of dentate granule cells to a sustained rhythmic mode in temporal lobe epilepsy. J Neurosci 31:10811–10818.

Behr J, Lyson KJ, Mody I (1998) Enhanced propagation of epileptiform activity through the kindled dentate gyrus. J Neurophysiol 79:1726–1732.

Ben-Ari Y (2002) Excitatory actions of gaba during development: the nature of the nurture. Nat Rev Neurosci 3:728–739.

Chawla MK, Guzowski JF, Ramirez-Amaya V, Lipa P, Hoffman KL, Marriott LK, Worley PF, McNaughton BL, Barnes CA (2005) Sparse, environmentally selective expression of Arc RNA in the upper blade of the rodent fascia dentata by brief spatial experience. Hippocampus 15:579–586.

Cho K-O, Lybrand ZR, Ito N, Brulet R, Tafacory F, Zhang L, Good L, Ure K, Kernie SG, Birnbaum SG, Scharfman HE, Eisch AJ, Hsieh J (2015) Aberrant hippocampal neurogenesis contributes to epilepsy and associated cognitive decline. Nat Commun 6:6606.

Claiborne BJ, Amaral DG, Cowan WM (1986) A light and electron microscopic analysis of the mossy fibers of the rat dentate gyrus. J Comp Neurol 246:435–458.

Cohen AS, Lin DD, Quirk GL, Coulter DA (2003) Dentate granule cell GABA(A) receptors in epileptic hippocampus: enhanced synaptic efficacy and altered pharmacology. Eur J Neurosci 17:1607–1616.

Collins RC, Tearse RG, Lothman EW (1983) Functional anatomy of limbic seizures: Focal discharges from medial entorhinal cortex in rat. Brain Res 280:25–40.

Coulter DA, Eid T (2012) Astrocytic regulation of glutamate homeostasis in epilepsy. Glia 60:1215–1226.

Cronin J, Obenaus A, Houser CR, Edward Dudek F (1992) Electrophysiology of dentate granule cells after kainate-induced synaptic reorganization of the mossy fibers. Brain Res 573:305–310.

de Almeida L, Idiart M, Lisman JE (2009a) A second function of gamma frequency oscillations: an E%-max winner-take-all mechanism selects which cells fire. J Neurosci 29:7497–7503.

de Almeida L, Idiart M, Lisman JE (2009b) The input-output transformation of the hippocampal granule cells: from grid cells to place fields. J Neurosci 29:7504–7512.

de Lanerolle NC, Kim JH, Robbins RJ, Spencer DD (1989) Hippocampal interneuron loss and plasticity in human temporal lobe epilepsy. Brain Res 495:387–395.

Dhaher R, Wang H, Gruenbaum SE, Tu N, Lee TSW, Zaveri HP, Eid T (2015) Effects of site-specific infusions of methionine sulfoximine on the temporal progression of seizures in a rat model of mesial temporal lobe epilepsy. Epilepsy Res 115:45–54.

do Nascimento AL, dos Santos NF, Campos Pelágio F, Aparecida Teixeira S, de Moraes Ferrari EA, Langone F (2012) Neuronal degeneration and gliosis time-course in the mouse hippocampal formation after pilocarpine-induced status epilepticus. Brain Res 1470:98–110.

Eid T, Thomas MJ, Spencer DD, Rundén-Pran E, Lai JCK, Malthankar G V., Kim JH, Danbolt NC, Ottersen OP, De Lanerolle NC (2004) Loss of glutamine synthetase in the human epileptogenic hippocampus: Possible mechanism for raised extracellular glutamate in mesial temporal lobe epilepsy. Lancet 363:28–37.

Estrada FS, Hernández VS, López-Hernández E, Corona-Morales AA, Solís H, Escobar A, Zhang L (2012) Glial activation in a pilocarpine rat model for epileptogenesis: a morphometric and quantitative analysis. Neurosci Lett 514:51–56.

Ewell LA, Jones M V (2010) Frequency-tuned distribution of inhibition in the dentate gyrus. J Neurosci 30:12597–12607.

Freund TF, Buzsáki G (1996) Interneurons of the hippocampus. Hippocampus 6:347–470.

Fricke R, Prince D (1984) Electrophysiology of dentate gyrus granule cells. J Neurophysiol 51.

Fyhn M, Hafting T, Treves A, Moser M-B, Moser EI (2007) Hippocampal remapping and grid realignment in entorhinal cortex. Nature 446:190–194.

Fyhn M, Molden S, Witter MP, Moser EI, Moser M-B (2004) Spatial representation in the entorhinal cortex. Science 305:1258–1264.

Guzowski JF, McNaughton BL, Barnes CA, Worley PF (1999) Environment-specific expression of the immediate-early gene Arc in hippocampal neuronal ensembles. Nat Neurosci 2:1120–1124.

Haas KF, Macdonald RL (1999) GABAA receptor subunit gamma2 and delta subtypes confer unique kinetic properties on recombinant GABAA receptor currents in mouse fibroblasts. J Physiol 514 (Pt 1:27–45.

Heinemann U, Beck H, Dreier JP, Ficker E, Stabel J, Zhang CL (1992) The dentate gyrus as a regulated gate for the propagation of epileptiform activity. Epilepsy Res Suppl 7:273–280.

Heng K, Haney MM, Buckmaster PS (2013) High-dose rapamycin blocks mossy fiber sprouting but not seizures in a mouse model of temporal lobe epilepsy. Epilepsia 54:1535–1541.

Henze DA, Wittner L, Buzsáki G (2002) Single granule cells reliably discharge targets in the hippocampal CA3 network in vivo. Nat Neurosci 5:790–795.

Hester MS, Danzer SC (2013) Accumulation of abnormal adult-generated hippocampal granule cells predicts seizure frequency and severity. J Neurosci 33:8926–8936.

Hollrigel GS, Ross ST, Soltesz I (1998) Temporal patterns and depolarizing actions of spontaneous GABAA receptor activation in granule cells of the early postnatal dentate gyrus. J Neurophysiol 80:2340–2351.

Houser CR (2007) Interneurons of the dentate gyrus: an overview of cell types, terminal fields and neurochemical identity. Prog Brain Res 163:217–232.

Houser CR, Esclapez M (1994) Localization of mRNAs encoding two forms of glutamic acid decarboxylase in the rat hippocampal formation. Hippocampus 4:530–545.

Houser CR, Miyashiro JE, Swartz BE, Walsh GO, Rich JR, Delgado-Escueta AV (1990) Altered patterns of dynorphin immunoreactivity suggest mossy fiber reorganization in human hippocampal epilepsy. J Neurosci 10:267–282.

Hu H, Gan J, Jonas P (2014) Fast-spiking, parvalbumin+ GABAergic interneurons: From cellular design to microcircuit function. Science (80-) 345:1255263–1255263.

Hu H, Martina M, Jonas P (2010) Dendritic mechanisms underlying rapid synaptic

activation of fast-spiking hippocampal interneurons. Science 327:52–58.

Iijima T, Witter MP, Ichikawa M, Tominaga T, Kajiwara R, Matsumoto G (1996) Entorhinal-Hippocampal Interactions Revealed by Real-Time Imaging. Science (80-) 272:1176–1179.

Isokawa M, Fried I (1996) Extracellular slow negative transient in the dentate gyrus of human epileptic hippocampus in vitro. Neuroscience 72:31–37.

Jung MW, McNaughton BL (1993a) Spatial selectivity of unit activity in the hippocampal granular layer. Hippocampus 3:165–182.

Jung MW, McNaughton BL (1993b) Spatial selectivity of unit activity in the hippocampal granular layer. Hippocampus 3:165–182.

Kobayashi M, Buckmaster PS (2003) Reduced inhibition of dentate granule cells in a model of temporal lobe epilepsy. J Neurosci 23:2440–2452.

Kron MM, Zhang H, Parent JM (2010) The developmental stage of dentate granule cells dictates their contribution to seizure-induced plasticity. J Neurosci 30:2051–2059.

Krook-Magnuson E, Armstrong C, Bui A, Lew S, Oijala M, Soltesz I (2015) In vivo evaluation of the dentate gate theory in epilepsy. J Physiol 593:2379–2388.

Krueppel R, Remy S, Beck H (2011) Dendritic integration in hippocampal dentate granule cells. Neuron 71:512–528.

Langston RF, Ainge JA, Couey JJ, Canto CB, Bjerknes TL, Witter MP, Moser EI, Moser M-B (2010) Development of the Spatial Representation System in the Rat. Science (80-) 328:1576–1580.

Leutgeb JK, Leutgeb S, Moser M-B, Moser EI (2007) Pattern separation in the dentate gyrus and CA3 of the hippocampus. Science 315:961–966.

Lisman J (2011) Formation of the non-functional and functional pools of granule cells in the dentate gyrus: role of neurogenesis, LTP and LTD. J Physiol 589:1905–1909.

Liu YB, Lio PA, Pasternak JF, Trommer BL (1996) Developmental changes in membrane properties and postsynaptic currents of granule cells in rat dentate gyrus. J Neurophysiol 76:1074–1088.

Lothman EW, Stringer JL, Bertram EH (1992) The dentate gyrus as a control point for seizures in the hippocampus and beyond. Epilepsy Res Suppl 7:301–313.

Lu Y, Zhong C, Wang L, Wei P, He W, Huang K, Zhang Y, Zhan Y, Feng G, Wang L (2016) Optogenetic dissection of ictal propagation in the hippocampal–entorhinal cortex structures. Nat Commun 7:10962.

Marín-Burgin A, Mongiat LA, Pardi MB, Schinder AF (2012) Unique processing during a period of high excitation/inhibition balance in adult-born neurons. Science 335:1238–1242.

Masukawa LM, Higashima M, Kim JH, Spencer DD (1989) Epileptiform discharges evoked in hippocampal brain slices from epileptic patients. Brain Res 493:168–174.

Masukawa LM, Wang H, O'Connor MJ, Uruno K (1996) Prolonged field potentials evoked by 1 Hz stimulation in the dentate gyrus of temporal lobe epileptic human brain slices. Brain Res 721:132–139.

McHugh TJ, Jones MW, Quinn JJ, Balthasar N, Coppari R, Elmquist JK, Lowell BB, Fanselow MS, Wilson MA, Tonegawa S (2007) Dentate gyrus NMDA receptors mediate rapid pattern separation in the hippocampal network. Science 317:94–99.

McNaughton BL, Morris RGM (1987) Hippocampal synaptic enhancement and information storage within a distributed memory system. Trends Neurosci 10:408–415.

Mori M, Abegg MH, Gähwiler BH, Gerber U (2004) A frequency-dependent switch from inhibition to excitation in a hippocampal unitary circuit. Nature 431:453–456.

Mtchedlishvili Z, Kapur J (2006) High-affinity , slowly desensitizing GABA A receptors mediate tonic inhibition in hippocampal dentate granule cells. Mol Pharmacol 69:564–575.

Nakashiba T, Cushman JD, Pelkey KA, Renaudineau S, Buhl DL, McHugh TJ, Barrera VR, Chittajallu R, Iwamoto KS, McBain CJ, Fanselow MS, Tonegawa S (2012) Young dentate granule cells mediate pattern separation, whereas old granule cells facilitate pattern completion. Cell 149:188–201.

Neunuebel JP, Knierim JJ (2012) Spatial firing correlates of physiologically distinct cell types of the rat dentate gyrus. J Neurosci 32:3848–3858.

Neunuebel JP, Knierim JJ (2014) CA3 retrieves coherent representations from degraded input: Direct evidence for CA3 pattern completion and dentate gyrus pattern separation. Neuron 81:416–427.

Nörenberg A, Hu H, Vida I, Bartos M, Jonas P (2010) Distinct nonuniform cable properties optimize rapid and efficient activation of fast-spiking GABAergic interneurons. Proc Natl Acad Sci U S A 107:894–899.

O'Reilly RC, McClelland JL (1994) Hippocampal conjunctive encoding, storage, and recall: avoiding a trade-off. Hippocampus 4:661–682.

Ortinski PI, Dong J, Mungenast A, Yue C, Takano H, Watson DJ, Haydon PG, Coulter DA (2010) Selective induction of astrocytic gliosis generates deficits in neuronal inhibition. Nat Neurosci 13:584–591.

Owens DF, Kriegstein AR (2002) Is there more to GABA than synaptic inhibition? Nat Rev Neurosci 3:715–727.

Parent JM (2007) Adult neurogenesis in the intact and epileptic dentate gyrus. Prog Brain Res 163:529–540.

Parent JM, Yu TW, Leibowitz RT, Geschwind DH, Sloviter RS, Lowenstein DH (1997)

Dentate granule cell neurogenesis is increased by seizures and contributes to aberrant network reorganization in the adult rat hippocampus. J Neurosci 17:3727–3738.

Pathak HR, Weissinger F, Terunuma M, Carlson GC, Hsu F-C, Moss SJ, Coulter DA (2007) Disrupted dentate granule cell chloride regulation enhances synaptic excitability during development of temporal lobe epilepsy. J Neurosci 27:14012–14022.

Patrylo PR, Schweitzer JS, Dudek FE (1999) Abnormal responses to perforant path stimulation in the dentate gyrus of slices from rats with kainate-induced epilepsy and mossy fiber reorganization. Epilepsy Res 36:31–42.

Patton PE, McNaughton B (1995) Connection matrix of the hippocampal formation .1. The dentate gyrus. Hippocampus 5:245–286.

Peng Z, Huang CS, Stell BM, Mody I, Houser CR (2004) Altered expression of the delta subunit of the GABAA receptor in a mouse model of temporal lobe epilepsy. J Neurosci 24:8629–8639.

Piatti VC, Ewell LA, Leutgeb JK (2013) Neurogenesis in the dentate gyrus: carrying the message or dictating the tone. Front Neurosci 7:50.

Pinheiro PS, Lanore F, Veran J, Artinian J, Blanchet C, Crépel V, Perrais D, Mulle C (2013) Selective block of postsynaptic kainate receptors reveals their function at hippocampal mossy fiber synapses. Cereb Cortex 23:323–331.

Rolls ET (2010) A computational theory of episodic memory formation in the hippocampus. Behav Brain Res 215:180–196.

Rudy JW, Stadler-Morris S, Albert P (1987) Ontogeny of spatial navigation behaviors in the rat: dissociation of “proximal”- and “distal”-cue-based behaviors. Behav Neurosci 101:62–73.

Salin PA, Scanziani M, Malenka RC, Nicoll RA (1996) Distinct short-term plasticity at two excitatory synapses in the hippocampus. Proc Natl Acad Sci U S A 93:13304–13309.

Saxena NC, Macdonald RL (1994) Assembly of GABAA receptor subunits: role of the delta subunit. J Neurosci 14:7077–7086.

Scharfman HE (1991) Dentate hilar cells with dendrites in the molecular layer have lower thresholds for synaptic activation by perforant path than granule cells. J Neurosci 11:1660–1673.

Scharfman HE, Sollas AE, Berger RE, Goodman JH, Pierce JP (2003a) Perforant path activation of ectopic granule cells that are born after pilocarpine-induced seizures. Neuroscience 121:1017–1029.

Scharfman HE, Sollas AL, Berger RE, Goodman JH (2003b) Electrophysiological evidence of monosynaptic excitatory transmission between granule cells after seizure-induced mossy fiber sprouting. J Neurophysiol 90:2536–2547.

Schenk F (1985) Development of place navigation in rats from weaning to puberty. Behav Neural Biol 43:69–85.

Shao L-R, Dudek FE (2005) Changes in mIPSCs and sIPSCs after kainate treatment: evidence for loss of inhibitory input to dentate granule cells and possible compensatory responses. J Neurophysiol 94:952–960.

Shao L-R, Dudek FE (2011) Repetitive perforant-path stimulation induces epileptiform bursts in minislices of dentate gyrus from rats with kainate-induced epilepsy. J Neurophysiol 105:522–527.

Sloviter RS (1987) Decreased hippocampal inhibition and a selective loss of interneurons in experimental epilepsy. Science 235:73–76.

Spruston N, Johnston D (1992) Perforated patch-clamp analysis of the passive membrane properties of three classes of hippocampal neurons. J Neurophysiol 67:508–529.

Staley KJ, Otis TS, Mody I (1992) Membrane properties of dentate gyrus granule cells: comparison of sharp microelectrode and whole-cell recordings. J Neurophysiol 67:1346–1358.

Stringer JL, Lothman EW (1992) Reverberatory seizure discharges in hippocampal-parahippocampal circuits. Exp Neurol 116:198–203.

Stringer JL, Williamson JM, Lothman EW (1989) Induction of paroxysmal discharges in the dentate gyrus: frequency dependence and relationship to afterdischarge production. J Neurophysiol 62:126–135.

Sun C, Mtchedlishvili Z, Bertram EH, Erisir A, Kapur J (2007) Selective loss of dentate hilar interneurons contributes to reduced synaptic inhibition of granule cells in an electrical stimulation-based animal model of temporal lobe epilepsy. J Comp Neurol 500:876–893.

Sutula T, Cascino G, Cavazos J, Parada I, Ramirez L (1989) Mossy fiber synaptic reorganization in the epileptic human temporal lobe. Ann Neurol 26:321–330.

Tamamaki N, Nojyo Y (1993) Projection of the entorhinal layer II neurons in the rat as revealed by intracellular pressure-injection of neurobiotin. Hippocampus 3:471–480.

Tashiro A, Makino H, Gage FH (2007) Experience-specific functional modification of the dentate gyrus through adult neurogenesis: a critical period during an immature stage. J Neurosci 27:3252–3259.

Tauck DL, Nadler J V (1985) Evidence of functional mossy fiber sprouting in hippocampal formation of kainic acid-treated rats. J Neurosci 5:1016–1022.

Thind KK, Yamawaki R, Phanwar I, Zhang G, Wen X, Buckmaster PS (2010) Initial loss but later excess of GABAergic synapses with dentate granule cells in a rat model of temporal lobe epilepsy. J Comp Neurol 518:647–667.

Treves A, Rolls ET (1994) Computational analysis of the role of the hippocampus in memory. Hippocampus 4:374–391.

Treves A, Tashiro A, Witter MP, Moser EI (2008) What is the mammalian dentate gyrus good for? Neuroscience 154:1155–1172.

van Groen T, Miettinen P, Kadish I (2003) The entorhinal cortex of the mouse: Organization of the projection to the hippocampal formation. Hippocampus 13:133–149.

van Praag H, Schinder AF, Christie BR, Toni N, Palmer TD, Gage FH (2002) Functional neurogenesis in the adult hippocampus. Nature 415:1030–1034.

Wei W, Zhang N, Peng Z, Houser CR, Mody I (2003) Perisynaptic localization of delta subunit-containing GABA(A) receptors and their activation by GABA spillover in the mouse dentate gyrus. J Neurosci 23:10650–10661.

Williamson A (1994) Electrophysiology of epileptic human neocortical and hippocampal neurons maintained in vitro. Clin Neurosci 2:47–52.

Xu Z, Xue T, Zhang Z, Wang X, Xu P, Zhang J, Lei X, Li Y, Xie Y, Wang L, Fang M, Chen Y (2011) Role of signal transducer and activator of transcription-3 in up-regulation of GFAP after epilepsy. Neurochem Res 36:2208–2215.

Yu EP, Dengler CG, Frausto SF, Putt ME, Yue C, Takano H, Coulter DA (2013) Protracted postnatal development of sparse, specific dentate granule cell activation in the mouse hippocampus. J Neurosci 33:2947–2960.

Zhang N, Wei W, Mody I, Houser CR (2007) Altered localization of GABA(A) receptor subunits on dentate granule cell dendrites influences tonic and phasic inhibition in a mouse model of epilepsy. J Neurosci 27:7520–7531.

Zhang W, Buckmaster PS (2009) Dysfunction of the dentate basket cell circuit in a rat model of temporal lobe epilepsy. J Neurosci 29:7846–7856.

CHAPTER 3: Protracted postnatal development of sparse, specific dentate granule cell activation in the mouse hippocampus

Abstract

The dentate gyrus (DG) is a critical entry point regulating function of the hippocampus. Integral to this role are the sparse, selective activation characteristics of the principal cells of the DG, dentate granule cells (DGCs). This sparse activation is important both in cognitive processing and in regulation of pathological activity in disease states. Using a novel, combined dynamic imaging approach capable of resolving sequentially both synaptic potentials and action potential firing in large populations of DGCs, we characterized the postnatal development of firing properties of DG neurons in response to afferent activation in mouse hippocampal-entorhinal cortical slices. During postnatal development, there was a protracted, progressive sparsification of responses, accompanied by increased temporal precision of activation. Both of these phenomena were primarily mediated by changes in local circuit inhibition, and not by alterations in afferent innervation of DGCs because $GABA_A$ antagonists normalized developmental differences. There was significant Θ and γ frequency-dependent synaptic recruitment of DGC activation in adult, but not developing, animals. Finally, we found that the decision to fire or not fire by individual DGCs was robust and repeatable at all stages of development. The protracted postnatal development of sparse, selective firing properties, increased temporal precision and frequency dependence of activation, and the fidelity with which the decision to fire is made are all fundamental circuit

determinants of DGC excitation, critical in both normal and pathological function of the DG.

Introduction

The dentate gyrus (DG) constitutes the first component of the canonical trisynaptic circuit in the hippocampus and functions as a key regulator of cortical input to the hippocampus. Its primary input, the perforant pathway (PP), arises from neurons in layer II of the entorhinal cortex (EC; Steward and Scoville, 1976; Amaral and Cowan, 1980). EC innervation of the principal cells of the DG (DGCs) is promiscuous, exhibiting massive convergence and divergence. Individual EC neurons innervate large areas of the DG (Tamamaki and Nojyo, 1993), and small regions of the DG receive input from widespread regions of the EC (van Groen et al., 2003). In recording studies *in vivo*, DGCs exhibit spatially selective firing in extremely small subpopulations of neurons (Jung and McNaughton, 1993a; Leutgeb and Moser, 2007; Neunuebel and Knierim, 2012). Therefore, based on the contrast with their broad afferent innervation pattern, it is likely that the sparse, specific firing characteristics of DGCs emerge from local factors within the DG.

These include intrinsic biophysical properties making these neurons extremely reluctant to fire, particularly in bursts, and the powerful feedforward, feedback, and tonic inhibition evident within the DG circuit originating from multiple interneuron populations (Coulter & Carlson, 2007; for review, see Acsády & Káli, 2007). This circuitry confers sparse firing characteristics onto DGCs and also endows the DG with the capability of preventing relay of pathological, synchronous cortical activity into the hippocampus, regulating seizure activity in states such as epilepsy. This latter

phenomenon has been termed dentate gating (Heinemann et al., 1992; Lothman et al., 1992). The majority of studies examining DG activation patterns have been conducted using unit recordings *in vivo*, which cannot resolve circuit determinants of firing behavior. Little attention has been focused on either the development of the ensemble neuronal firing characteristics or circuit gating behavior within the DG during early postnatal maturation.

In the present study, we investigated how properties of DG circuit gating function and DGC activation behavior varied during postnatal development by using a novel strategy involving combined sequential functional imaging of synaptic potentials and cellular activation patterns using voltage-sensitive dye (VSDI) and multicellular calcium imaging (MCI), respectively. We found that DGC action potential (AP) firing selectivity increased as postnatal development progressed, achieving adult levels of sparse activation by 30 d postnatal (P30). This was accompanied by both an increase in the temporal precision of activation and emergence of DG gating behavior. The developmental delays in achieving adult levels of sparse AP firing and temporal precision of responses were normalized between various age groups by perfusion with the $GABA_A$ antagonist picrotoxin, suggesting that emergence of these developmentally dependent phenomena were primarily the result of changes in local circuit inhibition. We also found that sparse activation of DGC firing was precise, with the same small set of cells responding similarly to multiple stimuli. The delayed postnatal development of DG gating, sparse activation behavior of DGCs, and temporal precision of activation have significant implications for both normal and pathological function of the hippocampus.

Materials and Methods

Animals and tissue preparation. Brains of male C57BL/6 mice (P12-P60) were removed and blocked in ice cold artificial cerebrospinal fluid (ACSF) with NaCl replaced with an equal osmolarity concentration of sucrose ACSF composed of the following (inmM): 87 NaCl, 2.5 KCl, 1.25 NaH_2PO_4, 75 sucrose, 10 glucose, 26 $NaHCO_3$, 1 $CaCl_2$-$2H_2O$, and 2 $MgSO_4$. Horizontal hippocampal entorhinal cortical slices (350 μm) were cut with a vibrating tissue slicer (zero *z* Vibratome 3000) and submerged in ice-cold sucrose ACSF. Slices were then incubated in a calcium indicator loading chamber and bubbled with 95% O_2/5% CO_2 at 37°C. The calcium indicator loading solution was composed of either 4 μl of 0.5% Fura-2-AM (for multiphoton imaging, Invitrogen) or 4 μl of 0.5% Oregon Green BAPTA-1 AM (for confocal imaging, Invitrogen), 4 μl of 20% pluronic acid (Invitrogen) in DMSO and 4 μl of 15% Cremophor (EL) (Invitrogen) in DMSO and 4ml of oxygenated ACSF (composition in mM: 125 NaCl, 2.5 KCl, 1.25 NaH_2PO_4, 10 glucose, 26 $NaHCO_3$, 2 $CaCl_2$-$2H_2O$, 1 $MgSO_4$). During loading, slices were maintained at 37°C and continuously exposed to humidified 95% O_2/5% CO_2 to maintain osmolarity, oxygen, and pH levels. Slices were loaded for 35 min and then washed and incubated in fresh oxygenated ACSF at room temperature for at least 45 min to allow AM-ester dyes to cleave. (Takano et al., 2012). Slices were then stored in oxygenated ACSF for up to 6 h without deterioration of response. Immediately before transferring slices to the microscope stage for imaging, Fura-2-AM-loaded slices were further stained in an oxygenated submersion chamber containing 0.0125 mg/ml of the VSD di-3-ANEPPDHQ (Invitrogen) in ACSF for 20 min (Carlson and Coulter, 2008). After staining, slices were placed in a 36°C heated submersion recording chamber.

Microelectrode stimulation and recording. For stimulation of the granule cell layer, a bipolar tungsten-stimulating electrode was placed adjacent to the hippocampal fissure between the suprapyramidal blade and apex of the granule cell layer (defined as the midpoint between the suprapyramidal and infrapyramidal blades; see **Fig. 3.2*A***). For extracellular recording, a tungsten recording electrode was positioned in the dentate molecular layer of the suprapyramidal or infrapyramidal blades. Recording electrodes were always > 500 μm away from the stimulating electrode and outside the imaging field to avoid electrical artifacts and electromagnetic noise from the excitation laser.
Stimulus intensity standardization. Stimulus intensity was standardized across developmental stages using field EPSP slope measurements. This was done because fEPSP and VSDI EPSP experiments record different information. fEPSP recordings sample current flux through the extracellular space and, in addition to changing amplitude with increasing stimulation intensity, will vary in slope, amplitude, and sign depending on the location of the recording site relative to the current sinks and sources created by the synaptic response. VSDI EPSP experiments record transmembrane voltage, which may vary slightly depending on the ROI sampled relative to the synaptic input site resulting from intrinsic cell properties, but otherwise are insensitive to sources and sinks generating current flux in the extracellular space. However, peak voltage measures of EPSPs will begin to flatten at higher stimulus intensities because of driving force changes during larger responses. This will not occur in fEPSP measurements. In addition, evoked synaptic responses are compound events, composed of both EPSPs and IPSPs. IPSPs tend to activate at longer latencies and to be recruited more at higher stimulus amplitudes because (1) they are polysynaptic and (2) they are mediated by channels with slower kinetics compared with EPSPs. Measuring fEPSP slope is likely to enhance contributions of EPSPs by sampling earlier during the synaptic event compared

with recording peak depolarizing PSP responses in VSDI recordings. This facilitates stimulus standardization. Slice viability was verified using local field potential recordings. Stimulating electrode placement was determined by ensuring that the stimulation site elicited similar responses in both suprapyramidal and infrapyramidal blades. Local field potential recordings were monitored online during the optical recordings to verify the ongoing viability of slices. Local field potentials were recorded using a Microelectrode AC Amplifier (Model 1800, AM Systems). Electrical data were collected using Clampex 9.0 (Molecular Devices) software.

Juxtacellular loose-patch recordings. Juxtacellular loose-patch current clamp recordings were conducted in Fura-loaded slices to explore the relationship between AP firing and calcium transients in DGCs. Patch electrodes (5–7 MΩ resistance, filled with ACSF) were positioned juxtacellularly to DGCs of interest, and negative pressure was applied to acquire low resistance seals of >50MΩ. Seal quality was monitored during recordings. Current-clamp recordings were made using a Multiclamp 700B amplifier (Molecular Devices) and sampled at 10 kHz with a Digidata 1332A analog-digital converter (Molecular Devices). Electrical data were collected using Clampex 9.0 (Molecular Devices). Data were analyzed and stimulation artifacts were removed in Clampfit 10 (Molecular Devices).

VSDI and MCI. An integrated multiphoton/epifluorescence microscopy system enabled the use of two sequential, distinct imaging techniques combined with simultaneous electrical recording in the same slice. An Olympus BX-61 fixed stage microscope with a 20x (XLUMPlanFl, NA=0.95) water immersion objective (Olympus) was used in this study. This magnification allowed individual cells to be readily resolved during MCI while still preserving the ability to visualize network activation and signal propagation with VSDI techniques. VSD fluorescence signals were captured with a high-speed 80 x

80 pixel CCD camera (NeuroCCD-SM, Redshirt Imaging) at a 1000 Hz frame rate. We used a collimated light-emitting-diode emitting with a peak intensity at 505 nm (LEDC9, ThorLabs) to excite the VSD (di-3-ANEPPDHQ). VSDI was achieved by using a Chroma U-N41002 (Chroma Technology) filter cube, comprised of an excitation filter (535 nm/50 nm), an emission filter (610 nm/70 nm), and a dichroic mirror (565 nm-LP). All filter widths are given as the full width at half maximum (**Fig. 3.1**). Electrical stimulation and onset of imaging trials were controlled by an electrical trigger with a delay of 1 s before stimuli to obtain a baseline for imaging analysis. Repeated measurements of 4 trials were taken, and trials were averaged to increase the signal-to-noise ratio. For MCI, Fura-2-AM was excited using a Prairie Technology Ultima Multiphoton Imaging System attached to the Olympus BX-61 fixed-stage microscope. The setup included external nondescanned dual-channel reflection/fluorescence detectors and a diode-pumped, wideband mode locked Ti:Sapphire femtosecond laser (720–950 nm, 140 fs; 90 MHz, Chameleon, Coherent; **Fig. 3.1**). Fura-2 (MCI) and di-3-ANEPPDHQ (VSDI) were selected based on the minimal overlap of emission and excitation spectra to allow adequate separation of signals in each imaging modality (**Table 3.1**). For the excitation/emission for the calcium imaging light path, emitted fluorescence was collected with the same objective lens, reflected by a dichroic mirror (660nmLP) and passed through an IR cutoff filter (650 nm SP) (Chroma Technology). An additional dichroic filter (495 nm LP) and bandpass filter (460 nm/50 nm) were used to further separate VSD and calcium indicator fluorescence (**Fig. 3.1**). The optical data were then passed through a preamplifier and a 12-bit analog to digital converter. Images were acquired at a frame rate of ~10 Hz. Stimuli were repeated four times.

In VSD imaging, 535 nm light, the center wavelength of the excitation band-pass (BP) filter (F in **Fig. 3.1**), effectively excites di-3-ANEPPDHQ in the single photon (1P)

excitation process, but not Fura-2. In calcium imaging, two-photon (2P) absorption cross-section at 780 nm for Fura-2 Ca^{2}-free form (8.1 GM) is much larger than the Ca^{2}-bound form (0.3 GM) (Wokosin et al., 2004), causing fluorescence signal to extinguish during neuronal activity (e.g., calcium influx through voltage-gated calcium ion channels). The fluorescence traces for calcium imaging in the subsequent figures were all inverted for visual intuition. For detecting Fura-2 signal, a 460 nm band-pass filter (G in **Fig. 3.1**) was chosen based on the peak Fura-2 emission spectra. The 2-photon absorption cross-section for di-3-ANEPPDHQ could not be found, but it was reported to be 4 GM for a similar molecule, di-8-ANESPPDHQ (Fisher et al., 2008). This indicates that the 780 nm light could excite di-3-ANEPPDHQ by the 2-photon excitation process, but emission 460 nm is very weak, and the majority of emission from VSD dye channel can be blocked by the filters (D and G in **Fig. 3.1**).

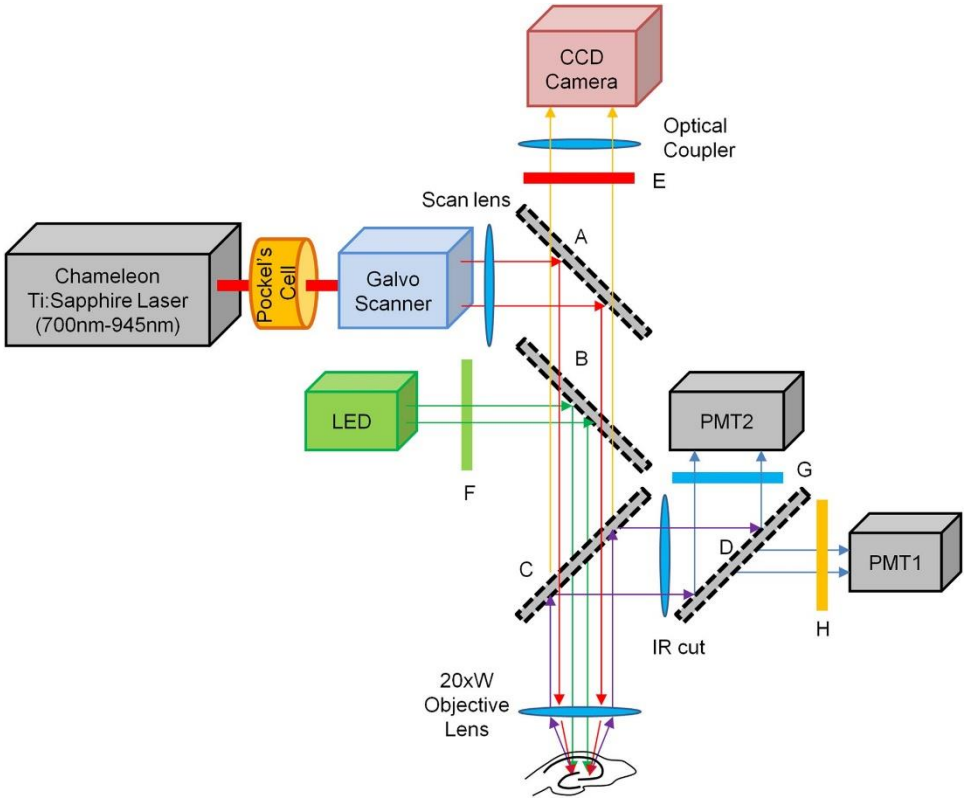

Table 3.1. Specifications for VSD and calcium imaging probes

Modality	Dye	Ex_{535} 1P	Ex_{780} 2P	Em_{460} (% max)	Em_{610} (% max)
Ca^2 imaging	Fura-2	0% max at 340 nm	Ca^2-free 8.1 GM Ca^2-bound 0.3 GM	98	0
VSD imaging	di-3-ANEPPDHQ	50% max at 510 nm	NA/4 GM	2	95

Figure 3.1. System diagram for the sequential VSD and calcium imaging microscope. A Prairie Technologies Ultima Multi-Photon Microscopy system mounted on an Olympus BX-61 microscope equipped with a sliding mirror (A) and a filter wheel, by which either a 565 nm LP (long-pass) filter (B) or a 660 nm LP filter (C) can be selected. For VSD imaging, the mirror (A) is removed and the LP filter (B) was inserted. Excitation light (505 nm center wavelength with 30 nm full width at half-maximum) from a collimated LED (LEDC9, Thorlabs) was guided through a 535 nm/50 nm (center wavelength/width) BP (band-pass) filter (F), reflected by a LP filter (B) and focused on the specimen by an objective lens (Olympus XLUMPlanFl, 20, NA = 0.95). Fluorescence emission was collected by the same objective lens and guided to the CCD camera (NeuroCCD-SM, Redshirt Imaging) through the LP filter (B), a 610 nm/70 nm BP filter (E), and an optical coupler. For calcium imaging, the mirror (A) and the LP filter (C) were selected and 780 nm excitation light from the Ti:Sapphire laser (Chameleon, Coherent) was guided by the mirror (A), through the LP filter (C) and focused on the specimen. Fluorescence emission was reflected by the LP filter (C) and separated into two channels by a 495 nm LP filter (D). A 460 nm/50 nm BP filter (G) and 607/45 nm BP filter (H) were placed in front of each PMT detector. PMT 2 detected the emission signals from the calcium indicator.

Confocal MCI. For confocal MCI, Oregon Green BAPTA-AM-loaded slices were imaged using a Live Scan Swept Field Confocal Microscope (Nikon Instruments) equipped with an Ar/Kr ion laser (Inova 70C, Coherent, excitation 488 nm) operated with NIS-elements software (Nikon). Images were acquired with a water immersion 40x lens (NA = 0.8) and a Cascade 128+ CCD camera (Photometrics). This system allowed capture of images at 320 Hz with full frame resolution (128x128 pixels).

Data analysis. VSDI data were analyzed using custom written algorithms in IGOR 6.0 (Wavemetrics). Reference frames were calculated as the average of 60 ms before stimulation. All data points were normalized using in-house algorithms to reflect the change in fluorescence compared with baseline (ΔF/F0) (Ang et al., 2006). Local VSD signals were calculated by integrating ROI encompassing the granule cell layer (GC), the hilus, and the molecular layer (**Fig. 3.2*A***). For MCI, the field of view at 20x magnification allowed us to capture 60–100 Fura-loaded cells per image, with multiple regions studied per slice (see **Fig. 3.4*A***). Manual construction of small oval or round ROI encompassing the soma was used to analyze activity of these cells. The average intensities of ROI were calculated as a function of time and exported as a text file (Takano et al., 2012). Stimulus-locked peaks were extracted in ROI response traces using a ΔF/F0 area as threshold to detect events in a given cell ROI, and responses were verified visually. This supervised detection algorithm was used to determine activation of each cell in response to the stimulus. Each cell's activity was observed over time and across conditions using an ID number attached to the ROI delineating each cell. Picrotoxin (PTX), a GABA receptor antagonist, was applied (50 μM) at the end of all experiments to confirm that individual neurons were able to be activated by the afferent stimulus. Cells that were inactive in both control and PTX conditions were excluded from further analysis. The proportion of these inactive cells did not differ between

developmental stages (36.7 ± 9.6% and 28.2 ± 5.8% for P12 and P60, respectively, not significantly different, *t* test). These inactive cells are likely to be a combination of glial cells, and damaged and/or deafferented neurons.

Calcium transient onset time estimation. For confocal recordings of calcium transient onset latencies at higher temporal resolution, we determined that the rising phase of ΔF/F0 responses was exponential in shape. To estimate onset time, windowed traces were fitted to a 4 parameter exponential equation, where *A* is amplitude, *B* is the time constant, *C* is the onset time, and *D* is an offset:

$$f(t) = D, \text{ where } t > C \text{ and}$$

$$f(t) = A\{1 - \exp[-B(t - C)]\} + D, \text{ where } t \pm C.$$

We estimated "onset time" from parameter C in the above equation. Transients in which the coefficient of determination, *R*2, was > 0.5 were omitted from further analysis.

Statistical analysis. All values are expressed as mean ± SEM. For comparisons between groups, statistical significance was tested using either a one- or two-way ANOVA, a *t* test, or for non-normally distributed data, a Mann–Whitney *U* test. Differences in population distributions were assessed using a Kolmorgorov–Smirnov test. *p* values < 0.05 were considered evidence of statistical significance.

Statistical assessment of DGC activation behavior using a logistic regression model. We fit two logistic regression models to test the null hypothesis that individual cells within a particular slice respond in a stochastic fashion to repeated stimuli, against the alternative that the probability of response in later stimuli is a function of the cell's earlier propensity to respond to stimulation. A response for each cell was collected for each of four sequential stimuli. We used the data from the final stimulus as the outcome in the model. Under the null hypothesis, the data can be adequately fit using a model that includes terms for each of the slices to adjust for differences in the overall rate of

response to stimuli. Under the alternative, the response patterns from the earlier stimuli predict response to the subsequent stimuli. We considered two alternative models, the first where we included a predictor (respond yes or no) for each of Stimuli 1, 2, and 3 and the second where we included only the response to Stimuli 2 and 3. The null and alternative models were identical except for the inclusion of the predictors using the earlier stimuli. We chose the model based on response to Stimuli 2 and 3 using the Akaike Information criteria. The significance of the pattern of response to each of the earlier two stimuli was assessed using a likelihood ratio test and the significance of individual terms in the model assessed using Wald tests. Estimates and SEs of the estimates of the probability of response conditional on the previous response pattern were computed from the model. The logistic regression models were implemented in R2.13

Results

Development of DG gating function–VSDI recordings

Anatomical studies have demonstrated that the rodent DG and its principal neurons, DGCs, exhibit a protracted, predominantly postnatal development. Within the DG, inhibitory interneurons are already present at birth and, although not mature, possess extensive dendritic and axonal arborizations (Schlessinger et al., 1978; Amaral and Kurz, 1985; Lubbers et al., 1985; Seay-Lowe and Claiborne, 1992). The principal cells of the DG, DGCs, however, are mostly generated in 2–3 weeks after birth and migrate to their appropriate locations (Schlessinger et al., 1978; Rickmann et al., 1987). In a relatively unique phenomenon, DGCs continue to be generated throughout life (Altman

and Das, 1965; Eriksson et al., 1998; van Praag et al., 2002). During the perinatal period, afferent innervation by the EC arrives early, before the birth of most DGCs, and, as DGCs are born and mature, EC synapses in the molecular layer of the DG increase up to eightfold by P21 (Fricke and Cowan, 1977; Amaral and Cowan, 1980). During this period of explosive synaptogenesis in the DG, rodent pups are navigating their environment, weaning, and accomplishing rudimentary, hippocampal-dependent cognitive tasks (Schenk, 1985; Ainge and Langston, 2012a). Clearly, a critical question is as follows: how does this protracted postnatal development of the anatomic circuit impact the function of the DG, and by extension, the cognitive capabilities of the animal?

To begin investigating postnatal development of function of the DG, VSDI was used to assess one major role of this circuit: regulating propagation of EC inputs to downstream structures in the hippocampus, in slices prepared from animals of varying ages. Network activation was measured separately in the granule cell layer (GC), hilus, and area CA3 in each slice using measurement of EC stimulation-evoked synaptic voltage signals in distinct ROI, as shown in **Figure 3.2*A***. To standardize stimulus intensities, we first measured input/output curves using field EPSP slope measurement in slices prepared from each age group (P12, P22-P30, and P60-P61). Input/output plots overlapped extensively and did not differ statistically, and there was no substantive difference in maximal fEPSP slope for all postnatal ages (two-way ANOVA and one-way ANOVA, respectively, not significant), justifying the use of identical stimulus intensities in all groups in subsequent imaging studies. We next used VSDI to examine how afferent input to the DG (PP stimulation) activated downstream structures in hilus and area CA3 (**Fig. 3.2*B–E***). In agreement with our field potential recordings, there was no difference in the amplitude of depolarization evident in the GC region between developmental stages, with similar response levels evident at all stimulus intensities in slices prepared

from P12, P22-P30, and P60 animals (**Fig. 3.2*B*,*C***). However, there were differences in the kinetics of the VSDI responses evident in GC ROI between P12 and P60 stages. Specifically, P12 responses had a pronounced slowing on the falling phase of the PP-evoked postsynaptic potential relative to P60 responses (**Fig. 3.2*B*, top**). We attribute this extended synaptic response to a combination of the longer membrane time constants in immature granule cells and the depolarizing effects of GABAergic inhibition evident in DGCs at these early developmental stages (Liu et al., 1996; Hollrigel et al., 1998). In support of this hypothesis, application of bumetanide (20 μM), a blocker of the chloride accumulator NKCC1, significantly accelerated the decay kinetics of the VSD-recorded postsynaptic potential in slices prepared from P12 animals (PSP decay = 229 ± 56 and 106 ± 20 ms for control and bumetanide exposed conditions, $p = .015$, paired t test). We have also seen a similar slowing in the decay phase of EC stimulus-induced synaptic depolarizations recorded using VSDI in adult animals during the development of epilepsy, when DGC transmembrane chloride gradients are disrupted (Pathak et al., 2007).

Despite the similarity in GC responses, the magnitude of postsynaptic potentials elicited in both the hilus and area CA3 varied significantly during postnatal development (**Fig. 3.2*B*,*D*,*E***). At the earliest stage of development examined (P12), there were large postsynaptic potentials elicited in both the hilus and area CA3 after PP stimulation, which gradually decreased as development progressed, with smaller postsynaptic potentials elicited in P22-P30 animals and very low levels of responses in these downstream structures in slices prepared from adult animals (**P60, Fig. 3.2*B*,*D***). We quantified this network propagation by calculating a ratio of responses in the GC area relative to area CA3 (GC/CA3). For this measure, ratios close to 1 signify little filtering of input, and ratios <1 indicate restriction in propagation of postsynaptic potentials to

downstream structures. When this ratio was plotted against developmental stage, a clear trend was evident ($p < 0.001$), with decreasing responses in downstream structures by PP stimulation as development progressed (**Fig. 3.2*E***).

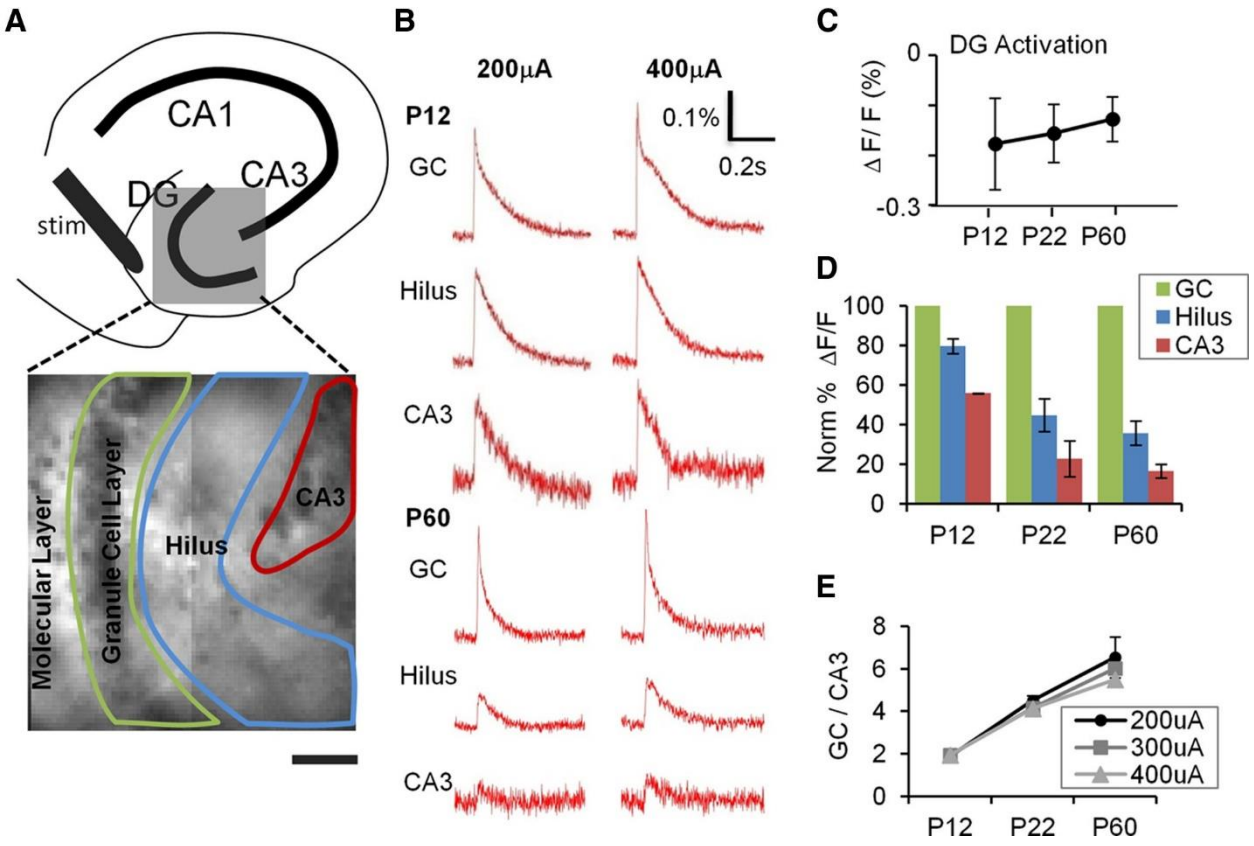

Figure 3.2. Postnatal development of DG gating behavior. ***A***, Top, A schematic illustration depicting subregions of the hippocampus. Bottom, The DG (gray box) is expanded in a VSD image with an overlay of the ROI delineating subregions used to measure DG responses elicited by PP stimulation. ***B***, VSDI time-resolved fluorescence plots for the subregions depicted in ***A*** for P12 (top) and P60 (bottom) animals. PP stimulation elicits comparable depolarizations in the GC, hilus, and CA3 at P12, but little depolarization of hilus and CA3 at P60, despite robust responses in GC. ***C***, DG response amplitude (F/F_0) is comparable at all developmental ages (elicited by a 400 A PP stimulus). ***D***, P12, P22, and P60 mice (*n*=8 slices in 3 animals, *n*=7 of 2 animals, and *n*=6 of 2 animals, respectively), show progressively less propagation of synaptic responses through GC (green) to hilus (blue) and CA3 (red). All data points are normalized to GC layer response at 400 A, which is equivalent across groups (see ***C***). ***E***, Plots of DG gating function, the ratio of GC to CA3 activation intensity, depict the significant increase in the DG gating property as postnatal development progresses, at several stimulus intensities (200 μA (circle), 300 μA (square), and 400 μA (triangle). $p < 0.001$ for the animal age factor affecting gating (two-way ANOVA). $p = 0.16$ for stimulus intensity affecting gating (two-way ANOVA).

MCI of DGC activation to afferent stimulation

The developmental reduction in downstream responses of hippocampal structures after PP stimulation could result from decreased DGC excitability and/or an alteration in properties of mossy fiber-induced synaptic responses or targets. VSDI is a useful tool to study the spatiotemporal properties of synaptic potentials in circuits but, because of requirements for signal averaging necessary to increase signal to noise, it has little utility in resolving cellular action potential activation (for review, see Carlson and Coulter, 2008). To compensate for this limitation in VSDI and allow examination of stimulus-induced AP activation in large numbers of individual DGCs simultaneously, each slice was loaded with both VSD and calcium indicator. This allowed us to combine imaging strategies sequentially in the same slice. Each slice was first imaged using VSDI and epifluorescence microscopy, followed by MCI using 2-photon microscopy. Because of activation of high threshold calcium channels, there is a selective influx of calcium ions in the neuronal soma linked to AP activation. Accompanying this influx is an alteration in fluorescence signal in calcium indicator-loaded neuronal cell bodies, which can be resolved in MCI studies (**Fig. 3.3**). This allows dynamic imaging-based assessment of AP responses in large populations of individual neurons with cellular resolution (Stosiek et al., 2003; Ikegaya et al., 2004; Cossart et al., 2005; Sasaki et al., 2008; Vogelstein et al., 2009; Ishikawa et al., 2010; Takano et al., 2012). Juxtacellular loosepatch current-clamp recordings were conducted in Fura-loaded slices to explore the relationship between AP firing and calcium transients in DGCs in response to PP activation. **Figure 3.3*A*** illustrates the juxtacellular placement of a patch electrode next to a Fura 2-AM-labeled DGC for loose-patch recording (specimen records for imaging and patch recording from this cell are illustrated in **Fig. 3.3*A*,*B***). Fura fluorescence

changes measured from this DGC in response to PP stimulation eliciting 1–4 APS are depicted in **Figure 3.3*B***. **Figure 3.3*C*** illustrates the simultaneously recorded APs measured from the same cell using loose-patch recording. The relationship between calcium transient amplitude and AP number is analyzed in the graph in **Figure 3.3*D***, where peak fluorescence response is plotted against the AP number observed in loose-patch recording. These two measures were linearly correlated (Pearson r = 0.9835), supporting the significant link between AP number and calcium transient amplitude. **Figure 3.3*E*** shows the peak calcium fluorescence ($\Delta F/F0$) responses recorded from 4 different DGCs, in response to activation of 1 and 4 APs, normalized to the SD of baseline signal noise (3 or 4 trials per cell). For single APs, each DGC had a calcium transient peak 4-fold higher than the SD of baseline noise (7.9 ± 1.48 SD). This demonstrates that calcium transients elicited by single APs can readily be resolved from baseline noise in all cells. Calcium transients for responses elicited by 4 APs were larger, averaging 13.64 ± 2.35 times noise. For all cells recorded, calcium transient peaks for 4 action potentials were significantly larger than for 1 action potential (Cell 1, p=0.016; Cell 2, p=0.0003; Cell 3, p=0.021; Cell 4, p=0.010, paired t test). On average, 1 AP generated a calcium transient that was 53% the magnitude of a 4 AP transient. We have previously reported a similar relationship between calcium transient peaks and action potential firing for Oregon Green BAPTA-AM-loaded hippocampal neurons in MCI studies using our fast confocal microscopy system (Takano et al., 2012, their Fig. 1).

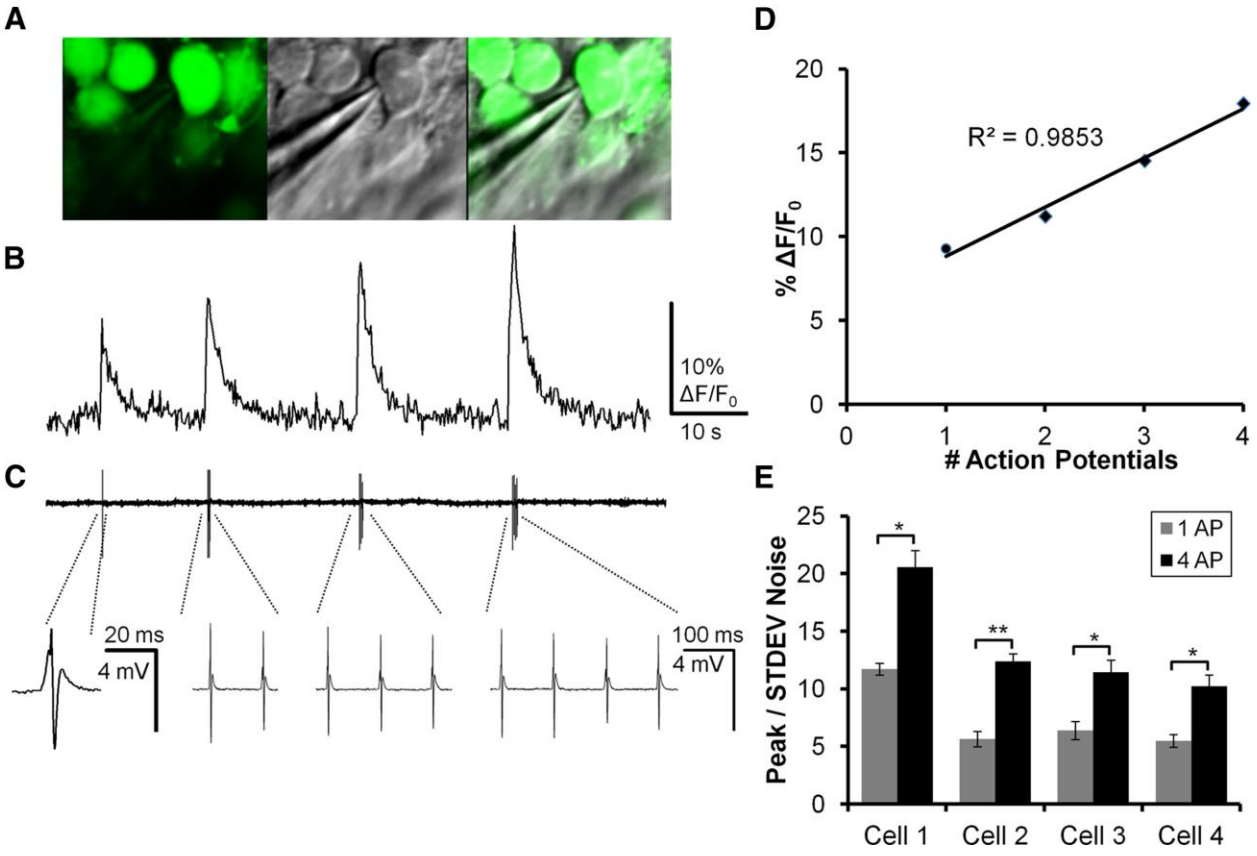
A
B
10%
ΔF/F0
10 s
C
20 ms
4 mV
100 ms
4 mV
D
R² = 0.9853
% ΔF/F0
# Action Potentials
E
1 AP
4 AP
Peak / STDEV Noise
Cell 1
Cell 2
Cell 3
Cell 4

Figure 3.3. Relationship of AP activation to calcium transient amplitude in DGCs. ***A***, Left, A 2-photon image of DGCs loaded with Fura2-AM in a P60 mouse. Middle, Dodt contrast image showing the electrode used for loose-patch recording of APs. Right, Merge of Fura2-AM and Dodt contrast depicting robust Fura labeling in the recorded DGC. ***B***, Calcium imaging transients elicited by stimulation of the PP with 10 Hz trains containing 1, 2, 3, and 4 pulses. ***C***, Top, Loose-patch recording time-locked with calcium imaging trace in ***B***. AP activation coincides with onset of calcium transients. Stimulus artifacts have been removed digitally. Bottom, Higher temporal resolution traces of loose-patch recordings in which individual APs can be resolved. The single AP to the left is depicted at an expanded time scale, whereas the remainder (2, 3, and 4 APs) are depicted at a compressed time scale. ***D***, Plot of AP activation versus calcium transient magnitude for the responses depicted in ***B***. Calcium transient amplitude correlated with AP firing (Pearson's coefficient $r^2 = 0.9853$). ***E***, Ratio of calcium transient amplitude to the SD of baseline noise for 4 patch-recorded DGCs. Every cell had a calcium transient peak ≥ 4 times the SD of baseline noise (mean ± SE, 7.9 ± 1.48). Calcium transients for responses elicited by 4 APs averaged 13.64 ± 2.35 times the SD of the noise (mean ± SE). Calcium transient peaks for 4 APs were significantly larger than for 1 AP (Cell 1, p=0.016; Cell 2, p=0.0003; Cell 3, p=0.021; Cell 4, p=0.010). On average, 1 AP generated a calcium transient that was 53% the magnitude of a 4 AP transient.

To accomplish our goal of determining cellular activation in populations of DGCs, calcium indicator fluorescence fluctuations were imaged in the same slice and regions in response to the same stimulus as VSDI recordings (**Fig. 3.4*A***). Select Fura 2-AM-loaded DG regions together with cellular ROI used for analysis are shown in representative P12 and P60 slices in **Figure 3.4*A***. **Figure 3.4*B*** depicts representative traces for individual cellular ROI (numbers correspond to image in **Fig. 3.4*A***) from P12 and P60 slices derived from calcium imaging of GCs. Asterisks denote calcium transients resolved with an automated detector (see Materials and Methods). There was a clear increased proportional activation of DGCs by PP stimulation in slices prepared from P12 compared with P60 animals, with 7 of 9 P12 DGCs exhibiting activation compared with 3 of 9 for P60 DGCs. To quantify this effect across development, we wanted to ensure that all DGCs included in the analysis had the capability of activating. To accomplish this, we applied PTX (50 μM), a $GABA_A$ antagonist, at the end of each experiment, and limited our subsequent analysis to neurons that exhibited stimulus-evoked calcium transients in the presence of PTX. Examining the proportion of PTX-active cells that also activated in normal ACSF across developmental ages (**Fig. 3.4*C***), we found that more than half of P12 DGCs activated in response to afferent stimulation, which decreased to 20% of neurons at P22-P30 and P60. This decrease in proportional activation was statistically significant (ANOVA, $p < 0.0001$, with Tukey's multiple-comparison *post hoc* testing demonstrating significant differences between P12 and P22 [$p < 0.05$] and P12 and P60 groups [$p < 0.01$]). In addition to serving as a method to ensure that we expressed responsive cell proportion relative to the overall population of viable neurons, PTX perfusion also demonstrated that the escalating sparsification in activation of DGCs during postnatal development was largely mediated by changes in local circuit inhibition rather than enhanced selectivity of afferent input targeting, because we observed that

blockade of inhibition normalized response proportion between postnatal developmental ages (63.3 ± 9.6%, and 71.8 ± 5.8% for P12 and P60 animals in PTX, not significantly different, *t* test).

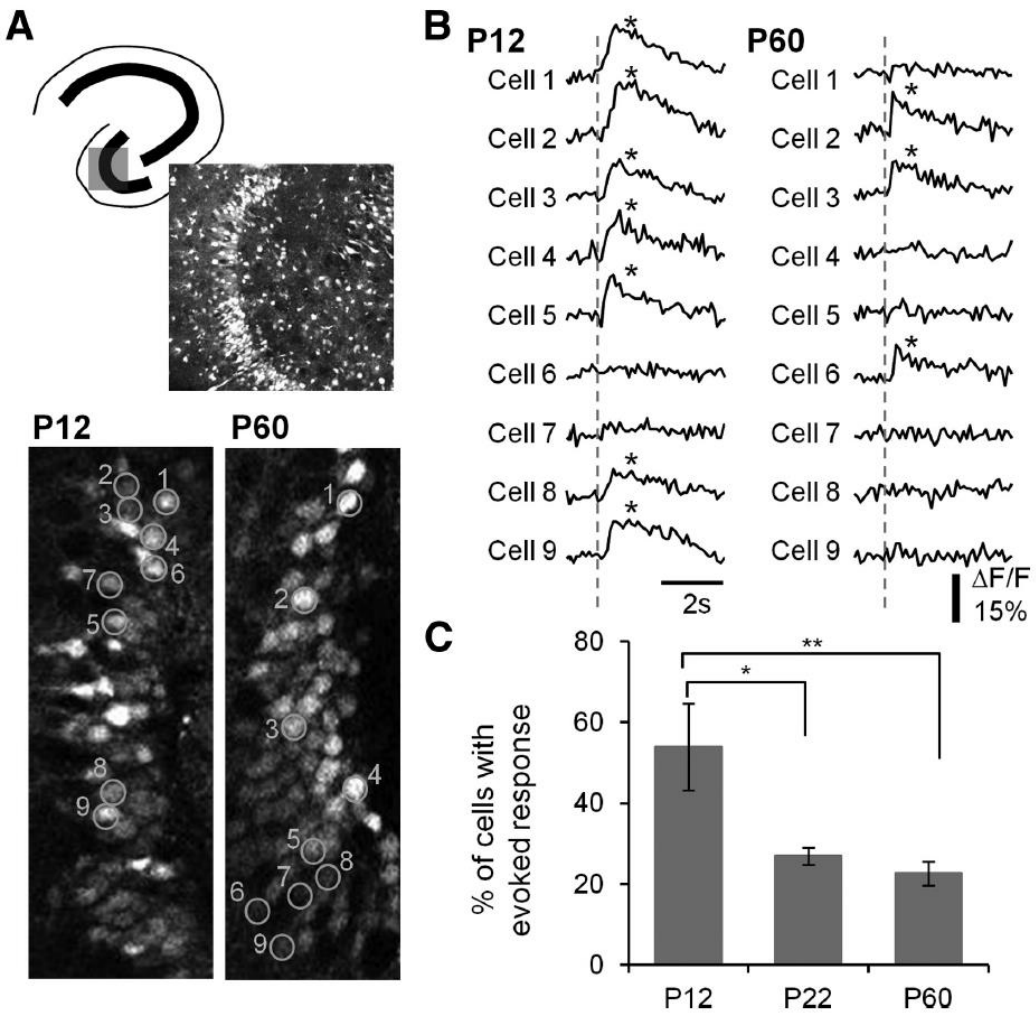
A
P12
P60
B
P12
P60
Cell 1
Cell 2
Cell 3
Cell 4
Cell 5
Cell 6
Cell 7
Cell 8
Cell 9
2s
ΔF/F
15%
C
% of cells with evoked response
80
60
40
20
0
*
**
P12
P22
P60

Figure 3.4. Decreased DGC activation during postnatal development. ***A***, Top, Schematic of a hippocampal slice depicting the imaged area in the DG and a Fura2-loaded DG of a P12 mouse (370μmx370μm). Bottom, Image of P12 and P60 DGCs, with ROI created on a random sample of cells (orange) (90 μm x 200 μm). Numbers denote cell identification with time-resolved fluorescence responses depicted in ***B***. ***B***, Representative traces of time-resolved calcium imaging responses for the ROI in the P12 and P60 images in ***A***. The dotted line indicates the time when PP stimulation (400μA) occurred. An asterisk indicates detection of a calcium transient. ***C***, Plot of the percentage DGC activation by PP stimulation for P12, P22, and P60 animals. Note the decrease in cell activation with postnatal development. $P<0.0001$ for the animal age factor (ANOVA). *$p<0.05$, significant differences between P12 and P22 (Tukey's multiple-comparison *post hoc* testing). **$p<0.01$, significant differences between P12 and P60 groups (Tukey's multiple-comparison *post hoc* testing). P12: $n = 322$ PTX-active cells in 10 imaged regions; P22: $n = 198$ in 10 imaged regions; P60: $n = 239$ of 12 imaged regions.

Information processing is mediated not only by the identity of cells that activate, but also by the temporal patterns of activation. Precise activation latencies time-locked to the occurrence of the afferent input retain specific information about the temporal properties of the stimulus. In the adult DG, the fast kinetics of excitatory synaptic potentials endows DGCs with the property of coincidence detectors resulting from the narrow activation and integration window generated by this characteristic (Schmidt-Hieber et al., 2007). To assess how the timing of cell activation relative to afferent input varied with postnatal development, we conducted a second set of MCI experiments on a specialized microscope capable of frame rates up to ~1 kHz (Nikon Live Scan Swept Field Confocal Microscope). Using this system, we were able to acquire MCI onset activation information from DGCs after PP stimulation at a 128x128 pixel frame rate of 320 Hz (**Fig. 3.5**). We determined this to be the highest temporal resolution possible using this microscope given the photon density emitted by the Oregon Green bulk-loaded cells during activation. Using this system increased our temporal resolution ~30-fold compared with the 10 Hz frame rates used on the multiphoton microscope during MCI (**Fig. 3.4**). Examining the time course of onset of MCI responses after PP stimulation and computing onset times using a curve-fitting algorithm (**Fig. 3.5*A***), we were able to resolve a large, statistically significant difference in the distribution of ensemble activation times between early postnatal (P12) and adult (P60) animals. This was evident in the histogram in **Figure 3.5*B*** as a multimodal distribution of response latencies for P12 animals, with early (5–15 ms) and late (15–100 ms) components (black bars), compared with a unimodal distribution of response latencies confined to early (5–15 ms) time points for P60 animals (gray bars; P12 distribution different from P60, p = 0.00068, Kolmogorov–Smirnov test; **Fig. 3.5*B***). The multimodal distribution of onset latencies in P12 animals may be the result of the wide variance in cell developmental

stage at this animal age (Liu et al., 1996), where birth, migration, and differentiation of neurons are still ongoing. Fast activating responses may reflect more mature DGCs, whereas slow, long latency responses may derive from less mature, more recently born DGCs (Schlessinger et al., 1978; Rickmann et al., 1987; Hollrigel et al., 1998). However, the late responses were not the result of spontaneous activity, which was evident in some P12 cells. Examining this activity in detail, we found that 2.4% of P12 granule cells exhibited spontaneous activity, with an event frequency of 0.013 Hz. Given that the activation window examined after stimulus in **Figure 3.5** was 100 ms, and activity in 160 P12 DGCs was plotted, <1 (0.05) spontaneous event would be expected to contribute to the ensemble activation for the entire population in **Figure 3.5**.

We also examined the role played by local circuit GABAergic inhibition in determining onset latencies of DGCs after PP stimulation. Application of the $GABA_A$ antagonist, PTX (50 μM), had distinct effects on activation times in the P12 and P60 age groups (**Fig. 3.5*C*, *D***). In the P12 group, PTX specifically blocked late activating responses, with little or no effect on early responses, which constituted the majority of the population. This suggested that GABAergic inhibition might exert a delayed, excitatory effect on a subpopulation of DGCs in this age group, presumably immature cells with depolarizing GABA responses (Hollrigel et al., 1998). The Kolmogorov–Smirnov test did not indicate differences in the overall distribution of latencies between PTX-treated and untreated cells (p = 0.123). We hypothesized that, although the overall distribution may have been similar between the two groups, components of the distribution differed. Examination of **Figure 3.5*C*** suggests that the distributions were largely similar, particularly at shorter response latencies. However, we noted that the P12 group appeared to be skewed to the right, with control cells tending to show longer response latencies. Thus, as a secondary analysis, we tested whether the means of the

two conditions were similar using a *t* test after log-transforming the data to achieve approximate normality. We found that control cells had a slightly longer mean latency than PTX-treated cells (p = 0.043, 10.1 vs 7.7 ms), which may reflect the shift in the distribution toward longer latency. Given the differing results for the two statistical tests and significance level near 0.05, these results should be interpreted with some caution and subject to confirmation in future studies. PTX had a different effect on P60 onset latencies, where it shifted the entire distribution to shorter AP activation times (Kolmogorov–Smirnov test, $p < 0.0001$, **Fig. 3.5*D***), suggesting that feedforward interneurons may activate so rapidly in adult animals that they affect the onset kinetics of monosynaptic, PP-originating EPSPs.

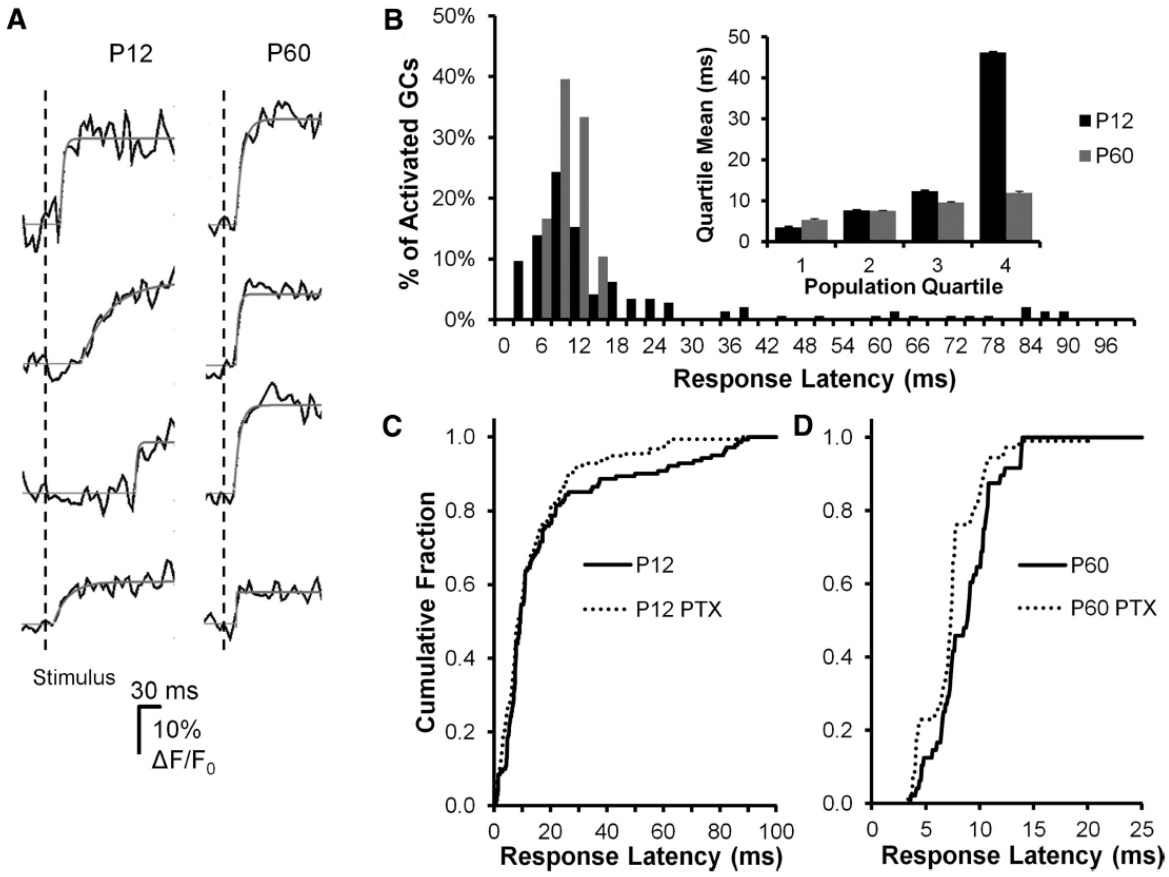
A
P12
P60
Stimulus
30 ms
10%
ΔF/F0
B
% of Activated GCs
Response Latency (ms)
Quartile Mean (ms)
Population Quartile
P12
P60
C
Cumulative Fraction
P12
P12 PTX
Response Latency (ms)
D
P60
P60 PTX
Response Latency (ms)

Figure 3.5. DGC activation timing precision increases during postnatal development. ***A***, Sample DGC calcium imaging traces from a P12 (left) and a P60 animal, demonstrating variability in response onset time after PP stimulation between groups. Onset time is estimated from exponential fits (solid lines, see Materials and Methods). The P12 response onsets are more variable, with frequent later events. PP stimulus time is indicated by the vertical line. ***B***, Histogram plotting population percentage against response latency for P12 (black bars) and P60 (gray bars) animals. The late events are restricted to the P12 population, whereas P60 responses are limited to the first 15 ms after stimulation. These population distributions of response latency were significantly different (Kolmogorov–Smirnov test, $p = 0.00068$). Inset, Further illustration of the differences between groups by plotting the mean response latencies broken down by population quartiles. For the first three quartiles, there is very little difference between groups, whereas in the fourth population quartile, there is a fivefold longer average response latency in P12 DGCs. ***C***, ***D***, Sensitivity of response onset time to GABA antagonist (PTX, 50μM) perfusion in P12 (***C***) and P60 (***D***) DGCs. Both populations exhibited PTX sensitivity in response latencies, but the nature of these effects differed. For P12 DGCs (***C***), PTX specifically blocked late activating responses (>20 ms latency), with little or no effect on early responses (0 –15 ms), which constituted the majority of the population. A Kolmogorov–Smirnov test for overall differences between populations was not significant ($p = 0.123$); however, untreated cells had a slightly longer mean latency ($p = 0.043$, 10.1 vs 7.7 ms, *t* test after log-transforming the data). For P60 DGCs (***D***), PTX shifted the entire curve to the left (Kolmogorov–Smirnov test $p < 0.0001$), consistent with a significant decrease in response latency. P12: $N = 3$ animals, 28 fields, 141 cells. P60: $N = 3$ animals, 22 fields, and 48 cells.

Repeatability of the active versus silent DGC response

PP innervation of the DG shows remarkable divergence and convergence (Tamamaki and Nojyo, 1993; van Groen et al., 2003). Given this apparent lack of input specificity, we were interested in determining how robust and repeatable is the decision made by individual DGCs to activate or fail to activate in response to PP stimulation. A deterministic, specific response would be reflected in a repeatable decision being made, in which cells that activate to a given stimulus continue to fire repeatedly and cells that fail to activate initially repeatedly fail to respond to subsequent stimuli. A stochastic process would be reflected in random activation, without evidence of repeatability. We were also interested in whether these response characteristics changed during postnatal development, as the DG circuit matures.

To examine these issues, we repeatedly stimulated the PP at 5 s intervals and assessed the overlap in populations of DGCs, which activate or do not activate at differing stages of postnatal development. At the end of the experiment, we applied PTX (50 μM) and repeated the stimulus. Only neurons that responded to stimulation in the presence of PTX were included in our analysis. We divided DGCs into responsive and nonresponsive populations, defined as PTX-responsive neurons that either activated or did not activate in response to the first stimulus in normal medium. We then examined how these two populations of cells responded to subsequent stimuli (**Fig. 3.6**). In Figure 3.6*A*, *B*, specimen records are depicted for 5 responsive (top) and 5 nonresponsive DGCs (bottom), in a slice prepared from a P12 (**Fig. 3.6*A***) and a P60 (**Fig. 3.6*B***) animal. Examining the responses to subsequent, identical stimuli at 5 s intervals, it is evident that DGCs responded similarly to subsequent stimuli. Cells that activated to the first

stimulus continued to activate frequently to subsequent stimuli, and cells that did not activate rarely activated to subsequent stimuli.

To analyze this trend evident in the specimen records in **Figure 3.6*A*, *B***, we fit a logistic regression model using the data from Stimulus 4 as the outcome and the data from the previous two stimuli as predictors, to assess whether the previous behavior of a neuron to stimulation influenced its subsequent behavior. The P12 dataset contained 240 cells across seven slices. Across all slices, 48.9% of cells responded to Stimulus 4. The propensity of a cell to respond in Stimulus 4 was highly dependent on its responses to Stimulus 3 ($p < 0.0001$) and Stimulus 2 ($p = 0.013$). **Figure 3.6*C*** shows the propensity to respond (top) or not respond (bottom) for cells from each slice as a function of their previous response pattern. For cells with no response at either Stimulus 2 or Stimulus 3 (N_N), the probability of response at Stimulus 4 ranged from 7.0% to 33% depending on slice; in contrast, for cells that responded to both Stimulus 2 and Stimulus 3 (Y_Y), the stimulation 4 response probability varied from 56.6% to 89.6%.

The propensity of a P60 cell to respond to stimulus 4 was highly dependent on its propensity to respond to Stimulus 2 ($p < 0.0001$), and also positively associated with its propensity to respond to Stimulus 3, although this association did not achieve statistical significance ($p = 0.075$). **Figure 3.6*D*** shows the propensity to respond (top) or not respond (bottom) for cells from each slice as a function of their previous response pattern. For cells with no response to Stimulus 2 and 3 (N_N), the probability of response at Stimulus 4 ranged from 3.4% to 29.3%; in contrast, for cells that responded to both Stimulus 2 and 3 (Y_Y_), the probability of response at stimulus 4 varied from 67.6% to 96.1%.

For both the P12 and P60 data, similar results were found using stimulus 3 as the outcome and the response from Stimulus 1 and 2 as predictors (results not shown). The

results for the P60 and P12 data differed in that, the propensity to respond at Stimulus 4 showed the strongest association with the propensity to respond at Stimulus 3 for the P12 group, and to the propensity to respond at Stimulation 2 for the P60 group. Nevertheless, the P12 and P60 data provide strong evidence against the hypothesis of stochastic response patterns.

The results of our analysis refute the null hypothesis of no relationship between previous and subsequent responses and strongly support the hypothesis of deterministic response patterns ($p < 0.0001$ for an association for both P12 and P60). This is concordant with the finding that ensemble activation of populations of DGCs to afferent stimulation was repeatable and precise, and therefore more consistent with a deterministic than a stochastic process.

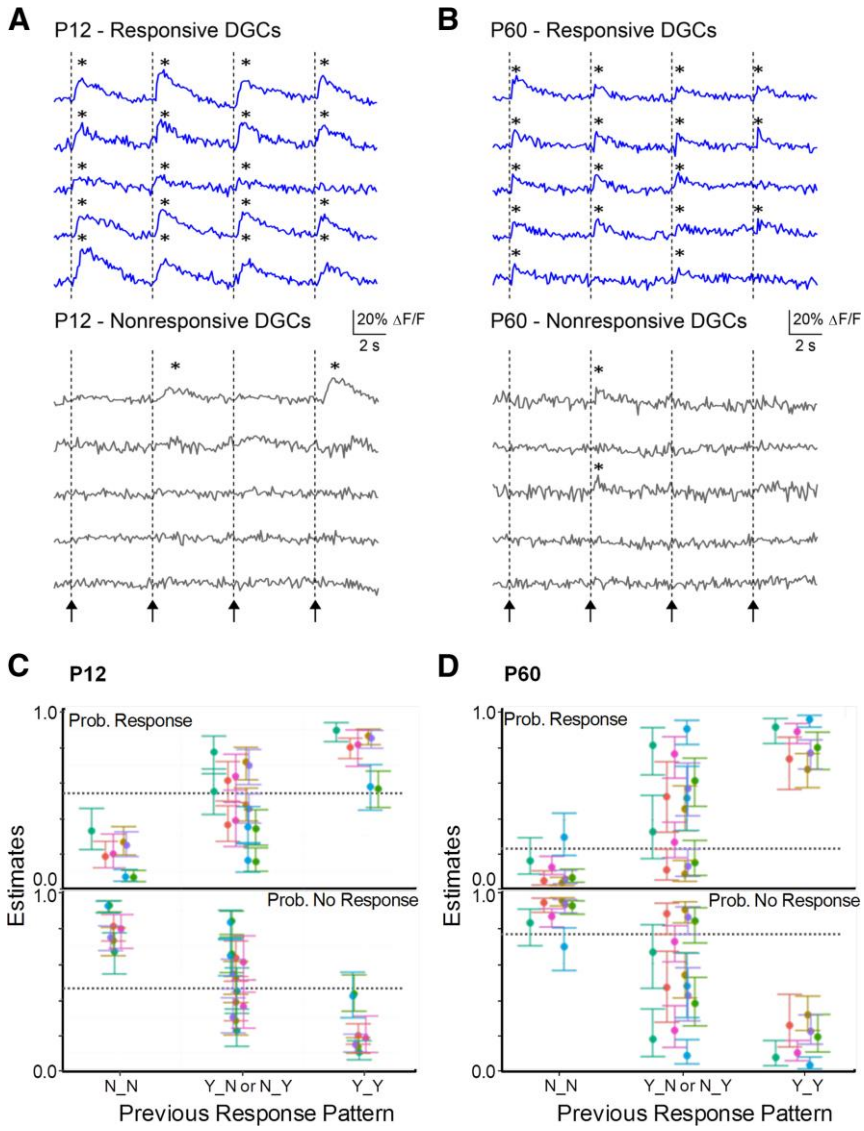
A
P12 - Responsive DGCs
P12 - Nonresponsive DGCs
20% ΔF/F
2 s
B
P60 - Responsive DGCs
P60 - Nonresponsive DGCs
20% ΔF/F
2 s
C
P12
Prob. Response
Prob. No Response
Estimates
1.0
0.0
N_N
Y_N or N_Y
Y_Y
Previous Response Pattern
D
P60
Prob. Response
Prob. No Response
Estimates
1.0
0.0
N_N
Y_N or N_Y
Y_Y
Previous Response Pattern

Figure 3.6. Repeatability of activate/remain silent DGC response. ***A***, ***B***, Calcium transient traces in representative DGCs in P12 and P60 animals, respectively, in response to 4 PP stimuli. Arrows/dotted lines indicate onset of PP stimulation (400 μA). Responsive cells (***A***,***B***, top) were defined as DGCs that activated to the first stimuli, and nonresponsive cells as DGCs that failed to activate to the first stimulus (***A***, ***B***, bottom). Responsive cells at both ages responded frequently to subsequent stimuli, whereas nonresponsive cells did not. *Calcium transient was detected. ***C***, ***D***, Estimate of probability of response or nonresponse in Stimulus 4 given the previous pattern of response in Stimuli 2 and 3 for P12 (***C***) and P60 (***D***) groups (see Materials and Methods for model details). N_N, no response in both; Y_N, response in Stimulus 2 and not Stimulus 3; N_Y, no response in Stimulus 2 but response in Stimulus 3; Y_Y, response to both. Error bars indicate SEM; each color indicates a different slice. The hyphenated line indicates the probability of a response at Stimulus 4 across all cells and slices. The activation behavior of both P12 and P60 DGCs was strongly influenced by their previous behavior: cells that exhibited responses to Stimuli 2 and 3 had a high probability of activating to Stimulus 4, whereas cells that did not activate to Stimuli 2 and 3 had a low probability of responding to Stimulus 4, in all slices (n = 7 for both P12 and P60) and at both developmental stages. Cells with mixed responses to Stimuli 2 and 3 (Y_N or N_Y) had variable probabilities of activating to Stimulus 4. Random behavior would be predicted by responses probabilities at the overall population mean (dotted line in plot).

Selective recruitment of DGC responses by θ and γ frequency stimulation

The data described above reflect DGC activation to single PP stimuli (**Fig. 3.4**) or to repeated stimuli at low frequencies (0.2 Hz, **Fig. 3.6**). During spatial navigation, the DG receives θ and γ frequency input from grid cells within the medial EC. How do these more natural stimulus patterns (θ and γ frequency inputs) modify DGC activation, and does this vary with postnatal development? To address this question, we used Oregon Green BAPTA-AM-loaded DGCs in slices prepared from P12 and P60 animals and examined activation in response to varying frequency inputs (δ, 1 Hz; θ, 5 and 10 Hz; and γ frequency, 60 Hz ranges) using the fast confocal microscope. The kinetics of Oregon Green are faster than Fura 2 during AP-elicited calcium transients, and the frequency response of the confocal microscope is much faster than the multiphoton microscope used in most experiments, allowing us to better resolve individual responses to varying frequency inputs in DGCs.

Figure 3.7*A* plots the proportional activation of DGCs from P12 (black bars) and P60 (gray bars) animals to 1, 5, 10, and 60 Hz PP stimulation. There is very little additional recruitment of P12 DGCs by higher frequency stimulation, whereas there is significant further DGC recruitment in P60 animals in response to 10 and 60 Hz stimulation (**Fig. 3.7*A***). This is better visualized by normalizing response recruitment to the proportional activation evident in response to 1 Hz stimulation (**Fig. 3.7*B***). There is little or no additional activation at 5, 10, and 60 Hz for cells from P12 animals, whereas there is a twofold and fivefold greater recruitment for 10 and 60 Hz stimulation, respectively, for P60 animals (P12 and P60 distributions differ significantly, $p < 0.0001$, two way ANOVA). Although P60 DGCs exhibit lower basal activation (**Fig. 3.4**), they are readily recruited at input frequencies overlapping those encountered during normal

cognitive processing in awake, behaving animals. This differs from P12 animals, which show significant basal activation (**Fig. 3.4**), but no additional recruitment with higher frequency inputs.

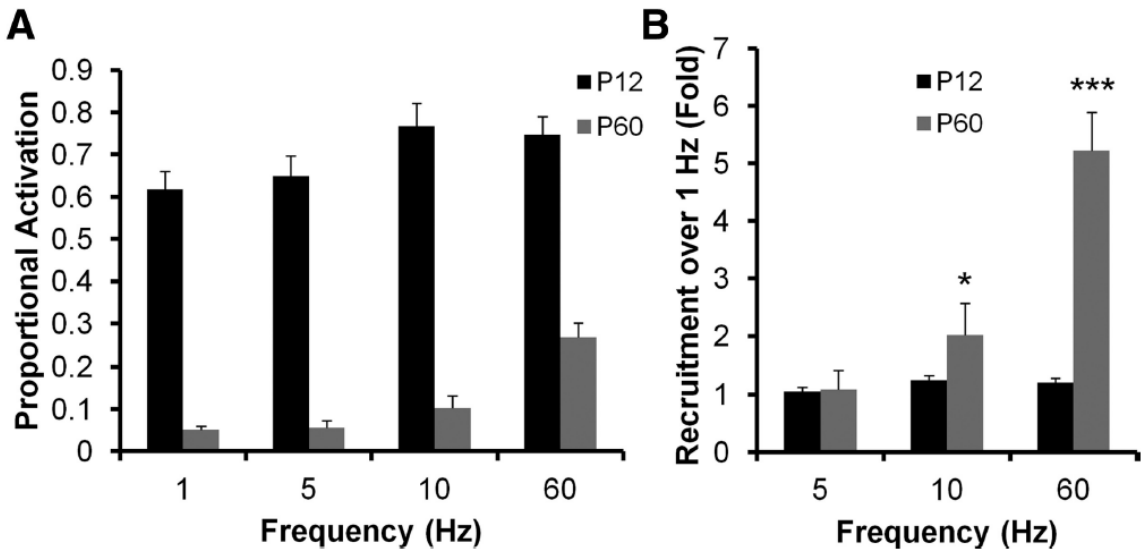

Figure 3.7. Increased θ and γ frequency recruitment of DGCs during postnatal development. ***A***, ***B***, Responses of DGCs from P12 (black bars) and P60 (gray bars) animals to varying frequency stimulation of the PP (1, 5, 10, and 60 Hz). ***A***, Raw mean percentage activation. ***B***, Percent recruitment normalized to the activation evident during 1 Hz stimulation. Note that P12 DGCs, although more active overall, exhibited very little frequency recruitment, whereas P60 DGCs were significantly recruited by θ (5–10 Hz) and γ (60 Hz) frequency stimulation of the PP (two-way ANOVA). Both frequency and age effect are significant ($p < 0.0001$). *$p < 0.05$, 1 vs 10 Hz for P60 (Bonferroni *post hoc* test). ***$p < 0.001$, 1 vs 60 Hz for P60 (Bonferroni *post hoc* test). n = 3 animals, 6 slices, 11 fields, 629 cells for P12; n = 3 animals, 4 slices, 5 fields, 366 cells for P60.

Regional distinction in proportion DGC activation

Anatomic studies have described regional distinctions between the infrapyramidal and suprapyramidal blades of the DG. The suprapyramidal blade of the DG has more GABAergic inhibitory interneurons than the infrapyramidal blade (Seress and Pokorny, 1981; Woodson et al., 1989), and interneurons in the suprapyramidal blade are more densely innervated by mossy fibers (Ribak and Peterson, 1991). Both of these distinctions have the potential to increase the strength of feedforward and feedback inhibition in the suprapyramidal blade relative to the infrapyramidal blade, critical processes regulating DGC activation. To assess possible functional differences in the suprapyramidal and infrapyramidal blades associated with these anatomic differences in inhibitory innervation, we examined DGC activation in response to PP stimulation in the two blades at varying stages of postnatal development using MCI. **Figure 3.8*A*** depicts the regions defined in our studies as suprapyramidal and infrapyramidal blades of the DG. In **Figure 3.8*B***, MCI specimen records of cell activation in response to PP stimulation are depicted for DGCs in the infrapyramidal and suprapyramidal blades in slices prepared from P12 (top traces) and P60 (bottom traces) animals. Note that all cells (P12 and P60) were responsive in PTX and that an increased proportion of DGCs exhibited activation in the infrapyramidal blade relative to the suprapyramidal blade. This trend, evident in these specimen records, was present in all recordings. **Figure 3.8*C*** plots the proportional activation of DGCs in the infrapyramidal and suprapyramidal blades at all postnatal developmental stages sampled. The distinction in proportional activation between the two blades was statistically significant and retained throughout development

($p < 0.01$ to $p < 0.05$, depending on developmental stage). Also, the gradual reduction in proportional DGC activation evident across ages (**Fig. 3.4*C***) was primarily the result of a pruning of activation in the infrapyramidal blade with development, which gradually decreases from 85% to 20% in P12 and P60 animals (**Fig. 3.8*C***). The suprapyramidal does not show a similar decrease, maintaining activation levels of 15–20% throughout postnatal development (**Fig. 3.8*C***). To the right of these MCI specimen records in **Figure 3.8*B*** are sequential VSDI traces (gray) recorded in the same slices from the same regions examining the EPSP amplitudes in the suprapyramidal and infrapyramidal blades at both postnatal ages. These responses were similar, so differences in proportional activation of DGCs between blades are not the result of gross differences in PP innervation strength in these two DG subregions. This was true for all recordings (**Fig. 3.8*D***).

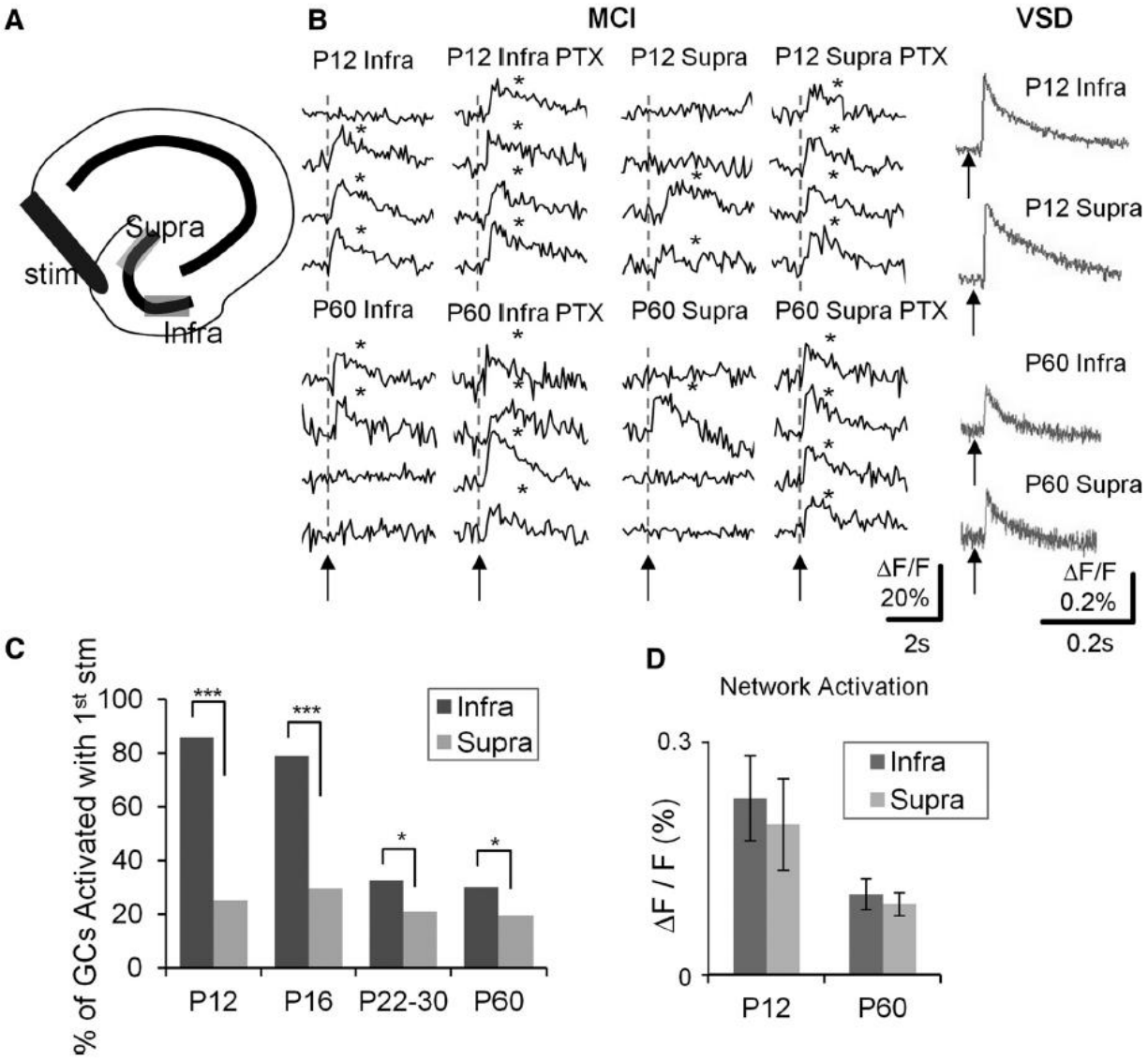
A
B
MCI
VSD
P12 Infra
P12 Infra PTX
P12 Supra
P12 Supra PTX
P60 Infra
P60 Infra PTX
P60 Supra
P60 Supra PTX
Supra
stim
Infra
ΔF/F
20%
2s
ΔF/F
0.2%
0.2s
C
% of GCs Activated with 1st stm
Infra
Supra
P12
P16
P22-30
P60
D
Network Activation
ΔF / F (%)
Infra
Supra
P12
P60

Figure 3.8. Enhanced proportional activation of DGCs in the infrapyramidal blade of the DG. ***A***, Schematic depicting the hippocampus with the suprapyramidal and infrapyramidal blades. ***B***, Traces are calcium imaging responses from representative DGCs in the infrapyramidal (Infra) and suprapyramidal (Supra) blade of the DG, in P12 (top) and P60 (bottom) animals. Responses were recorded in control medium, and in the presence of the GABA antagonist, PTX (50 μM). Gray traces (right) represent VSDI responses of PP-evoked EPSPs in the infrapyramidal and suprapyramidal blades of P12 (top) and P60 (bottom) animals. Asterisks denote detection of a calcium transient. Note that there is enhanced proportional activation of DGCs in the infrapyramidal compared with the suprapyramidal blades at both ages, despite the fact that VSDI-recorded EPSPs were comparable. ***C***, Aggregate population plots of percentage DGC activation in infrapyramidal and suprapyramidal blades in 4 developmental ages (P12, P16, P22–P30, and P60). Note that enhanced DGC activation is evident at all ages. *$p < 0.05$ (Fisher's exact test). ***$p < 0.001$ (Fisher's exact test). P12: $n = 10$ samples of 2 animals; P16: $n = 10$ of 2; P22–P30: $n = 20$ of 3; P60: $n = 24$ of 4. ***D***, Averaged VSDI-recorded PP-evoked EPSPs in P12 and p60 animals. Note that there was no difference between the infrapyramidal and suprapyramidal blades (P12, $n = 7$ slices of 2 animals; P60, $n = 6$ of 1).

Discussion

In adult mice, DGCs exhibited sparse, selective, and tightly tuned activation in response to PP stimulation. In these adult animals, ~20% of the viable neuronal population responded to strong afferent stimulation. These properties of activation depended on inhibitory modulation within the circuit because the majority of cells responded in the presence of a GABA antagonist, PTX. The adult pattern of DGC activation emerged in a protracted manner during postnatal development. In animals during the first 2 postnatal weeks, there was much less selectivity, with 60% of DGCs activating in response to afferent stimulation, with significantly less precise temporal tuning. Both the developmental regulation of sparse activation behavior and increased temporal fidelity of responses were dependent, at least partly, on changes in local circuit GABAergic inhibition because blockade of GABA receptors normalized responses across developmental stages. Even on a background of this large difference in AP firing selectivity, several aspects of DGC responses appeared early in development and were retained. These included the robust, repeatable nature of an individual cell's propensity to activate or remain silent in response to afferent activation, and a preferential developmental decline in active cells in the infrapyramidal compared with the suprapyramidal blade.

The proportion of neurons within a circuit that respond to stimulation of an afferent input, and the mechanisms that regulate this decision to activate in individual neurons are among the most fundamental aspects of circuit function. The activation process is most frequently examined *in vivo*, often during execution of behavioral tasks. However, *in vitro* approaches such as those used in the present study may also be important in characterizing these fundamental aspects of circuit behavior because more

variables can be controlled, and neurons are more accessible for detailed biophysical analysis. The applicability of *in vitro* studies can be controversial, however. Issues center around two main caveats, which could complicate interpretation: (1) Has the circuit been disrupted by the experimental preparation? (2) Are the mechanisms regulating activation elucidated *in vitro* also relevant to *in vivo* processing?

Our combined imaging approach has allowed us to examine the spatiotemporal properties of afferent activation in the DG using VSDI approaches, as well as patterns of cellular activation in large numbers of neurons with single-cell resolution using MCI and 2-photon microscopy. This allows determination of afferent pathway function while still permitting proportional cell activation to be assessed. We also verify that the majority of cells we image and all the neurons that we analyze are viable and able to activate appropriately. These constitute unique strengths of our combined approach. The question concerning the relevance of the present findings to developmental regulation of cell activation propensity *in vivo* remains to be determined. However, there is one remarkable similarity to *in vivo* studies: the sparse but specific firing in DGCs described during spatial navigation (Jung and McNaughton, 1993a; Leutgeb et al., 2007; Neunuebel and Knierim, 2012) is very similar to our findings *in vitro* in more mature animals.

New data are emerging which suggest that the same sparse population of DGCs may activate in multiple environments (Leutgeb et al., 2007; Alme et al., 2010), rather than sparse firing of multiple distinct populations of DGCs in diverse environments (Jung and McNaughton, 1993a; Chawla et al., 2005). This may be mediated by combined activation of both newly born and perinatally born DGCs in the adult brain (Marín-Burgin et al., 2012). The concept that sparse populations of DGCs activate in multiple environments may require significant modification in the conceptual framework

describing cognitive processing within this circuit (Clelland et al., 2009; Nakashiba et al., 2012). Regardless of the identity of active DGCs, they play a critical role in hippocampal function. A recent study used optogenetic techniques to reactivate neurons within the DG which had activated during acquisition of a fear memory task. This reactivation of this small population of DGCs recapitulated the learned behavior, supporting the importance of DGC coding in cognitive processing (Liu et al., 2012).

Some characteristic components of DGC activation were present early in postnatal development and maintained into adulthood. One of these was the robustness of the decision to activate or not activate in response to a given stimulus. This is a characteristic seen in DGC recordings during spatial navigation (Jung and McNaughton, 1993a; Leutgeb et al., 2007; Neunuebel and Knierim, 2012), and in activity reporter studies examining *Arc* RNA expression patterns after repeated similar environmental exposures (Chawla et al., 2005). In a slice study of DG inhibitory circuitry responding to PP activation, Ewell and Jones (2010) described frequency-tuned basket cell-mediated inhibition, which contributed to sparsification of DGC output that was present in P12-P21 animals. Thus, significant components of the DG inhibitory circuit are online early during postnatal development and may be the substrate defining the robust nature of the decision to activate or remain silent evident at this age.

A recent study used MCI to examine PP stimulation-induced DGC activation, focusing on differential properties of newborn and perinatally born neurons in adult animals (Marín-Burgin et al., 2012). Notably, there were significant increases in the proportional activation of DGCs in adult animals reported in this study (60%) relative to the present findings (20%, **Fig. 3.4**). This 60% level of activation could not be considered sparse, an important conclusion of the present study. This conflict in proportional activation measures could be the result of methodological differences

between the two studies. Both studies normalized responses to the proportion of cells activated in the presence of GABA antagonists. However, Marin-Burgin et al. (2012) used epifluorescence microscopy and averaged multiple trials to derive their 60% activation estimate, whereas the present study used 2-photon microscopy and reported activation in individual trials. Both of these methodological differences could contribute to differences in proportional activation estimates. Epifluorescence microscopy collects fluorescence from the focal plane, and out of focus regions, whereas 2-photon microscopy only excites fluorescence within a narrow focal plane with a 1–2 μm depth. This could account for the difference in proportional activation reported in the two studies because neurons out of the focal plane can factor into the overall estimate of activation proportion. A second contributor might be the 5 trial signal averaging used by Marin-Burgin et al. (2012) to calculate activation. Our imaging approach could resolve activation of individual APs in single trials with signals ~5 SD larger than noise levels. Averaging over multiple trials would increase activation estimates by 30–50% because initially nonactive cells can be recruited ~40% of the time by additional stimuli.

The preferential recruitment of DGCs in the infrapyramidal compared with the suprapyramidal blade was particularly strong in early postnatal animals and may be mediated by differences in anatomic measures of inhibition between the two regions. The suprapyramidal blade has more GABA-inhibitory interneurons than the infrapyramidal blade (Seress and Pokorny, 1981; Woodson et al., 1989), and the inhibitory neurons in the suprapyramidal blade are more densely innervated by mossy fibers (Ribak and Peterson, 1991). Our findings of enhanced DGC activation in the infrapyramidal blade are not in agreement with *Arc* RNA expression studies of cellular activity during spatial navigation (Chawla et al., 2005) or with a combined physiology/imaging study (Scharfman et al., 2002). These groups found that the

suprapyramidal blade exhibited greater proportional activation. However, these studies were conducted in more septal regions of the hippocampus than the temporal pole studied in the present study, which may explain these divergent findings. The suprapyramidal blade activation preference disappears in more temporal locations (Scharfman et al., 2002).

Given that local circuit inhibition is a prime mediator of sparse, specific activation properties of DGCs (Nitz and McNaughton, 2004; Schmidt-Hieber et al., 2007; Ewell and Jones, 2010; Sambandan et al., 2010), and that there is significant variation in inhibitory properties in the DG during postnatal development (Hollrigel et al., 1998), the sensitivity of developmental changes in DGC activation propensity and AP firing precision to GABA blockers is not unexpected. However, what is surprising is that both of these developmental changes in DGC activation completely normalize in the presence of PTX. This raises the intriguing possibility that the identity and characteristics of DGC activation may not be defined exclusively by specificity in PP inputs onto DGCs. Rather, they may also be defined to a significant extent by feedforward inhibition, which in turn must be mediated by precise PP inputs onto interneurons. This provides a permissive environment allowing small populations of DGCs to activate, potentially to multiple sets of inputs (Leutgeb et al., 2007; Alme et al., 2010). This suggests that, because information is not coded exclusively in the identity of granule cells that activate, these cells may use a combination of a rate code and cellular identity output to discriminate input properties, a hypothesis requiring further testing.

The neuronal representation of space within the hippocampus and EC of rodents exhibits a protracted postnatal development, stabilizing at adult levels by 3.5–4 weeks postnatal (Langston et al., 2010a). Capabilities in conduct of spatial memory tasks also exhibit a similar protracted postnatal development (Schenk, 1985; Rudy et al., 1987;

Ainge and Langston, 2012a). Given that appropriate activity within the DG is an important component of these tasks, the delays in development of adult levels of sparse and selective DGC activation, temporal tuning, and frequency-dependent recruitment in response to EC activation described in the present study may contribute to delays in development of both neuronal representations of space and of adult levels of competence in spatial memory tasks.

Chapter 3 Bibliography

Acsády L, Káli S (2007) Models, structure, function: the transformation of cortical signals in the dentate gyrus. Prog Brain Res 163:577–599.

Ainge JA, Langston RF (2012) Ontogeny of neural circuits underlying spatial memory in the rat. Front Neural Circuits 6:1–10.

Alme CB, Buzzetti RA, Marrone DF, Leutgeb JK, Chawla MK, Schaner MJ, Bohanick JD, Khoboko T, Leutgeb S, Moser EI, Moser M-B, McNaughton BL, Barnes CA (2010) Hippocampal granule cells opt for early retirement. Hippocampus 20:1109–1123.

Altman J, Das GD (1965) Autoradiographic and histological evidence of postnatal hippocampal neurogenesis in rats. J Comp Neurol 124:319–335.

Amaral DG, Cowan WM (1980) Subcortical afferents to the hippocampal formation in the monkey. J Comp Neurol 189:573–591.

Amaral DG, Kurz J (1985) The time of origin of cells demonstrating glutamic acid decarboxylase-like immunoreactivity in the hippocampal formation of the rat. Neurosci Lett 59:33–39.

Carlson GC, Coulter DA (2008) In vitro functional imaging in brain slices using fast voltage-sensitive dye imaging combined with whole-cell patch recording. Nat Protoc 3:249–255.

Chawla MK, Guzowski JF, Ramirez-Amaya V, Lipa P, Hoffman KL, Marriott LK, Worley PF, McNaughton BL, Barnes CA (2005) Sparse, environmentally selective expression of Arc RNA in the upper blade of the rodent fascia dentata by brief spatial experience. Hippocampus 15:579–586.

Clelland CD, Choi M, Romberg C, Clemenson GD, Fragniere A, Tyers P, Jessberger S, Saksida LM, Barker RA, Gage FH, Bussey TJ (2009) A functional role for adult hippocampal neurogenesis in spatial pattern separation. Science 325:210–213.

Cossart R, Ikegaya Y, Yuste R (2005) Calcium imaging of cortical networks dynamics. Cell Calcium 37:451–457.

Coulter DA, Carlson GC (2007) Functional regulation of the dentate gyrus by GABA-mediated inhibition. Prog Brain Res 163:235–243.

Eriksson PS, Perfilieva E, Björk-Eriksson T, Alborn AM, Nordborg C, Peterson DA, Gage FH (1998) Neurogenesis in the adult human hippocampus. Nat Med 4:1313–1317.

Ewell LA, Jones M V (2010) Frequency-tuned distribution of inhibition in the dentate gyrus. J Neurosci 30:12597–12607.

Fricke R, Cowan WM (1977) An autoradiographic study of the development of the entorhinal and commissural afferents to the dentate gyrus of the Rat. J Comp Neurol 173:231–250.

Heinemann U, Beck H, Dreier JP, Ficker E, Stabel J, Zhang CL (1992) The dentate gyrus

as a regulated gate for the propagation of epileptiform activity. Epilepsy Res Suppl 7:273–280.

Hollrigel GS, Ross ST, Soltesz I (1998) Temporal patterns and depolarizing actions of spontaneous GABAA receptor activation in granule cells of the early postnatal dentate gyrus. J Neurophysiol 80:2340–2351.

Ikegaya Y, Aaron G, Cossart R, Aronov D, Lampl I, Ferster D, Yuste R (2004) Synfire chains and cortical songs: temporal modules of cortical activity. Science 304:559–564.

Ishikawa D, Takahashi N, Sasaki T, Usami A, Matsuki N, Ikegaya Y (2010) Fluorescent pipettes for optically targeted patch-clamp recordings. Neural Networks 23:669–672.

Jung MW, McNaughton BL (1993) Spatial selectivity of unit activity in the hippocampal granular layer. Hippocampus 3:165–182.

Langston RF, Ainge JA, Couey JJ, Canto CB, Bjerknes TL, Witter MP, Moser EI, Moser M-B (2010) Development of the spatial representation system in the rat. Science 328:1576–1580.

Leutgeb J, Moser E (2007) Enigmas of the dentate gyrus. Neuron:176–178.

Leutgeb JK, Leutgeb S, Moser M-B, Moser EI (2007) Pattern separation in the dentate gyrus and CA3 of the hippocampus. Science 315:961–966.

Liu X, Ramirez S, Pang PT, Puryear CB, Govindarajan A, Deisseroth K, Tonegawa S (2012) Optogenetic stimulation of a hippocampal engram activates fear memory recall. Nature 484:381–385.

Liu YB, Lio PA, Pasternak JF, Trommer BL (1996) Developmental changes in membrane properties and postsynaptic currents of granule cells in rat dentate gyrus. J Neurophysiol 76:1074–1088.

Lothman EW, Stringer JL, Bertram EH (1992) The dentate gyrus as a control point for seizures in the hippocampus and beyond. Epilepsy Res Suppl 7:301–313.

Lubbers K, Wolff JR, Frotscher M (1985) Neurogenesis of GABAergic neurons in the rat dentate gyrus: a combined autoradiographic and immunocytochemical study. NeurosciLett 62:317–322.

Marín-Burgin A, Mongiat LA, Pardi MB, Schinder AF (2012) Unique processing during a period of high excitation/inhibition balance in adult-born neurons. Science 335:1238–1242.

Nakashiba T, Cushman JD, Pelkey KA, Renaudineau S, Buhl DL, McHugh TJ, Barrera VR, Chittajallu R, Iwamoto KS, McBain CJ, Fanselow MS, Tonegawa S (2012) Young dentate granule cells mediate pattern separation, whereas old granule cells facilitate pattern completion. Cell 149:188–201.

Neunuebel JP, Knierim JJ (2012) Spatial firing correlates of physiologically distinct cell

types of the rat dentate gyrus. J Neurosci 32:3848–3858.

Nitz D, McNaughton B (2004) Differential modulation of CA1 and dentate gyrus interneurons during exploration of novel environments. J Neurophysiol 91:863–872.

Pathak HR, Weissinger F, Terunuma M, Carlson GC, Hsu F-C, Moss SJ, Coulter DA (2007) Disrupted dentate granule cell chloride regulation enhances synaptic excitability during development of temporal lobe epilepsy. J Neurosci 27:14012–14022.

Ribak CE, Peterson GM (1991) Intragranular mossy fibers in rats and gerbils form synapses with the somata and proximal dendrites of basket cells in the dentate gyrus. Hippocampus 1:355–364.

Rickmann M, Amaral DG, Cowan WM (1987) Organization of radial glial cells during the development of the rat dentate gyrus. J Comp Neurol 264:449–479.

Rudy JW, Stadler-Morris S, Albert P (1987) Ontogeny of spatial navigation behaviors in the rat: dissociation of "proximal"- and "distal"-cue-based behaviors. Behav Neurosci 101:62–73.

Sambandan S, Sauer J-F, Vida I, Bartos M (2010) Associative Plasticity at Excitatory Synapses Facilitates Recruitment of Fast-Spiking Interneurons in the Dentate Gyrus. J Neurosci 30:11826–11837.

Sasaki T, Takahashi N, Matsuki N, Ikegaya Y (2008) Fast and accurate detection of action potentials from somatic calcium fluctuations. J Neurophysiol 100:1668–1676.

Scharfman HE, Sollas AL, Smith KL, Jackson MB, Goodman JH (2002) Structural and functional asymmetry in the normal and epileptic rat dentate gyrus. J Comp Neurol 454:424–439.

Schenk F (1985) Development of place navigation in rats from weaning to puberty. Behav Neural Biol 43:69–85.

Schlessinger AR, Cowan WM, Swanson LW (1978) The time of origin of neurons in Ammon's horn and the associated retrohippocampal fields. Anat Embryol (Berl) 154:153–173.

Schmidt-Hieber C, Jonas P, Bischofberger J (2007) Subthreshold dendritic signal processing and coincidence detection in dentate gyrus granule cells. J Neurosci 27:8430–8441.

Seay-Lowe SL, Claiborne BJ (1992) Morphology of intracellularly labeled interneurons in the dentate gyrus of the immature rat. J Comp Neurol 324:23–36.

Seress L, Pokorny J (1981) Structure of the granular layer of the rat dentate gyrus. A light microscopic and Golgi study. J Anat 133:181–195.

Steward O, Scoville SA (1976) Cells of origin of entorhinal cortical afferents to the

hippocampus and fascia dentata of the rat. J Comp Neurol 169:347–370.

Stosiek C, Garaschuk O, Holthoff K, Konnerth A (2003) In vivo two-photon calcium imaging of neuronal networks. Proc Natl Acad Sci U S A 100:7319–7324.

Takano H, McCartney M, Ortinski PI, Yue C, Putt ME, Coulter DA (2012) Deterministic and stochastic neuronal contributions to distinct synchronous CA3 network bursts. J Neurosci 32:4743–4754.

Tamamaki N, Nojyo Y (1993) Projection of the entorhinal layer II neurons in the rat as revealed by intracellular pressure-injection of neurobiotin. Hippocampus 3:471–480.

van Groen T, Miettinen P, Kadish I (2003) The entorhinal cortex of the mouse: Organization of the projection to the hippocampal formation. Hippocampus 13:133–149.

van Praag H, Schinder AF, Christie BR, Toni N, Palmer TD, Gage FH (2002) Functional neurogenesis in the adult hippocampus. Nature 415:1030–1034.

Vogelstein JT, Watson BO, Packer AM, Yuste R, Jedynak B, Paninski L (2009) Spike inference from calcium imaging using sequential Monte Carlo methods. Biophys J 97:636–655.

Woodson W, Nitecka L, Ben-Ari Y (1989) Organization of the GABAergic system in the rat hippocampal formation: a quantitative immunocytochemical study. J Comp Neurol 280:254–271.

CHAPTER 4: Massively augmented hippocampal dentate granule cell activation accompanies epilepsy development.

Abstract

In a mouse model of temporal lobe epilepsy, multicellular calcium imaging revealed that disease emergence was accompanied by massive amplification in the normally sparse, afferent stimulation-induced activation of hippocampal dentate granule cells. Patch recordings demonstrated reductions in local inhibitory function within the dentate gyrus at time points where sparse activation was compromised. Mimicking changes in inhibitory synaptic function and transmembrane chloride regulation was sufficient to elicit the dentate gyrus circuit collapse evident during epilepsy development. Pharmacological blockade of outward chloride transport had no effect during epilepsy development, and significantly increased granule cell activation in both control and chronically epileptic animals. This apparent occlusion effect implicates reduction in chloride extrusion as a mechanism contributing to granule cell hyperactivation specifically during early epilepsy development. Glutamine plays a significant role in local synthesis of GABA in synapses. In epileptic mice, sparse granule cell activation could be restored by glutamine application, implicating compromised GABA synthesis. Glutamine had no effect on granule cell activation earlier, during epilepsy development. We conclude that compromised feedforward inhibition within the local circuit generates the massive dentate gyrus circuit hyperactivation evident in animals during and following epilepsy development. However, the mechanisms underlying this disinhibition diverge significantly as epilepsy progresses.

Introduction

Situated as the initial component of the canonical trisynaptic circuit, the dentate gyrus (DG) is a critical entry point to the hippocampus, regulating access of cortical input to the limbic system. Essential to this role are the sparse, selective activation properties of the DG's principal cells, dentate granule cells (DGCs). *In vivo* recording studies have demonstrated that these neurons exhibit spatially selective firing in extremely small populations (Jung and McNaughton, 1993b; Leutgeb et al., 2007; Neunuebel and Knierim, 2012). Moreover, studies examining immediate-early-gene expression, a molecular readout for sustained neuronal activity, have described exceptionally sparse labeling in DGCs, even after exposure to multiple environments or spatial cognitive tasks (Chawla et al., 2005; Alme et al., 2010).

This characteristic, sparse activation of DGCs is thought to enable them to participate in the execution of cognitive functions such as pattern separation and novelty detection (Jung and McNaughton, 1993b; Bakker et al., 2008). The propensity for DGCs to generate action potentials (APs) is tightly constrained by cell-intrinsic biophysical properties (Fricke and Prince, 1984; Staley et al., 1992; Krueppel et al., 2011) and robust local inhibitory control (Buzsáki, 1984; Coulter and Carlson, 2007; Pardi et al., 2015), culminating in a population of neurons that are extremely reluctant to activate (Heinemann et al., 1992). However, the circuit mechanisms defining how the few responsive DGCs are recruited during cognitive tasks remain unknown.

A secondary consequence of the DG's low excitability is its ability to restrict the relay of pathological, synchronous cortical activity into downstream hippocampal and limbic structures, regulating seizure activity in diseases such as epilepsy - a phenomenon termed 'dentate gating' (Lothman et al., 1991; Heinemann et al., 1992). Artificially

inducing failure of normal DG gating is sufficient to induce seizure generation and propagation (Krook-Magnuson et al., 2015). DG circuit properties are significantly disrupted in humans with epilepsy and in animal models of the disorder. Alterations include sprouting of recurrent mossy fiber synapses (Tauck and Nadler, 1985), molecular and cellular alterations of local inhibitory circuits (Kobayashi and Buckmaster, 2003; Zhang et al., 2009; Yu et al., 2013b; Sun et al., 2014; Buckmaster et al., 2016), aberrant neurogenesis (Parent et al., 1997), astrocytic gliosis (Eid et al., 2004), and alterations in the intrinsic properties of DGCs (Bender et al., 2003). This aggregation of cellular and circuit changes in the DG accompanying epilepsy development has generated a prevalent hypothesis that its normal gating function is compromised, and this, in turn, may contribute to increased seizure propensity. However, to date, DG gate failure has primarily been described using field potential recordings, which are not cell specific and do not identify cellular mechanisms underlying this epilepsy-associated circuit collapse.

In the present study, we used multicellular calcium imaging (MCI) to investigate possible alterations in DG circuit activation properties during and following epilepsy development in a mouse-pilocarpine model of temporal lobe epilepsy. We report that epilepsy development was accompanied by massive augmentation in the normally sparse activation of DGCs. Whole-cell patch recordings demonstrated reductions in local DG inhibitory function at time points when sparse activation was compromised. Pharmacologically mimicking changes in inhibitory receptor function in control slices was sufficient to reproduce the DG circuit collapse evident in epileptic animals. Chloride extrusion blockade elevated DGC activation in control and epileptic animals, but these effects were occluded early during the epilepsy development, suggesting altered transmembrane chloride gradients may contribute to hyperexcitability specifically at this time point. Finally, metabolic reversal of astrogliosis-mediated disinhibition in slices

from chronically epileptic animals restored normal DGC activation. We conclude that the massive circuit hyperactivation evident in animals during and following epilepsy development is generated in large part by compromised local circuit inhibition, but the underlying contributory mechanisms mediating this disinhibition differ at these varying time points.

Results

Changes in DGC activation during epileptogenesis

To assess changes in aggregate DG network activation during epileptogenesis, we assayed DGC proportional activation in response to perforant path (PP) stimulation using MCI in slices from control animals, and at several time points following status epilepticus (SE). MCI exploits the finding that the strong depolarization during APs induces activation of high-threshold Ca^{2+} channels. Because of this, a Ca^{2+} influx into neuronal somata occurs only during spiking, and not in response to subthreshold depolarizations. Bulk-loading cell populations with Ca^{2+}-sensitive indicators transduces these AP-induced Ca^{2+} influxes into fluorescence changes and allows dynamic imaging-based assessment of APs in large neuronal populations with single-cell resolution (Cossart et al., 2005; Takano et al., 2012; Yu et al., 2013a). We previously showed that Oregon Green BAPTA-1 (OGB), used in this study, is capable of detecting single APs in hippocampal neurons (Takano et al., 2012; Yu et al., 2013a). Use of a swept field confocal microscope capable of frame rates up to 400 Hz enhances the temporal resolution of these MCI recordings (Takano et al., 2012; Yu et al., 2013a).

In response to moderate and strong PP stimulation (100 and 400 μA, ~60% and 100% maximal fEPSP [**Fig. 4.1**]), slices prepared from control animals (control slices) displayed extremely sparse DGC proportional activation, typical of activity observed *in*

vivo (**Fig. 4.4a-c**), with only 4% and 21% of DGCs responding, respectively. Subconvulsive pilocarpine treatment and/or electrode implantation had no effect on DGC activation (**Fig. 4.2**). Sparse activation deteriorated significantly following status epilepticus (SE; Kruskal-Wallis test, $p < 0.0001$). At 3-7 days post-SE, activation was significantly higher, with 57% and 82% of DGCs responding ($p = 0.0006$ and $p < 0.0001$, respectively), indicating an immediate, massive collapse in the normally sparse activation of DGCs. By 14 days post-SE, a time point when ~80% of mice have become epileptic (**Fig. 4.3**), proportional activation recovered to levels indistinguishable from controls, with only 13% and 43% of DGCs responding ($p > 0.9999$ and $p = 0.9082$). Subsequently, DGCs exhibited a secondary, permanent deterioration in sparse activation evident at 2-3 and 6 months post-SE, with 54% and 81% ($p = 0.0001$ and 0.0023) and 54% and 91% ($p = 0.0034$ and 0.0003) of cells responding to 100 and 400 μA stimulation, respectively **(Fig. 4.4 a-c)**. By the time this secondary collapse occurred, all animals had developed epilepsy (**Fig. 4.3**).

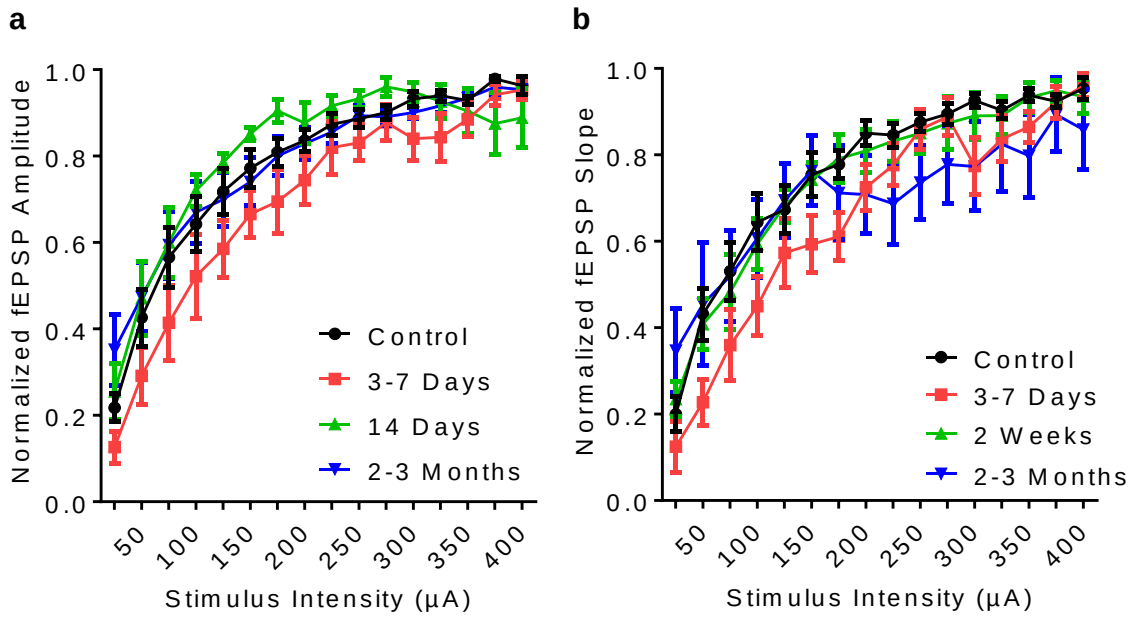

Figure 4.1. Input-output relationships of perforant path stimulation during epileptogenesis. To assess the input-output relationship of stimulus intensity to DG stimulus response in DG dendrites during epileptogenesis, we conducted extracellular field recordings with our recording electrode placed in the middle third of the molecular layer and recorded responses to single 200 µs electrical stimuli applied to the angular bundle of the perforant path approximately 100 µm away from the DG molecular layer. **a**, fEPSP amplitudes normalized to maximal value plotted against stimulus intensity. Input-output relationships following pilocarpine-SE were not significantly different from controls. (2-way ANOVA, F (45,400) = 0.7478, p=0.8842). **b**, fEPSP slope normalized to maximal value plotted against stimulus intensity. Input-output relationships were not significantly different from controls following pilocarpine-SE. (2-way ANOVA, F (45,336) = 0.6979, p=0.9293). n (slices): Control n = 9; 3-7 days, n = 4; 14 days, n = 6, 2-3 months, n= 6. Slices prepared from at least 3 animals.

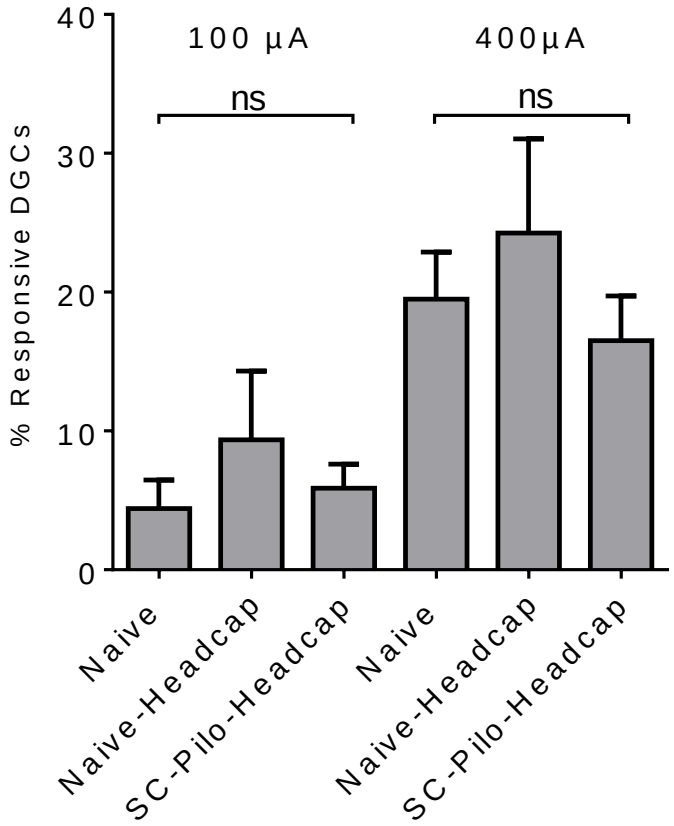

Figure 4.2. EEG-instrumentation (headcaps) and sub convulsive pilocarpine treatment do not alter DGC responsiveness. Proportional activation of DGC% in slices prepared from naïve control mice, naïve mice implanted with recording headcaps, and mice subjected to subconvulsive pilocarpine (30mg/kg pilocarpine (10%) dose and 2.5 mg/kg diazepam quelling) implanted with recording headcaps, 100 µA (left) and 400 µA (right) PP stimulation. Samples sizes as (n [slices], replicates [mice], total number cells [ROIs]): Control: (11, 5, 557), Naïve-headcap: (5, 3, 251); SC-Pilo-Headcap: (7, 3, 255). ANOVA, 100 µA: $F[2,20] = 0.7769$, $p = 0.4732$; 400 µA: $F[2,20] = 0.6704$, $p = 0.4732$. Histograms indicate mean ± S.E.M.

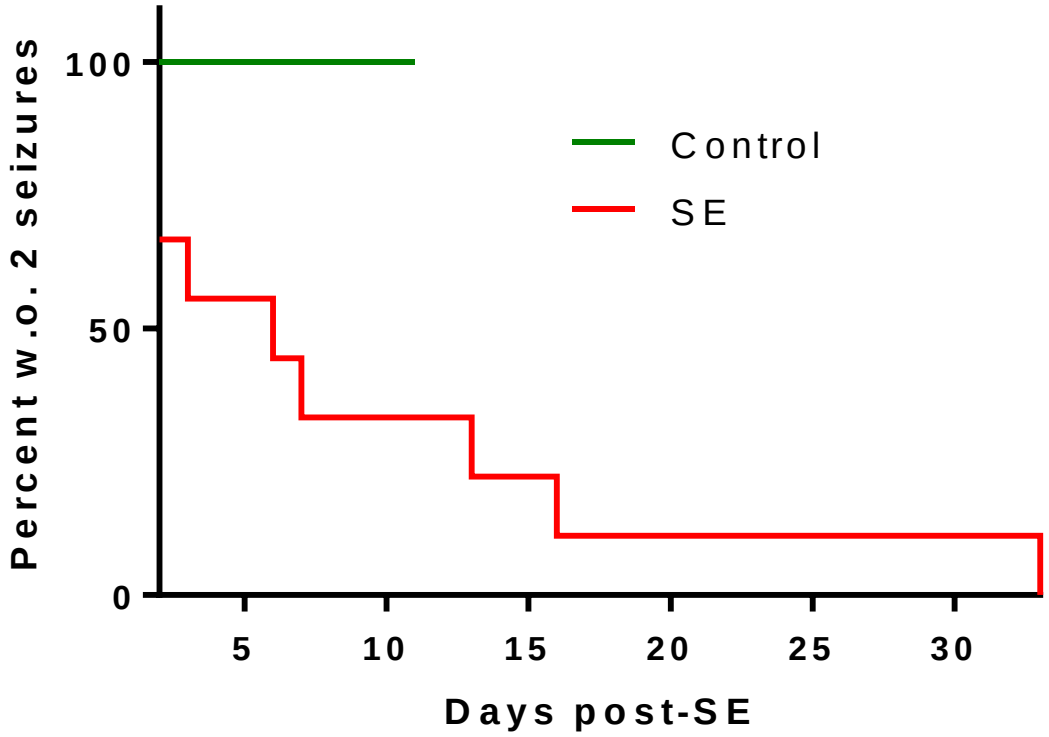

Figure 4.3. Meier Kaplan survival curve depicting epilepsy onset in pilocarpine treated mice. Epilepsy onset is defined as day on which 2nd recurrent, spontaneous, seizure occurred, excluding the first 2 days following SE in which some acute post-SE seizures were noted. By 8 days post SE, 50% of SE mice were confirmed as epileptic and all mice became epileptic by day 33, n = 9 pilocarpine treated mice. Control mice (naïve headcapped, n = 3, and subconvulsive pilocarpine treated -headcapped mice, n = 3) exhibited no seizures in 11 days of recordings, total n = 6.

To ensure all DGCs in our analysis were capable of activating, and that there were no variations in slice viability across different experimental groups following SE, we applied a saturating concentration of the $GABA_A$ antagonist, picrotoxin (PTX, 50 μM), at the end of each experiment and assessed DGC activation in response to a 400 μA tetanic stimulus (10 pulses, 60 Hz). We limited analysis to viable neurons, defined as neurons that exhibited stimulus-evoked Ca^{2+} transients under these conditions. Inactive cells were assumed to be either deafferented or not viable. Inhibitory blockade combined with strong stimulation resulted in activation of nearly all DGCs (>90%) in each group (**Fig. 4.4c**), indicating that the vast majority of DGCs in our preparations were viable, had not been deafferented, and were capable of firing APs. There were no significant differences in DGC activation between groups in the presence of PTX (Kruskal-Wallis test, $p = 0.17$), indicating consistent levels of slice viability.

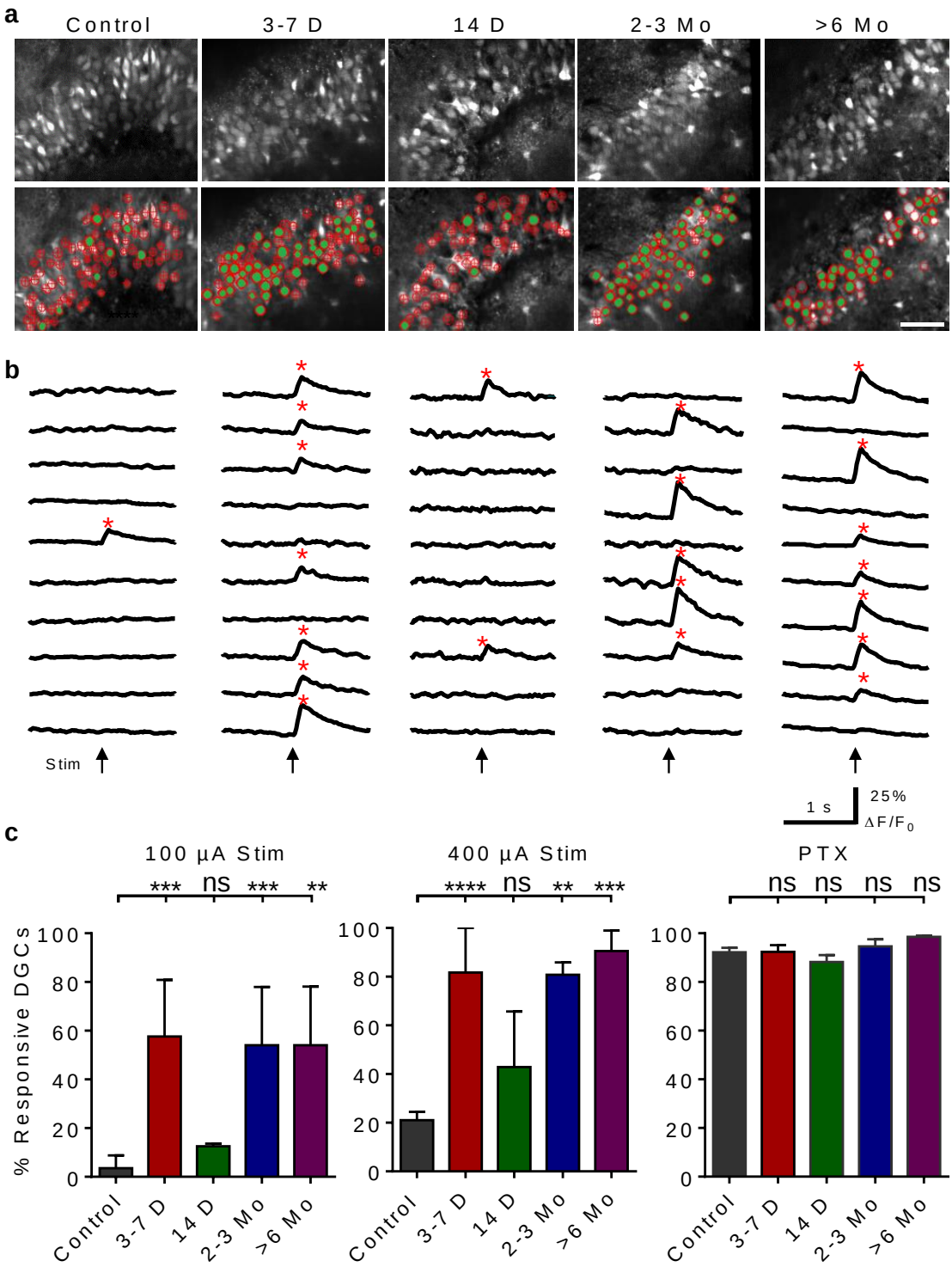
a
Control
3-7 D
14 D
2-3 Mo
>6 Mo
b
Stim
1 s
25%
ΔF/F0
c
100 µA Stim
400 µA Stim
PTX
*** ns *** **
**** ns ** ***
ns ns ns ns
% Responsive DGCs
0
20
40
60
80
100
Control
3-7 D
14 D
2-3 Mo
>6 Mo

Figure 4.4. Changes in DGC activation during epileptogenesis. **a**, Confocal micrographs of OGB-1-loaded DGCs from control mice and at defined time-points post-SE. Below are same images with overlaid ROIs depicting non-activating (hollow red ROIs) and activating DGCs (red ROIs filled green) in response to 100 µA PP stimulation. Scale bars: 50 µm. **b**, Representative traces of time-resolved calcium imaging responses from representative ROIs selected from images above**.** Arrows below traces indicate the time of stimulation. *** (red)** denote cellular activation detected with Ca^{2+} transient detection software. **c**, Plots of the proportional DGC activation (%) to 100 µA (left) and 400 µA (middle) PP stimulation, as well as 400 µA stimulation in the presence of 50 µM PTX (right). Note the significantly augmented DGC activation at 3-7 days, 2-3 months and >6 months post-SE compared to Controls. Samples sizes as (n [slices], replicates [mice], total number cells [ROIs]): Control: (23,9,1020); 3-7 Days: (9,6,517); 14 days: (7,3,405); 2-3 Months: (8,3,443); 6 Months: (6,3,372). Kruskal-Wallis test with Dunn's multiple-comparison *post hoc* testing, left and center are log(value+1) transformed to equalize variance before statistical testing, 100µA: $H(4,48) = 32.74$; 400µA: $H(4,48) = 35.49$, PTX $H(4,48) = 6.418$. Levels of significance indicated as: ns $p > 0.05$, * $p < 0.05$, ** $p < 0.01$, *** $p < 0.001$, **** $p < 0.0001$. Histograms indicate median ± interquartile range.

Taken together, these data demonstrate a novel, trimodal 10-20 fold elevation in DGC excitability during epilepsy development and expression. DGCs transition from a sparsely activating network in controls to one that collapses rapidly following SE. Normal activation recovers transiently, and then exhibits a secondary - likely permanent - collapse towards hyperexcitability as epilepsy manifests.

Alterations in amplitudes of evoked Ca^{2+} transients during epileptogenesis

In addition to changes observed in proportional DGC activation, we also noted significant alterations in stimulus-elicited Ca^{2+} transient amplitudes (normalized as % $\Delta F/F_0$) during epileptogenesis **(Fig. 4.4b)**. Neuronal Ca^{2+} transient amplitudes correlate closely with the number of APs fired by a cell (Takano et al., 2012; Yu et al., 2013a). These changes may capture alterations in the spike firing patterns in DGCs post-SE.

In response to 100 μA stimulation, DGCs in control slices had a median Ca^{2+} transient amplitude of 5.2% $\Delta F/F_0$ (**Fig. 4.5a**). Responses of this magnitude are the smallest seen in this study, and likely indicate firing of single APs. In order to assess this, we conducted juxtacellular patch recordings in active, control DGCs, determined that they were firing single APs, and found the mean Ca^{2+} transient amplitude in these neurons to be 6.6 ± 0.5% $\Delta F/F_0$ (n = 13 cells, data not shown). This was consistent with single AP firing in the control population MCI studies. The amplitudes of cellular responses were altered significantly following SE (Kruskal-Wallis test, $p < 0.0001$). At 3-7 days post-SE, Ca^{2+} transient amplitudes were significantly larger than control responses (median = 9.8% $\Delta F/F_0$, $p = 0.0019$), with the entire distribution shifted towards larger events (**Fig. 4.5a**). Lower transient amplitudes were restored 14 days

post-SE (median = 6.43% $\Delta F/F_{0,}$ p = > 0.9999). However, at 2-3 and > 6 months post-SE, transient amplitudes were increased significantly again compared to control levels (2-3 months median = 12.3% $\Delta F/F_0$, p < 0.0001; >6 months median = 10.1%, p = 0.0002). Combined juxtacellular patch recordings and MCI in 2-3 month post-SE DGCs determined that single AP Ca^{2+} transients in DGCs from epileptic animals had amplitudes of 10.93 ± 1.23% ΔF/F0 (significantly larger than controls, unpaired, Welch-corrected t-test, t(14,60)=3.253, p = 0.0055). One possible alternate contributor to larger Ca^{2+} transient amplitudes post-SE may be altered Ca^{2+} buffering in DGCs. SE down-regulates expression of calbindin, an endogenous Ca^{2+} buffering protein present in DGCs (Tang et al., 2006) that strongly reduces global Ca^{2+} signals in neurons (Müller et al., 2005). Reduced DGC-calbindin expression may contribute to the increased signal amplitudes observed during epileptogenesis. The combined juxtacellular/imaging data described above suggests that this might be the case, as opposed to the alternative explanation of DGCs firing more APs in response to afferent stimulation.

For each group, we also measured Ca^{2+} transient amplitudes following supramaximal stimulation (400 μA, **Fig. 4.5b**) and compared the results to those from moderate (100 μA) stimulation. Stronger stimulation failed to elicit significantly larger Ca^{2+} signals in control slices (medians for 100/400 μA: 5.2%/6.6% $\Delta F/F_0$, p = 0.2575, significance set at p = 0.001 *a priori*), demonstrating the DG's ability to restrict further activation of DGCs. However, supramaximal stimulation was sufficient to elicit significantly larger Ca^{2+} transients 3-7 days post-SE (medians for 100/400 μA: 9.8/13.6% $\Delta F/F_0$, p < 0.0001), suggesting that the stronger stimulus generated more APs from responsive DGCs or, alternatively, that APs were broadened with supramaximal stimulation. This effect was also evident 14 days post-SE (medians for 100/400 μA: 6.4%/10.4% $\Delta F/F_0$, p < 0.0001).

Interestingly, there was no significant difference in Ca^{2+} transient amplitudes elicited by 100 and 400 μA stimulation 2-3 months post-SE (medians for 100/400 μA: 12.33/12.68% $\Delta F/F_0$, p = 0.0520). Finally, at >6 months post-SE, stronger stimulation produced a significant shift in response amplitudes to values much higher than any other groups in our study (Medians for 100/400 μA: 10.2/19.7% $\Delta F/F_0$, p = 0.0001). Responses of this magnitude may reflect network burst activity within the epileptic DG. Such activity may be generated in slices prepared from chronically epileptic animals as a result of the well-established recurrent mossy fiber sprouting present in models of epilepsy.

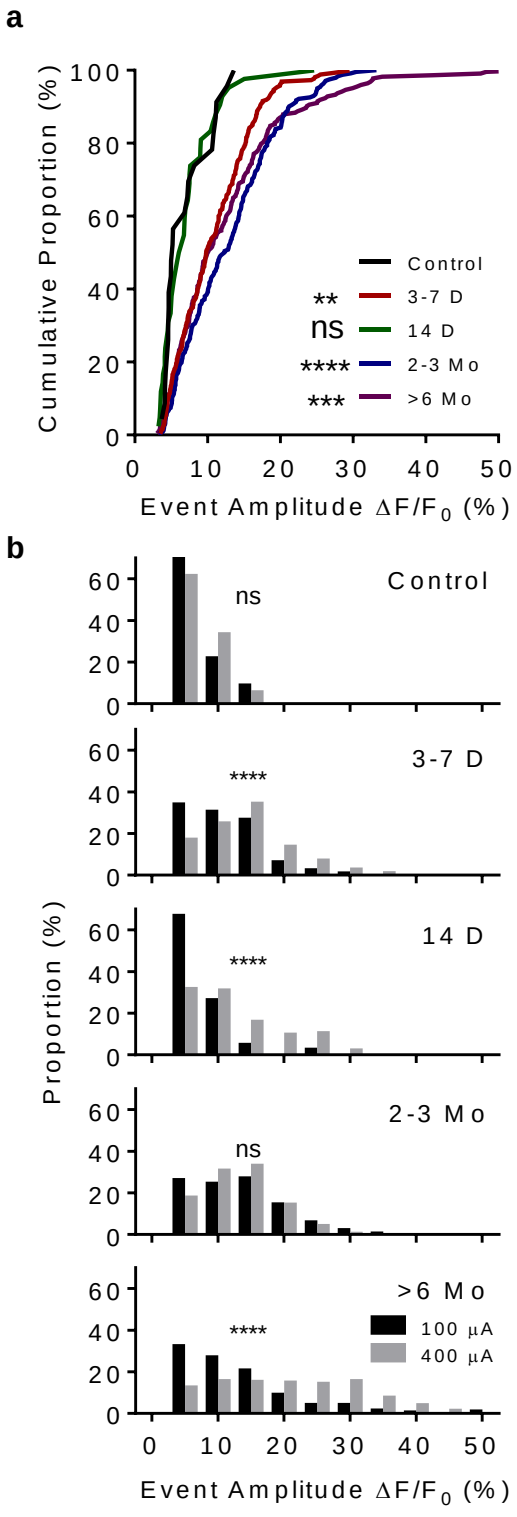
a
Cumulative Proportion (%)
100
80
60
40
20
0
0
10
20
30
40
50
Event Amplitude ΔF/F0 (%)
Control
3-7 D
14 D
2-3 Mo
>6 Mo
**
ns
****
***
b
Proportion (%)
Control
ns
3-7 D
****
14 D
****
2-3 Mo
ns
>6 Mo
****
100 µA
400 µA
60
40
20
0
0
10
20
30
40
50
Event Amplitude ΔF/F0 (%)

Figure 4.5. Alterations in evoked Ca2+ transient amplitudes during epileptogenesis. **a**, Cumulative proportion distribution of 100 µA stimulus-evoked Ca^{2+} transient amplitudes ($\Delta F/F_0$) during epileptogenesis (Kruskal-Wallis test with Dunn's multiple-comparison *post hoc* testing against controls, $H(4,27) = 56.5$, $p < 0.0001$). Note the significantly increased Ca^{2+} transient amplitudes at time points corresponding to augmented DGC activation (3-7 days, 2-3 months and >6 months). **b**, Histograms comparing distributions of 100 and 400 µA stimulus evoked Ca^{2+} transients at each time point during epileptogenesis. Kolmogorov-Smirnov test, 100 vs. 400 µA, Control: $D(32) = 0.2319$; 3-7 Days: $D(605) = 0.2542$; 14 Days; $D(186) = 0.4093$, 2-3 Months: $D(534) = 0.052$; >6 Months: $D (552) = 0.3974$. Sample sizes for (**a**, **b**) as (n = number OGB transients for 100/400 µA stimuli, slices, mice): Control (23/111, 11, 5); 3-7 Days (260/347,6,3); 14 days (42/146,7,3); 2-3 Months (242/294,8,3); >6 Months (223/331,6,3). Levels of significance indicated as: ns $p > 0.05$, * $p < 0.05$, ** $p < 0.01$, *** $p < 0.001$, **** $p < 0.0001$.

Location of responsive DGCs within the granule cell layer

The DG is a unique brain structure in that it continuously generates new, functional neurons throughout life (van Praag et al., 2002). Adult-born DGCs have temporally evolving electrophysiological properties distinct from their mature counterparts. Some studies suggest that these newborn cells may be activated preferentially compared to mature DGCs (Alme et al., 2010; Marín-Burgin et al., 2012). New DGCs are born in the DG's sub-granular proliferative zone, and even after maturing and establishing connectivity within the DG, typically remain confined to the inner portion of the granule cell layer (GCL). We validated this preferential localization using a transgenic approach. **Fig. 4.6a** is a representative confocal micrograph of a 7 week old TdTomato-expressing adult-born DGC in a slice prepared from a Gli1-Cre^{ERT} x Rosa-TdTomato mouse, which "birthdates" DGCs with the fluorescent marker TdTomato in a tamoxifen-inducible Cre-recombinase system (Scobie et al., 2009). This cell is located near the inner GCL/hilar border; its location was stereotypic. We analyzed 13 imaging fields in slices prepared from control mice 7 weeks following tamoxifen-TdTomato birth-dating of DGCs, and found that 33/34 newborn cells were localized to the inner half of the GCL.

Pilocarpine-induced SE greatly increased DGC neurogenesis (**Fig. 4.6b**). We analyzed 4 imaging fields from slices prepared from post-SE mice 7 weeks after tamoxifen-induced TdTomato DGC birthdating, and found that 327/373 of these newborn cells were localized to the inner half of the GCL. Since we used MCI to study granule cell activation exclusively in normotopic neurons within the granule cell layer, we restricted our analysis of activation position to the granule cell layer—the only region in which we had activation data. The location of Td-Tomato labeled cells within the GCL was similar in control and epileptic animals (Fisher's exact test, $p = 0.7099$). Although

this was our initial intent, we were unable to assess directly responses of Gli1-Cre^{ERT} birth-dated DGCs using MCI post-SE. Gli1-Cre^{ERT}xRosa-TdTomato mice did not survive pilocarpine-induced SE in sufficient numbers to be useful in our MCI studies, possibly due to some unknown effect of transgene insertion.

To assess the possible contribution of newborn DGCs to overall responses in an indirect manner, we examined the location of active cells within the granule cell layer, and compared this to the total number of DGCs, generating a proportional activity/cell location plot. **Fig. 4.6c** depicts the distribution of locations (plotted as % distance from the inner to outer GCL border) corresponding to DGCs activated in response to a 100 μA stimulus, as well as the location of all measured regions of interest (ROIs). There was no significant difference between these two distributions in slices prepared from control animals (active and total medians, 41%, and 41%, respectively, $p = 0.3281$), suggesting that newborn DGCs within the GCL do not activate disproportionally in comparison to the rest of the DGC population. Similarly, in slices prepared from epileptic mice >2 months post-SE, the distribution of responsive DGCs did not differ significantly from the entire population of imaged cells (active and total medians 49% / 47%, respectively, $p = 0.9393$), again suggesting that the activity of GCL DGCs generated after SE also did not contribute disproportionately to overall cellular activation (**Fig. 4.6d**).

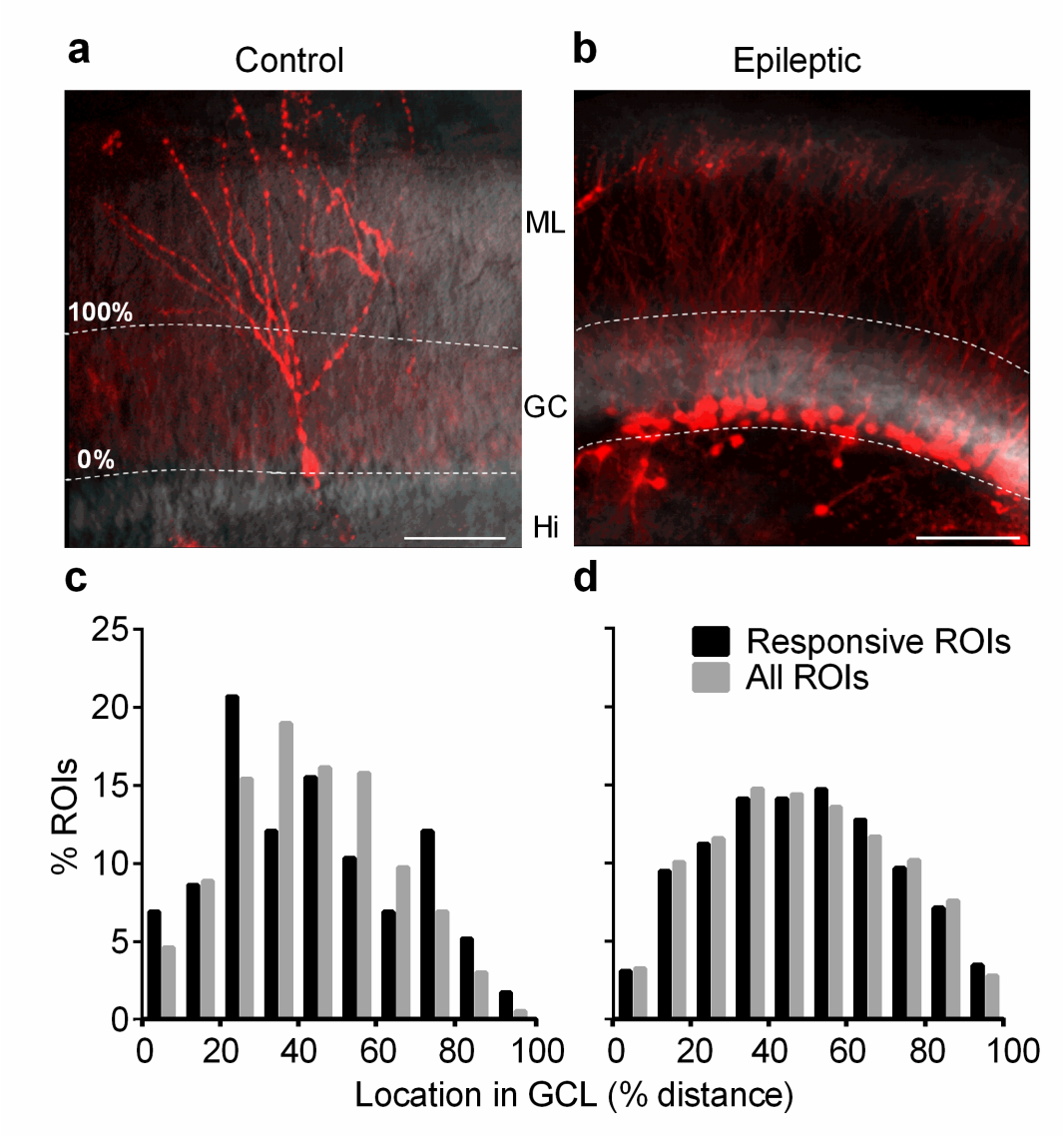
a
Control
b
Epileptic
ML
GC
Hi
100%
0%
c
d
Responsive ROIs
All ROIs
% ROIs
25
20
15
10
5
0
0
20
40
60
80
100
Location in GCL (% distance)

Figure 4.6. Location of responsive DGCs within the GCL. Confocal micrograph of birthdated, TdTomato-expressing, adult-born DGCs in Gli1-Cre^{ERT} x Rosa-TdTomato crossed mice. **a**, Adult-born DGC labeled 7 weeks following 1 week of tamoxifen administration (7 d, 1/d, 150 mg/kg, I.P.) in naive animal. Scale bar: 100 microns. **b,** Adult-born DGCs labeled 7 weeks after 1 week of tamoxifen administration (7 d, 1/d, 150 mg/kg, I.P.) immediately following pilocarpine-induced status epilepticus. Note, that in both control and epileptic slices, newborn DGCs are restricted to the inner portion of the molecular layer. White dashed lines indicate the boundaries of the granule cell layer with molecular layer (ML), granule cell layer (GC) and Hilus (Hi) labeled in center. **c**, Histogram of responsive DGC locations and all DGC (responsive and non-responsive) locations within GCL in control slices; there was no significant difference between location distributions (Kolmogorov-Smirnov test, D (620) = 0.1132, p = 0.3281). Number of cells (Responsive/Total): n = 83/589 cells from 5 mice. **d**, Histogram of cell locations from epileptic slices; there was no significant difference between location distributions (Kolmogorov-Smirnov test, D (1257) = 0.02967, p = 0.9393) n = 338/855 cells from 6 mice.

Juxtacellular recordings of DGCs during epileptogenesis.

The identity and proportion of cells that fire APs when a circuit is activated are critical aspects of appropriate neural circuit function, regulating information processing. Precise activation latency time-locked to an afferent stimulus also retains specific information about the temporal properties of the stimulus and is a critical component of information coding in a circuit. Both cell-intrinsic integrative properties of DGCs (Schmidt-Hieber et al., 2007; Krueppel et al., 2011) and activation of extensive feedforward and feedback inhibitory circuits (Coulter and Carlson, 2007; Ewell and Jones, 2010) determine DGC activation latencies. As such, possible alteration in DGC activation latency during epileptogenesis may reflect degraded information processing within the circuit, and may provide insight into network determinants of DG dysfunction associated with epilepsy development.

To assess directly the temporal properties of DGC activation during epileptogenesis, we conducted MCI-guided juxtacellular patch recordings of DGCs activating in response to afferent stimulation. Since DGC activation can be extremely sparse, particularly in control slices, we employed MCI to identify activating DGCs with reliable stimulus-elicited Ca^{2+} transients, and targeted our juxtacellular patch recordings to those cells (**Fig. 4.7a**). In control slices, DGCs responding to PP stimulation activated with an AP latency of 7.28 ± 0.50 ms (**Fig. 4.7b**). Early following SE, AP latency was significantly reduced to 5.82 ± 0.23 ms (3-7 days, ANOVA $p = 0.0083$, with Dunnett's multiple-comparisons test *post hoc,* $p = 0.0217$). Later following SE, AP latency averaged 6.94 ± 0.52 ms (14 days, not significantly different from control, $p > 0.8938$). Two months post-SE, AP latency decreased to 5.65 ms ± 0.35 (significantly reduced from control levels, $p = 0.0149$). Time points post-SE with significantly altered AP latencies also were time points in which sparse DGC firing had collapsed.

We have shown previously that both proportional activation of DGCs and the temporal windows in which APs are generated are significantly influenced by local inhibitory function (Yu et al., 2013a). To understand the role of local GABAergic inhibition in determining DGC AP latency, we applied 50 μM PTX to our preparations. As seen in **Fig. 4.4c**, PTX significantly increases proportional DGC activation, so we did not restrict our analysis to only cells activating in the absence of PTX. Inhibitory blockade significantly reduced control DGC AP latencies to 5.18 ± 0.83 ms (unpaired t-test, $t(28) = 3.673$, $p = 0.0010$), a reduction of 29% (**Fig. 4.7c**). This suggests that disynaptic feedforward interneurons may respond with sufficient rapidity to alter the onset kinetics of monosynaptic EPSPs, resulting in delay or prevention of DGC activation. This constitutes a surprising role for feed-forward inhibitory circuitry in the DG. This form of inhibition is typically thought to decrease jitter in AP activation in its targets, not to delay or prevent firing (Pouille and Scanziani, 2001; Higley and Contreras, 2006).

At 3-7 days post-SE, we found that inhibitory blockade did not significantly reduce AP latencies compared to normal ACSF (ACSF mean, 5.82 ± 0.23 ms; 50 μM PTX mean, 5.00 ± 0.36 ms (unpaired t-test, $t(36) = 1.974$, $p = 0.0561$; **Fig. 4.7b&c**). That inhibitory blockade failed to affect AP latency at 3-7 days post-SE suggests either that there is diminished feedforward inhibition or that chloride reversal changes could make GABA less effective. Consistent with this latter hypothesis, blockade of chloride extrusion in control slices, using the KCC2-selective transporter blocker, R-(+)-[(2-*n*-Butyl-6,7-dichloro-2-cyclopentyl-2,3-dihydro-1-oxo-1H-inden-5-yl)oxy]acetic acid (DIOA), mimicked this AP latency decrease seen in 3-7 day post-SE animals [from 7.28 ± 0.49 ms in ACSF to 5.85 ± 0.28 ms in the presence of DIOA (unpaired, Welch-corrected t-test, $p = 0.0192$, control: $n = 16$; DIOA: $n = 14$, $t(23.14) = 2.516$), data not shown]. At 14 days

post-SE, there was no difference in AP latency compared to controls. However, PTX failed to reduce AP latencies significantly when compared to control ACSF (Control ACSF mean 6.95 ± 0.51 ms, PTX mean 7.294 ± 1.01 ms, unpaired t-test, $t(23) = 0.3348$, $p = 0.7408$; **Fig. 4.7**). There was, however, a significant difference between the normalized relative effects of PTX between control mice and mice 14 days post-SE; in control slices, PTX reduced AP latencies by 28.81 ± 3.06%, while it increased AP latency 5.10 ± 14.58% in slices 14 days post-SE (one-way ANOVA, with *post hoc* Dunnett's test, $p = 0.0102$; **Fig. 4.7c**). Two months following SE, PTX had a paradoxical effect: it caused a significant increase in AP latency from 5.66 ms ± 0.035 in control ASCF to 6.86 ± 0.319 ms in PTX (unpaired t-test, $t(29) = 2.502$, $p = 0.0183$; **Fig. 4.7b&c**). This PTX-induced increase in AP latency could be consistent either with excitatory actions of GABA, or with disinhibition-induced unmasking of polysynaptic excitatory inputs onto DGCs through the recurrent mossy fiber network present in epileptic animals (Tauck and Nadler, 1985).

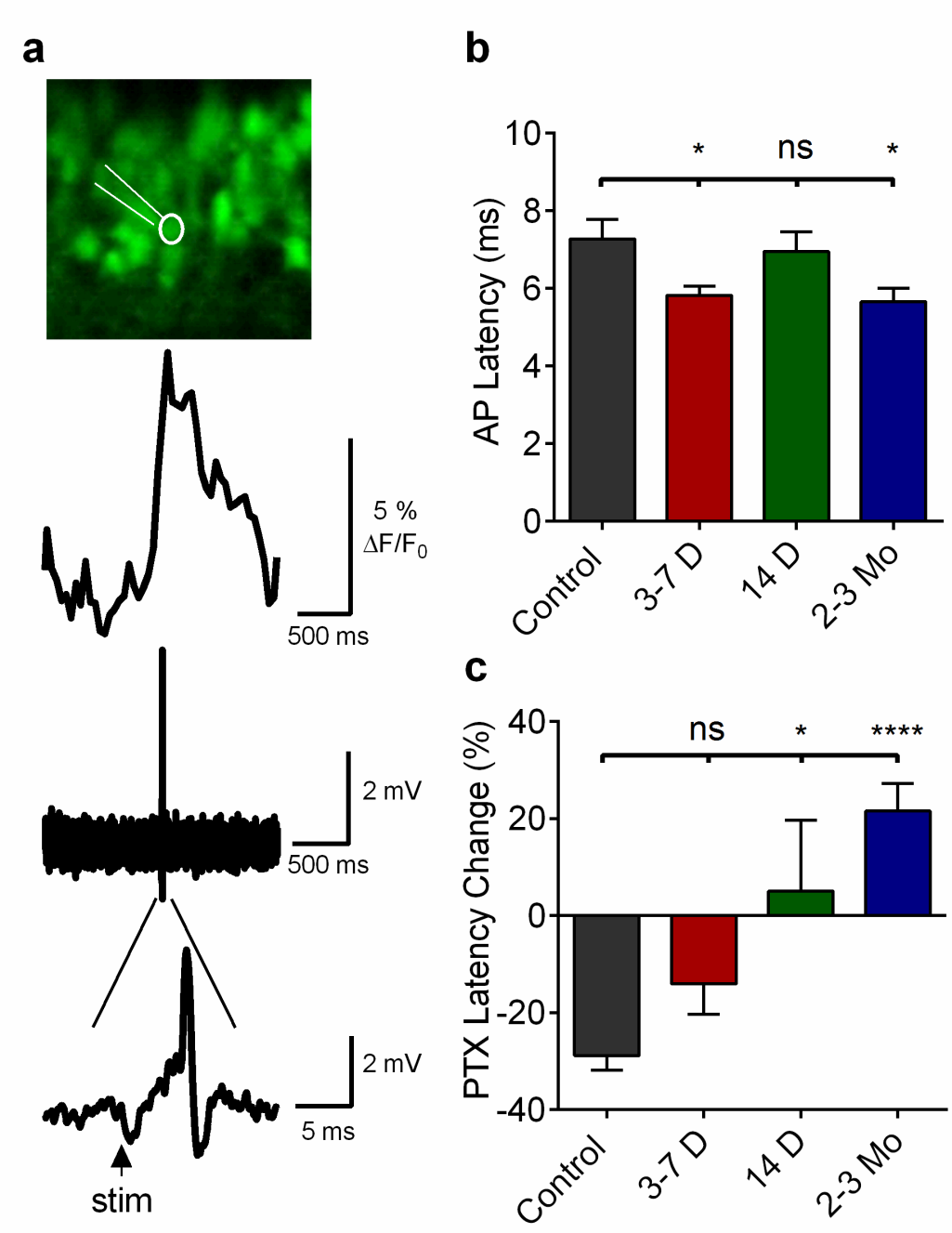
a
5 %
ΔF/F0
500 ms
2 mV
500 ms
2 mV
5 ms
stim
b
AP Latency (ms)
10
8
6
4
2
0
*
ns
*
Control
3-7 D
14 D
2-3 Mo
c
PTX Latency Change (%)
40
20
0
-20
-40
ns
*
****
Control
3-7 D
14 D
2-3 Mo

Figure 4.7. Juxtacellular recordings from active DGCs during epileptogenesis. **a**, Top, confocal micrograph of DGCs loaded with OGB-1 in a slice prepared from a control mouse. Highlighted white is a fluorescently labeled micropipette (Alexa-488 Conjugated BSA) juxtacellularly attached to an activating DGC in a slice prepared from a control mouse. Middle, Ca^{2+} imaging transient elicited by 400 µA PP stimulus. Bottom, juxtacellular-patch recording in which individual APs can be resolved, with expanded timescale presented below depicting the latency between stimulus and AP onset can be resolved. **b**, AP latencies obtained from juxtacellular recordings of DGCs activating in response to a 400 µA PP stimulus in slices prepared from mice at several time points post-SE. Note the significant reduction in AP latency at 3-7 days and 2-3 months post-SE compared to controls. One-way ANOVA, $F(3,66) = 4.247$, $p = 0.0083$, with Dunnett's multiple-comparison *post hoc* testing. Levels of significance: ns $p > 0.05$, * $p < 0.05$, **** $p < 0.0001$ **c**, Change in AP latencies (%) with picrotoxin application (50 µM). One-way ANOVA, $F(3,50) = 9.310$, $p < 0.0001$, with Dunnett's multiple-comparison *post hoc* testing. Levels of significance: * $p < 0.05$, **** $p < 0.0001$) Sample sizes as (ACSF [cells], PTX [cells], replicates [mice]: Control: (16,14,5); 3-7 Days: (23,16,3); 14 Days: (15,10,3); 2-3 Months: (17,14,3). Histograms indicate means ± S.E.M. The ROUT outlier elimination method (with false discovery rate of 1%) identified 1 outlier in the 3-7 day, Control PTX, and 2 month PTX dataset; these cells were omitted from analysis.

Alterations in GABAergic efficacy during epileptogenesis

GABAergic inhibition plays a predominant role in restricting DGC activation and generating the concomitant sparse activation of DGCs in control animals (Coulter and Carlson, 2007; Dieni et al., 2013). We therefore assessed inhibitory function by obtaining whole cell patch recordings of DGCs during epileptogenesis to determine whether alterations in inhibitory function accompanied changes in DGC activation properties (**Fig. 4.8**). Control mean miniature inhibitory postsynaptic current (mIPSC) amplitude was 31.6 ± 1.03 pA (**Fig. 4.8b**). At 3-7 days post-SE, mIPSC amplitude decreased to 22.58 ± 1.39 pA, (a 29% reduction, $p < 0.0001$). mIPSC amplitude was also significantly reduced 14 days post-SE, albeit to a lesser extent, by 13% (to 27.46 ± 1.39 pA; $p = 0.0170$). Finally, 2-3 months post-SE, mIPSC amplitudes was again reduced by 32% relative to controls (to 21.57 ± 1.39 pA; $p < 0.0001$]). mIPSC frequencies did not differ between controls and post-SE groups (ANOVA, $p = 0.58$, **Fig. 4.9a**).

We also recorded spontaneous inhibitory postsynaptic currents (sIPSCs), which exhibited parallel changes to mIPSCs (**Fig. 4.8c**). sIPSC mean amplitudes were: Control: 40.66 ± 1.90; 3-7 days: 24.37 ± 1.19; 14 days: 34.42 ± 2.22; and 2-3 months: 23.48 ± 1.53 pA (mean ± SEM). sIPSC amplitudes were significantly reduced 3-7 days and 2-3 months post-SE (by 40%; $p < 0.0001$ and 42%; $p < 0.0001$, respectively). sIPSC frequencies at 3-7 days and 2-3 months post-SE did not differ significantly from controls; interestingly, sIPSC frequency was significantly increased from control levels 14 days post-SE (ANOVA with *post hoc* Dunnet's Test, $p = 0.0338$, **Fig. 4.9b**). The correlation between DGC activation and relative reduction in both m- and sIPSC amplitudes post-SE further supports compromised inhibitory function as a contributory mechanism

underlying the deterioration in sparse DGC activation during both the development and expression of epilepsy.

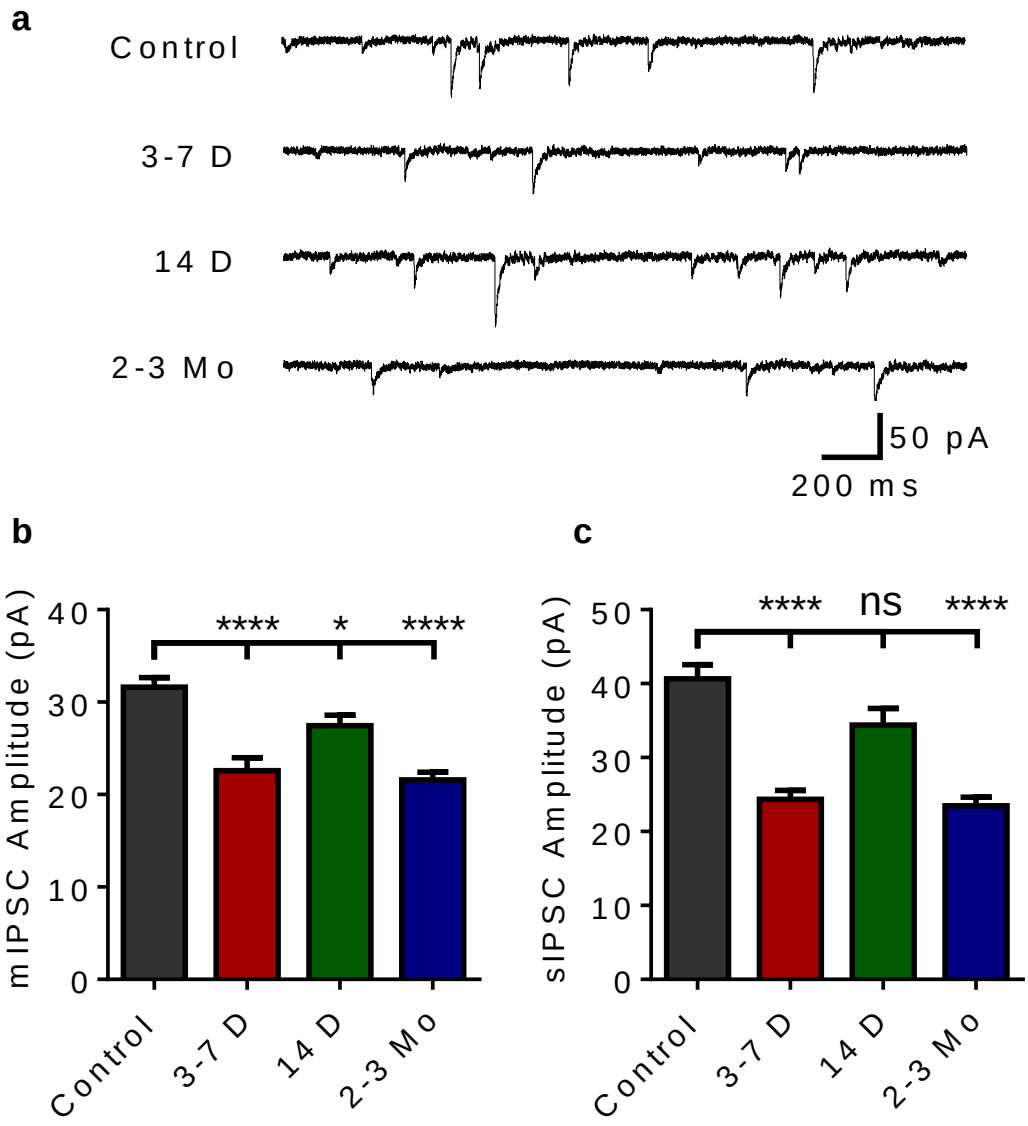
a
Control
3-7 D
14 D
2-3 Mo
50 pA
200 ms
b
mIPSC Amplitude (pA)
0
10
20
30
40
****
*
****
Control
3-7 D
14 D
2-3 Mo
c
sIPSC Amplitude (pA)
0
10
20
30
40
50
****
ns
****
Control
3-7 D
14 D
2-3 Mo

Figure 4.8. IPSC alterations during epileptogenesis. **a**, Representative mIPSC traces of control DGCs and DGCs recorded from slices prepared from mice at 3-7 days, 14 days, and 2-3 months post-SE. **b**, Plot of mean mIPSC amplitudes in control slices and slices prepared during epileptogenesis. **c**, Plot of mean sIPSC amplitudes in control slices and slices prepared during epileptogenesis. (**b, c**) Note the significant decrease in both m- and sIPSC ampltitudes at 3-7 days and 2-3months post-SE. Cell numbers (mIPSC, sIPSC) are as follows: Control: (17, 15); 3-7 days (13, 20); 14 days: (19, 20); 2 months: (15, 17). All cells were recorded in slices prepared from at least 3 mice. One-way ANOVA with Tukey's multiple-comparison *post hoc* testing, mIPSC $F(3,60) = 17.63$, sIPSC $F(3,68) = 22.12$, $p < 0.0001$. Levels of significance: ns $p > 0.05$, * $p < 0.05$, **** $p < 0.0001$. Histograms indicate means ± S.E.M. The ROUT outlier elimination method (with false discovery rate of 1%) identified 1 outlier in the control dataset; this cell was omitted from analysis.

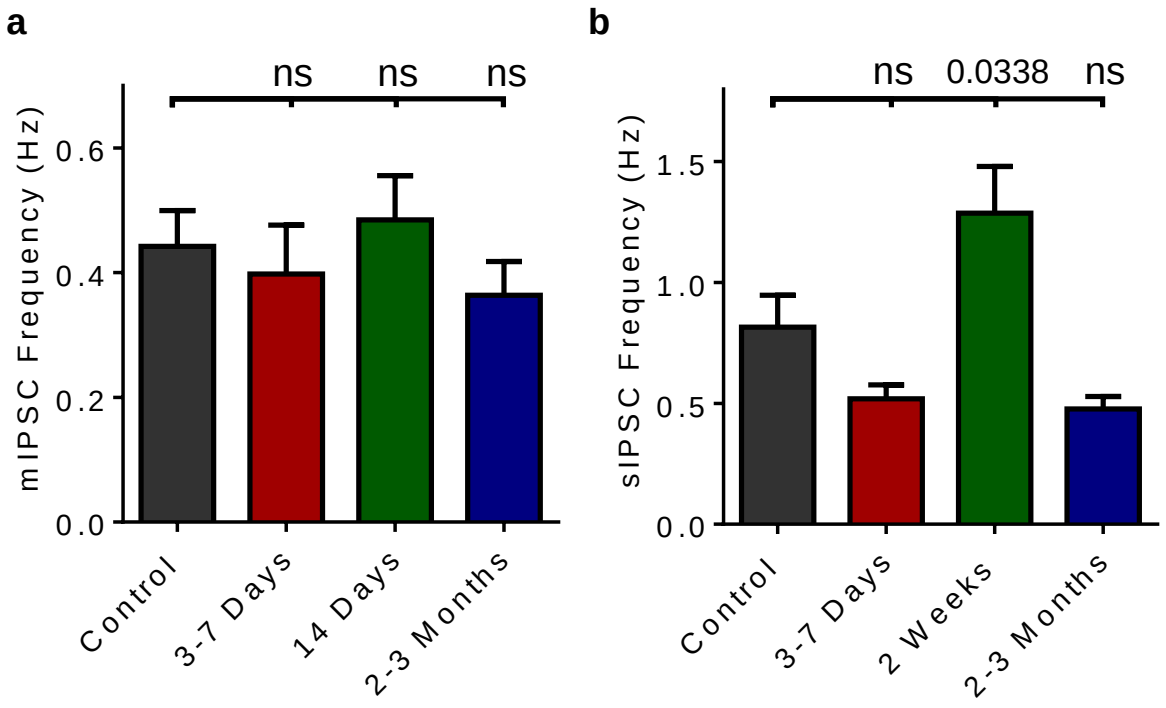

Figure 4.9. m- and s-IPSCs during epileptogenesis. **a**, Plot of mIPSC frequencies in control slices and slices prepared during epileptogenesis. **b**, Plot of sIPSC frequency in control slices and slices prepared during epileptogenesis. (**a, b**) Cell numbers (mIPSC, sIPSC) are as follows: Control; n = (17,15); 3-7 days: n = (13,20); 14 days: n = (19,20), 2 months n = (15,17). All cells were recorded in slices prepared from at least 3 mice. One way ANOVA with Dunnett's multiple-comparison *post-hoc* testing, mIPSC $F(3,60) = 0.6592$, $p = 0.58$; sIPSC $F(3,68) = 9.272$, $p < 0.001$. Histograms indicate mean ± S.E.M.

Disruption in inhibitory function degrades sparse DGC activation

Sparse activation of DGCs depends on tight inhibitory control from local GABAergic inhibitory interneurons (Freund and Buzsáki, 1996; Yu et al., 2013a; Pardi et al., 2015). Since a 30-40% reduction in mIPSC and sIPSC amplitude was evident during epileptogenesis (**Fig. 4.8**), we mimicked this change pharmacologically by application of the $GABA_A$ receptor antagonist, PTX (5 μM) in control slices and assayed DGC activation using MCI to examine whether this level of reduced inhibitory function was sufficient to enhance DGC excitability. We selected 5 μM PTX because it reduced mIPSC amplitudes in DGCs from control slices by ~35% (Control mean 31.62 ± 1.03 pA [n =17 cells], 5 μM PTX mean 20.64 ± 2.55 [n = 12 cells], Welch-corrected, unpaired two-tailed t-test, t[14.59] = 3.995, p = 0.0012).

In normal ACSF, PP stimulation (400 μA) activated 13.0 ± 3.0% of cells (**Fig. 4.10a**). Perfusion of PTX (5 μM) significantly enhanced DGC activation ~4-fold (52 ± 9.8%; p < 0.0001), demonstrating that a reduction in inhibitory function comparable to that observed during epileptogenesis is sufficient to compromise sparse activation in DGCs. Saturating PTX concentrations (50 μM) further enhanced DGC activation to 88.1 ± 10.4% (p < 0.0001). These results implicate reduced inhibitory drive onto DGCs as a critical mechanism contributing to DGC hyperexcitability during epileptogenesis.

However, the efficacy of ionotropic GABAergic synapses depends not only on the pre- and postsynaptic function of synaptic machinery but also on the driving force of Cl^- ions across the synaptic membrane. Following SE, reduced expression of the Cl^--extruding K^+/Cl^- cotransporter, KCC2, causes intracellular accumulation of Cl^- ions and contributes to enhanced DGC excitability via reduced inhibitory shunting efficacy of ionotropic $GABA_A$ receptors (Pathak et al., 2007). This change in chloride regulation was not assessed in our whole cell patch recordings. We therefore mimicked this

dysregulation in transmembrane Cl^- in our slice preparations by application of DIOA. DIOA perfusion (20 μM) elevated DGC activation 3-fold (from 13 ± 3.1% to 39 ± 5.6%; p = 0.0011). Combined application of 20 μM DIOA and 5 μM PTX had a synergistic effect, producing even more robust activation of DGCs (> 5-fold) and a near complete collapse of dentate gating, with 71 ± 4.2% of DGCs responding under these conditions (**Fig. 4.10a**). We went on to assay DIOA (20 μM) effects on DGC activation in slices prepared from control, 3-7 days, and 2-3 month post-SE mice. DIOA enhanced DGC excitability in both control and 2-3 month post-SE, but not in 3-7 day post-SE slices (**Fig. 4.10b**). This is consistent with an occlusion effect on DIOA actions, indicating KCC2 function may be compromised at 3-7 days post-SE. These results demonstrate that compromised local GABAergic inhibitory input onto DGCs, as well as the inappropriate regulation of intracellular $[Cl^-]$, are each sufficient to degrade sparse activation of DGCs, and that this combined mechanism may be operative to degrade DG circuit functions 3-7 days post-SE.

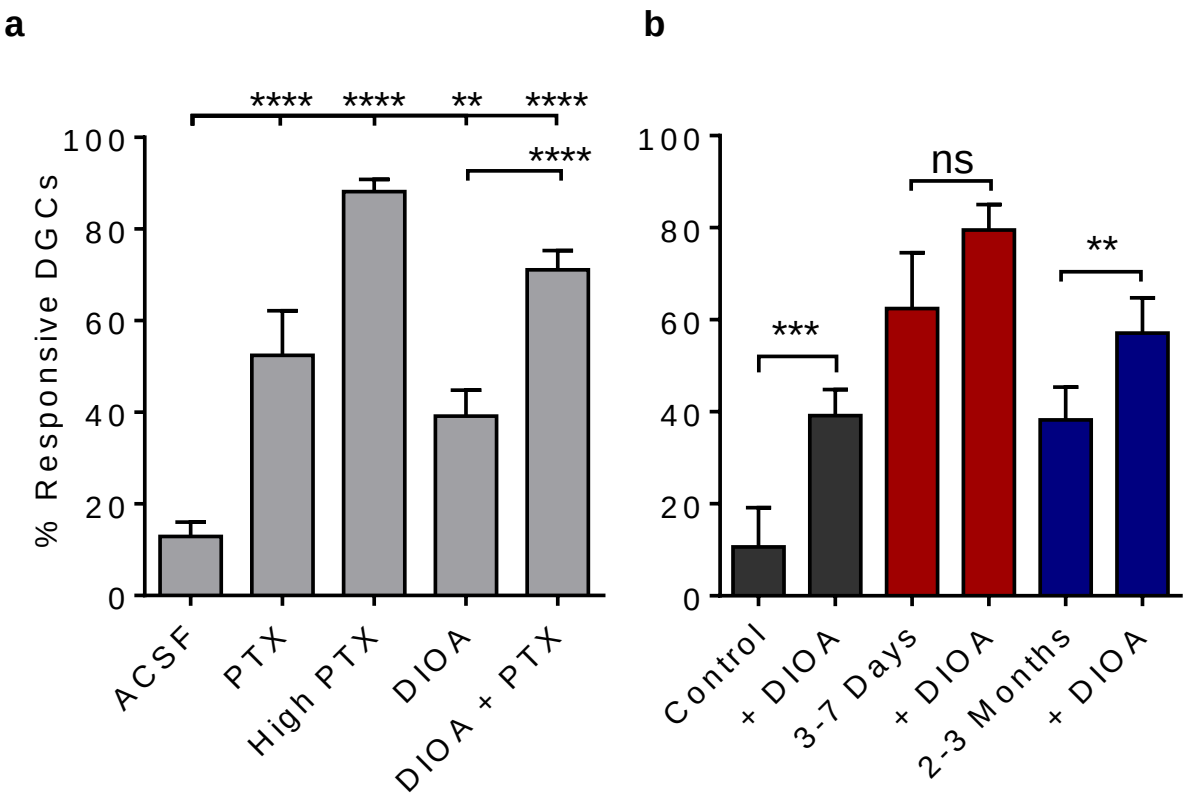
a
b
% Responsive DGCs
100
80
60
40
20
0
****
****
**
****
****
ACSF
PTX
High PTX
DIOA
DIOA + PTX
***
ns
**
Control
+ DIOA
3-7 Days
+ DIOA
2-3 Months
+ DIOA

Figure 4.10. Disruption in inhibitory function degrades sparse DGC activation. **a**, Plot of the proportional DGC activation (%) in control slices following 400 µA PP stimulation in control ACSF, 20 µM DIOA, 5 µM PTX, 20 µM DIOA + 5 µM PTX, and 50 µM PTX. Samples sizes are as follows as (n [slices], total number of cells [ROIs]), Control ACSF: (15,565); 5 µM PTX: (6, 239); 50 µM PTX: (15,565); 20 µM DIOA: (9,326); 20 µM DIOA + 5 µM PTX: (15, 565); Slices prepared from 4 naïve mice. Significance tested with one-way ANOVA, $F(4.55) = 54.25$, $p < 0.0001$, with Tukey's multiple-comparison *post hoc* testing. **b**, Plots of DIOA (20 µM) effects on the proportional DGC activation (%) to 400 µA PP stimulation in slices prepared from control, 3-7 days post-SE, and 2-3 months post-SE mice. Note the occlusion of DIOA effects at the 3-7 days post-SE. Samples sizes as (n [slices], replicates [mice], total number of cells [ROIs]), Control: (9,3,367); 3-7 days post-SE: (8,4,348); 2-3 months post-SE: (8,3,355). Significance tested with two-tailed, paired t-tests, Control: $t(8) = 6.025$; 3-7 days: $t(7) = 1.524$; and 2-3 months: $t(7) = 3.956$. **a&b**, Histograms indicate means ± S.E.M. Levels of significance: ns $p > 0.05$, ** $p < 0.01$, *** $p < 0.001$, **** $p < 0.0001$.

Metabolic rescue of circuit collapse in the chronically epileptic DG

While postsynaptic disinhibition and altered chloride regulation are likely mechanisms for the collapse of sparse firing in the DG during epileptogenesis, other circuit mechanisms may contribute to the DGC hyperexcitability observed in slices from chronically epileptic mice. Reactive astrocytosis is a prominent pathology in epilepsy (and present in the DG [**Fig. 4.11a**]), and can reduce the efficacy of inhibitory neurotransmission via downregulation of glutamine synthetase (Eid et al., 2004). In the brain, glutamine is exclusively supplied to neurons by astrocytes as the rate-limiting step in neurotransmitter recycling. Application of exogenous glutamine, which normally has no effect, can rescue this glutamine synthetase deficiency in gliotic regions of the brain by acting as the missing synthetic precursor and replenishing GABA in inhibitory presynaptic terminals (Ortinski et al., 2010). In order to understand the potential role of gliosis in the epileptic DG, we treated slices prepared from control, 3-7 days post-SE, and chronically epileptic mice with 5 mM glutamine (2 hours, Fluka, Buchs, Germany), and imaged activation of DGCs via MCI. This metabolic treatment had no effects on control and 3-7 days post-SE slices, but was sufficient to partially restore normal DGC activation in slices prepared from chronically epileptic animals (**Fig. 4.11b**). In normal ACSF, 74 ± 5% of epileptic DGCs activated in response to a 400 μA PP stimulus. Glutamine treatment resulted in a significant decrease in this activation to 38 ± 9% ($p = 0.0030$). Glutamine treatment had no significant effect on DGC activation in control slices ($p = 0.7303$; **Fig. 4.11b**), or in slices prepared 3-7 days post-SE ($p = 0.4935$). We conclude that glutamine effects are restricted to chronically epileptic mice, and are consistent with a contribution of astrogliosis to DGC hyperexcitability in these animals. Earlier results (**Fig. 4.7)** showed that GABA blockade increased AP latency in DGCs, due to either

excitatory actions of GABA or activation of recurrent mossy fibers. Here, results in 2-3 month post-SE animals demonstrate that glutamine-mediated GABA increase reduces proportional DGC activation, indicating that GABA is in fact inhibitory at this time point. It further suggests that the earlier observed PTX-effect on AP latency (Fig. 4.7) is likely due to the unmasking and activation of the recurrent mossy fiber network present in 2-3 month post-SE animals. These recurrent synapses are enriched in postsynaptic kainate receptors relative to normal mossy fiber terminals and PP synapses, making them more sensitive to kainate antagonists than other excitatory synapses within the DG (Pinheiro et al., 2013). Consistent with a role for recurrent mossy fiber synapses in proportional DG activation in epileptic animals, application of the kainate receptor antagonist (S)-1-(2-Amino-2-carboxyethyl)-3-(2-carboxy-thiophene-3-yl-methyl)-5-methylpyrimidine-2,4-dione (UBP-310, Santa Cruz Biotechnology, Santa Cruz, California)(5 μM) was sufficient to reduce DGC activation significantly in epileptic slices (from 74 ± 5% of DGCs to 54 ± 7%; one tailed, paired t-test, p = 0.0119 (**Fig. 4.12**, right), but had no effect on control DGC activation (one-tailed, paired t-test, p = 0.7131, **Fig. 4.12**, left).

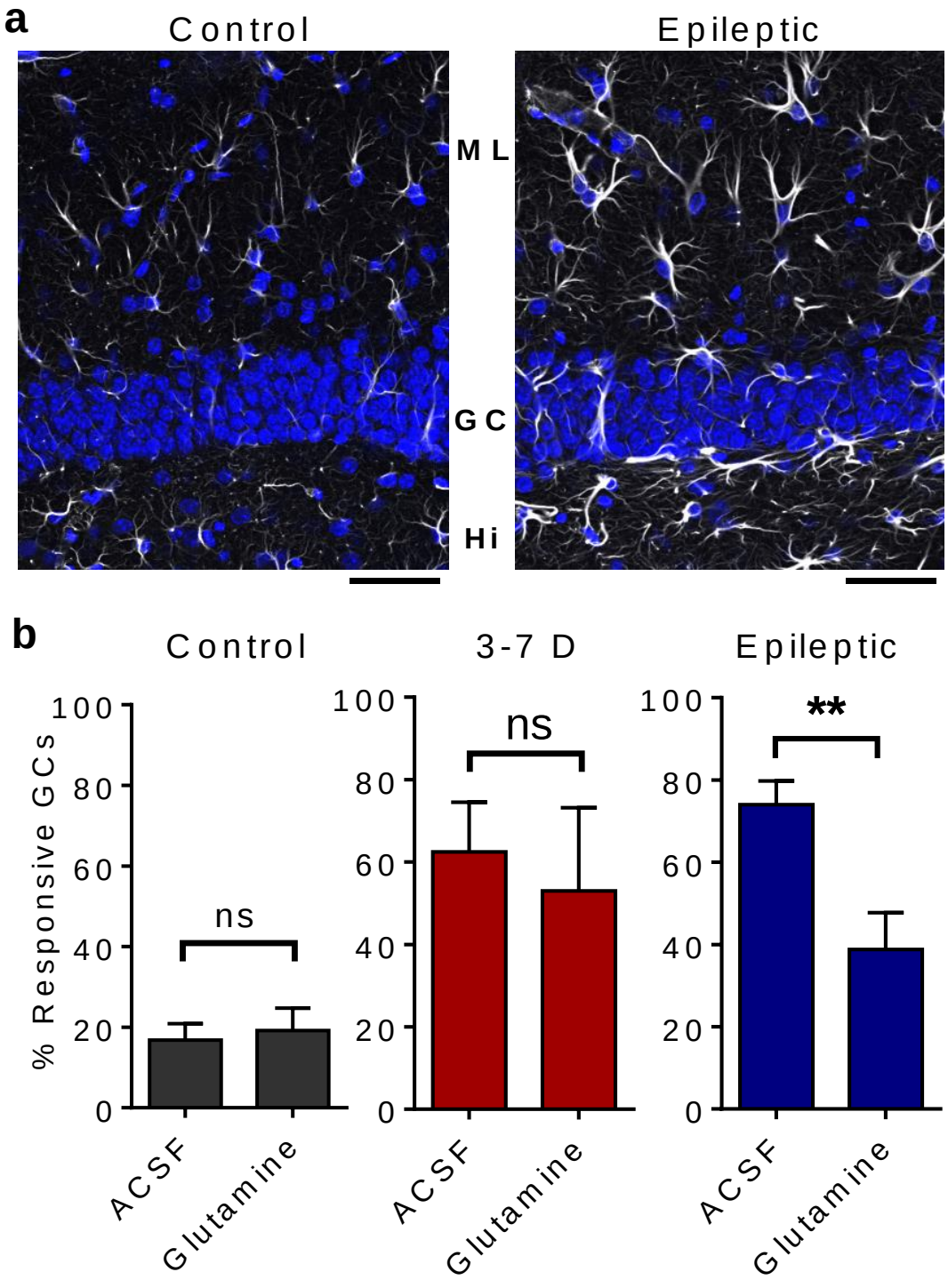
a
Control
Epileptic
M L
G C
Hi
b
Control
3-7 D
Epileptic
% Responsive GCs
100
80
60
40
20
0
ns
ns
**
ACSF
Glutamine
ACSF
Glutamine
ACSF
Glutamine

Figure 4.11. Metabolic rescue of circuit collapse in chronically epileptic DG. **a**, GFAP immunostaining of astrocytes in control and epileptic brain slices. (Greyscale: GFAP immunostaining; Blue; DAPI labeled nuclei). Note the increased expression of GFAP and hypertrophy of astrocytes in epileptic tissue. Immunostaining repeated in 4 control and 9 epileptic slices. Scale bars represent 50 µm. **b**, Proportional DGC activation (%) to 400 µA PP stimulation in slices from control (left), 3-7 days (middle) and epileptic mice (right, 2 months post-SE) when perfused with ACSF and 5 mM Glutamine. Notes that glutamine's effect in reducing DGC activation was only present in epileptic mice, 2-3 months post-SE. Control: unpaired 2 sided t-test, $t(15) = 0.3512$, $p = 0.7303$; 3-7 days: Welch-corrected, two-sided, unpaired t-test, $t(10.06) = 0.7106$, $p = 0.4935$: Epilepsy: Welch-corrected, one-tailed, unpaired t-test, $t(12.71) = 3.298$, $p = 0.0030$. Right, individual data points are plotted. Sample sizes as follows, n = (ACSF slices, Glutamine slices): Control ACSF: (9, 8); 3-7 days: (8, 14); and Epileptic: (8, 8). Slices taken from at least 3 mice. Histograms indicate means ± S.E.M.

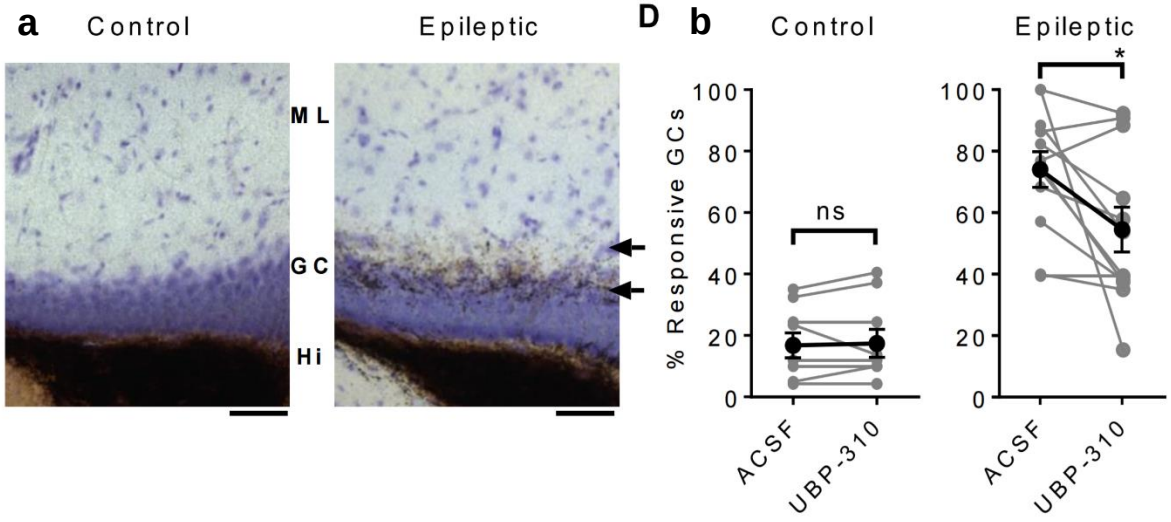

Figure 4.12. Pharmacologic blockade of recurrent mossy fiber synapses. a, Timm's staining of mossy fiber terminals in slices prepared from control and epileptic mice. Arrows mark the presence of silver-sulfide labelled mossy fiber terminals sprouted aberrantly into the inner molecular layer and on granule cell somata in epileptic tissue. Timm's staining repeated in 5 control and 12 epileptic slices. **b,** Proportional DGC activation (%) to 400 μA perforant path stimulation in control ACSF, 5 μM UBP-310, with before after plot of each slice on right. Control two-tailed, paired t-test t(8) = .3811, p = 0.7131. Epilepsy: one tailed, paired t-test, t(11) =2.619, p= 0.0119. Black plot is mean +/- S.E.M, gray are individual paired measurements. Sample sizes are as follows (slices): Control ACSF: n= 8; Glutamine: n = 8; UBP-310: n = 8; Epilepsy, ACSF: n= 12; Glutamine: n = 8; UBP-310: n = 12. Slices taken from at least 3 mice. Scale bars represent 50 μm.

Discussion

This study examines DG circuit function as it transforms during and following epileptogenesis. Using MCI, we found that epilepsy development was accompanied by massive enhancement of the normally sparse activation of DGCs. Further experiments revealed alterations in DGC activation latency during epileptogenesis that were likely mediated by compromised GABAergic inhibition. Pharmacologically mimicking these changes in inhibitory synaptic function in controls was sufficient to generate the DG circuit collapse evident in epileptic animals. Circuit function in chronically epileptic mice was rescued by application of exogenous glutamine. We conclude that the massive DG circuit hyper-activation evident in animals during and following epilepsy development is generated in large part by mechanistically complex compromises in local circuit inhibition.

Although few other studies examining DG circuit behavior in epilepsy have utilized MCI techniques, as we have done in the present study, many field potential and patch clamp recording studies have been published both in post-SE rat models of epilepsy and in hippocampal tissue resected from patients with epilepsy. There are a number of interesting similarities and differences in results obtained from rats and humans, compared to the mouse data in the present study.

The most directly comparable sets of studies to those presented here have been conducted in rats, where a number of reports have examined responses in the DG during and following epilepsy development in pilocarpine, kainate, and electrical stimulation post-SE models. A general, but variable, trend in both field potential, voltage-sensitive dye imaging, and patch clamp recording studies in post-chemically or -electrically evoked SE rats from both our own laboratory and others is that there is an early (within days post-SE) hyperexcitability in the DG (Sloviter, 1991; Pathak et al., 2007; Nakashiba

et al., 2009) accompanied by a reduction in synaptically recorded inhibition or paired pulse extrapolated inhibition in DGCs (Sloviter, 1991; Hellier et al., 1999; Cohen et al., 2003). In many studies, this early DG hyperexcitability then resolves within the next few weeks (Ang et al., 2006; Pathak et al., 2007; but see Patrylo et al., 1999), accompanied by a normalization in inhibitory synaptic responses, which persists long term (Buckmaster and Dudek, 1997; Gibbs et al., 1997; Hellier et al., 1999; Cohen et al., 2003; Thind et al., 2010; but see Sloviter, 1987; Shao and Dudek, 2005; Sun et al., 2007). The early post-SE DG hyperexcitability appears similar to the enhanced recruitment of DGCs evident in mice in the present study, as does the reduction in synaptic inhibition. However, the recovery of DG hyperexcitability and synaptic inhibition described in mice in the present study is only transient, with a later, permanent failure in both properties evident in mice (current study; see also Kobayashi and Buckmaster, 2003; Zhang et al., 2007). The partial recovery and then secondary collapse of appropriate DGC excitability we describe in mice may be mediated by the failed induction of a compensatory mechanism following injury, which is ineffective and suffers a secondary reversal due to ongoing seizures. In addition to species (rats vs. mice) dissimilarities potentially contributing to specific time course differences in inhibitory compromise post-SE, there are frequent divergent methodologies, including variation in the duration of SE (e.g. 40 min in the present study compared to 90 min (Yu et al., 2013a) and 120 min (Kobayashi and Buckmaster, 2003; Buckmaster et al., 2016)). This could induce distinct patterns of pathology, particularly interneuron loss, which might contribute to discrepancies in m- and sIPSC frequency effects between studies (Kobayashi and Buckmaster, 2003).

How does this compare with studies conducted in hippocampal tissue resected from patients with TLE? Although human recordings suffer from an unavoidable lack of rigorous controls, studies comparing DG excitability and inhibition in hippocampal slices

have reported significant stimulus-associated hyperexcitability and disinhibition, which is most strongly apparent in tissue from patients with mesial temporal sclerosis (classic TLE), and not in tissue from patients with tumor-associated TLE, or from control rats (Masukawa et al., 1989, 1996; Williamson, 1994). This chronic DG hyperexcitability in epilepsy appears most similar to the profile evident in the mouse studies presented here, and not to many rat post-SE epilepsy models, which frequently exhibit little in the way of circuit alterations in normal extracellular media (discussed above).

Within the DG, sparse DGC AP firing depends on GABAergic inhibition, and the initial determination to activate is accomplished within milliseconds. This implicates feedforward inhibition as a prime candidate regulator of DGC sparse activity. Feedforward inhibition is tuned to define an integrative window in principal cells, temporally locking circuit output to afferent input, and sharpening the timing of circuit responses (Pouille and Scanziani, 2001; Higley and Contreras, 2006). In the DG, this function is modified to regulate strongly the ability of DGCs to activate (Coulter and Carlson, 2007). Experimental support for this unique role of feedforward inhibition includes the effects of GABA antagonists to increase the proportion of cells that activate in a circuit lacking recurrent excitatory collaterals (**Figs. 4.4c & 4.10**) and to reduce activation latency (**Fig. 4.7c**). The KCC2 antagonist, DIOA, also reduces DGC activation latency, also consistent with early GABAergic inhibition regulating DGC firing. Feedforward inhibition can modulate cell firing in cortical circuits (Pouille et al., 2009; Dieni et al., 2013), but the magnitude of this effect in the DG constitutes an uncommonly extreme example where feedforward inhibition prevents most cells from firing, while also regulating the timing of firing in the residual active population (Pardi et al., 2015).

Active DGCs exhibited no preferential localization within the GCL (**Fig. 4.6**). The cell somata of adult-born DGCs coalesce almost exclusively in the inner portion of this

layer in both control and epileptic animals (**Fig. 4.6a&b** see also Parent et al., 1997). The lack of preferential location of active DGCs provides indirect evidence that, in our studies, both adult-born and mature DGCs within the GCL contribute equivalently to ensemble activation. This contrasts recent reports predicting enhanced excitability of adult-born DGCs during synaptic processing within the DG (Marín-Burgin et al., 2012; Dieni et al., 2013; Pardi et al., 2015), and during cognition (Alme et al., 2010). However, we characterized only the activity of normotopic DGCs and did not examine ectopic DGCs within the hilus, distant from our imaging regions within the DG cell layer. Many adult-born DGCs in epilepsy migrate to ectopic locations within the hilus and integrate abnormally into hippocampal circuitry (Scharfman et al., 2003a). The accumulation of these ectopic, but not normotopic, adult-born DGCs correlates with epilepsy severity (Hester and Danzer, 2013).

The normal sparse DGC activation evident in control animals increases 10-20 fold during and following epilepsy development (3-7 d and >60 d post-SE, respectively). Based on previous studies examining hippocampal alterations during epileptogenesis and in chronically epileptic animals, the underlying mechanisms responsible for this massive alteration in circuit function are likely to differ at these two distinct phases following SE. However, in both cases, compromised GABAergic inhibition is a likely contributor, given the pivotal role of interneurons in regulating DGC activation. Immediately following SE, there is compromised regulation of transmembrane chloride levels in DGCs, resulting in elevated intracellular chloride, compromised GABAergic inhibition, and loss of the gating function of the DG (Pathak et al., 2007). In addition, patch studies conducted immediately following SE in the rat pilocarpine model of epilepsy (3-7 days) have demonstrated reductions in inhibitory function in DGCs (Cohen et al., 2003; Kobayashi and Buckmaster, 2003) similar to those we report in mice (**Fig.**

4.8). To evaluate the possible contributions of these two mechanisms to DGC hyperactivation post-SE, we generated similar effects in control DG through partial blockade of GABA receptors and/or perfusion with a KCC2 blocker, and found that both of these manipulations were sufficient to elicit enhanced DGC activation similar to that seen 3-7 d post-SE (**Fig. 4.10a**). In addition, the action of DIOA to increase DGC activation was occluded in slices prepared from 3-7 days post-SE but not in chronically epileptic (2-3 months post-SE) mice, further supporting the specific role of chloride disequilibrium in DG hyperexcitability during epilepsy development (**Fig. 4.10b**).

As epilepsy manifests later following SE, additional cellular and circuit processes also emerge within the hippocampus, distinct from those seen during epileptogenesis. These other factors may also have a prominent role in the DGC hyperactivation evident in epileptic animals. In addition to the disinhibition evident both 3-7 and >60 d post-SE (**Fig. 4.8**), chronically epileptic animals display marked gliosis (**Fig. 4.11a**). Astrogliosis, a hallmark of temporal lobe epilepsy, is associated with downregulated expression of glutamine synthetase, the astrocyte-specific keystone enzyme in the glutamate-glutamine cycle (Eid et al., 2004; Ortinski et al., 2010). The astrocytic glutamate-glutamine cycle mediates neurotransmitter recycling in CNS synapses, and compromised function of this cycle rapidly depletes synaptic GABA and generates disinhibition (Liang et al., 2006; Ortinski et al., 2010). Within the brain, glutamine is exclusively generated by astrocytes. Glutamine has no effect on control brain (Ortinski et al., 2010; Coulter and Eid, 2012) since this amino acid is normally not rate limiting in neurotransmitter synthesis. To determine whether astrogliosis may contribute to DGC hyperactivation in epileptic animals, we incubated slices prepared from control, early (3-7 days post-SE), and chronically (2-3 months post-SE) epileptic animals in exogenous glutamine. We found that this reversed DGC hyperactivity specifically at the 2-3 month

post-SE time point. This suggests that gliosis may be a significant contributor to circuit collapse evident in chronically epileptic mice. In combination, these data demonstrate that, although the circuit disruptions evident during and following epilepsy development appear similar in extent, they are due to distinct underlying mechanisms, and so would require different therapeutic manipulations to restore normal DG function at these two time points during the disease process.

Given that the sparse ensemble activation of DGCs is a critical determinant of both hippocampal-dependent cognitive function and regulation of aberrant excitability in the limbic system, erosion in this circuit property may play a significant role both in cognitive comorbidities and seizure propensity in epilepsy. The time course of emergence and persistence of excess DGC activation links this aberrant circuit property both with the induction and expression of epilepsy. Studies providing mechanistic insight into how epilepsy development alters the basic circuit properties of hippocampal structures may be important not only in targeting new therapies for the treatment of seizures and the cognitive comorbidities accompanying epilepsy, but also, ultimately, in therapies designed to prevent and/or cure this disorder in at-risk patients.

Acknowledgments

We thank Alicia White and Shareen Nelson for technical assistance, Jillian Ma for help with data analysis and generating software used in analyzing cell locations in our imaging data sets and Dr. Fu Chun Hsu for assistance with calcium dye loading. This research was supported by NIH grants from the National Institute of Neurological Disorders and Stroke (NINDS RO1s NS082046 and NS38572 to D.A.C and NRSA F31 NS080403 to C.G.D), the Intellectual and Developmental Disabilities Research Center at

CHOP/PENN 1U54HD086984-01, as well as the American Epilepsy Society's Predoctoral Fellowship to C.G.D.

Methods

Animals and tissue preparation. All animal use was performed in accordance and with the approval of the Children's Hospital of Philadelphia's Institutional Animal Care and Use Committee and all methods were in accordance with the relevant guidelines and regulations. Male C57BL/6 were used in this study, except for in (**Fig. 4.6 a&b**), where Gli1-Cre^{ERT} x Rosa-TdTomato mice (C57BL/6 background) were used. Naïve control mice were aged 9-11 weeks, except for two older control mice aged 130-150 days in **Fig. 4.4**. Control mice were housed with up to 4 animals per cage. Mice that underwent pilocarpine-induced SE were singly housed post-SE. Vivarium light/dark cycle was 12/12 hours. For slice preparation, mice were perfused transcardially with ice cold, oxygenated (95% O_2 / 5% CO_2) artificial cerebrospinal fluid (ACSF) in which NaCl partially replaced an equal osmolarity concentration of sucrose. Sucrose ACSF was composed of (in mM): 87 NaCl, 2.5 KCl, 1.25 NaH_2PO_4, 75 sucrose, 10 glucose, 26 $NaHCO_3$, 0.5 $CaCl_2$-$2H_2O$, and 4 $MgSO_4$. After perfusion, brains were removed, and submerged in ice cold sucrose ACSF. Horizontal hippocampal-entorhinal cortex slices (350 μm) were cut using a Vibratome VT1200S (Leica, Wetzlar, Germany). Slices were then incubated in a calcium indicator loading chamber and humidified with 95% O_2/5% CO_2 at 37°C. The calcium indicator loading solution was composed of 4 μl of 0.5% Oregon Green BAPTA-1 AM (OGB; Invitrogen), 4 μl of 20% pluronic acid (Sigma) in DMSO, 4 μl of 15% Cremophor (EL) (Sigma) in DMSO (Sigma) and 4 ml of oxygenated sucrose ACSF. Slices were loaded for 15 min and then washed and incubated in fresh oxygenated ACSF (composition in mM: 125 NaCl, 2.5 KCl, 1.25 NaH_2PO_4, 10 glucose, 26 $NaHCO_3$, 2 $CaCl_2$-$2H_2O$, 1 $MgSO_4$)

at room temperature for at least 45 min to allow AM-ester linkages to cleave. Slices were then stored in oxygenated ACSF for up to 6 h without any evident deterioration of responses. For optical and electrical recordings, slices were placed in a 36°C heated submersion recording chamber, instrumented with electrodes, and allowed to acclimate for 10 minutes before commencing recordings.

Pilocarpine-induced status epilepticus (SE) model of epilepsy. Mice aged 6 weeks were injected with scopolamine (1 mg/kg), and 30 min later with pilocarpine (350 mg/kg). This triggered SE. Forty minutes after SE onset, diazepam (5 mg/kg) was administered to quell seizure activity. Ages of pilocarpine-SE mice varied depending on time post-SE as tracking circuit and cellular properties developing following SE was the primary goal of this study. Time post-SE is reported in each figure.

Video/EEG monitoring. Seizure events were monitored using video behavioral monitoring as well as depth electrode EEG recording to confirm the manifestation of epilepsy in all mice at time points > 2 months post-SE. EEG recordings were performed using a Stellate-Harmonie (Stellate Inc., Montreal, Canada) 16-bit, 32 channel digital EEG machine, sampling at 200 Hz. Cortical electrodes consisted of self-tapping screws and hippocampal electrodes of bipolar 0.005 inch stainless steel wire. The depth electrode was placed into area CA1 of the right hippocampus. Cortical electrodes were placed directly in front of the Bregma suture on both sides of the midline. Once in the correct position, all electrodes were held in a six pin pedestal. Ground and reference electrodes were placed directly behind the Lambda suture on either side of the midline. The pedestal of electrodes and screws were further held in place by dental cement. EEG tracings were reviewed to detect electrographic seizures. If a seizure was suspected, the occurrence of a behavioral seizure was confirmed. The time course and prevalence of

epilepsy development in our mouse model are depicted in **Figure 4.3**. Epilepsy onset was rapid, with 50% of animals developing epilepsy within 5 days, and occurred in all animals by 35 days post-SE. Additionally, we confirmed that EEG electrode implantation and headcap instrumentation, with or without subconvulsive pilocarpine treatment ($1/10^{th}$ dose pilocarpine, 35 mg/kg) did not induce epilepsy development, (**Fig. 4.3**) nor did it alter DGC responsiveness in our MCI recordings (**Fig. 4.2**).

Microelectrode stimulation and recording. For stimulation of PP granule cell afferents, a 125 μm diameter concentric, bipolar tungsten stimulating electrode (FHC Inc., Bowdoin, ME) was placed ~100 μm on the entorhinal cortical side of the hippocampal fissure, in a region neighboring the suprapyramidal blade and apex of the GCL (defined as the midpoint between the suprapyramidal and infrapyramidal blades;). For extracellular recordings, a glass recording microelectrode was positioned in the middle of the DG molecular layer. Recording electrodes were placed >500 μm away from the stimulating electrode and outside the imaging field to avoid stimulus and excitation laser-indued artifacts.

Stimulus intensity standardization. PP stimulus intensity was standardized across groups using local field EPSP slope and amplitude measurements recorded using glass microelectrodes (5–7 MΩ resistance, filled with ACSF) positioned in the middle third of the molecular layer to assess activation of the medial PP. Input-output relationships normalized to maximal response were invariant across all experimental groups (**Fig. 4.1**). In these studies, two stimulus intensities were used regularly, 100 μA and 400 μA, which corresponded to ~60% and 100% maximal stimulation. Additionally, local field potential recordings were monitored online during the optical recordings to verify the ongoing viability of slices. Local field potentials were recorded using an Axopatch 200B

amplifier (Molecular Devices, Sunnyvale, CA). Electrical data were collected using Clampex 10 (Molecular Devices) software.

Juxtacellular loose-patch recordings. Juxtacellular loose-patch current-clamp recordings were conducted in OBG-loaded slices to assess AP firing and timing associated with calcium transients in DGCs. Patch electrodes (5–7 MΩ resistance, filled with ACSF) were fluorescently labeled with 0.04% Alexafluor 488 conjugated bovine serum albumin (A13100, ThermoFischer), and then positioned onto DGCs of interest. Negative pressure was applied to acquire and maintain low resistance seals of >30 MΩ. Seal quality was monitored during recordings. Current-clamp recordings were made using a Multiclamp 700B amplifier (Molecular Devices) and sampled at 20 kHz with a Digidata 1332A analog-digital converter (Molecular Devices). Electrical data were collected and analyzed in Clampfit 10 (Molecular Devices).

Confocal multicellular calcium imaging (MCI). For confocal MCI, Oregon Green BAPTA-AM (OGB)-loaded slices were imaged using a Live Scan Swept Field Confocal Microscope (Nikon Instruments, Melville, NY) equipped with an Ar/Kr ion laser (Innova 70C, Coherent) or solid state laser (OBIS; both laser's excitation wavelength 488 nm) operated with NIS-elements software (Nikon). Images were acquired using a water immersion 40X lens (NA = 0.8) and a Cascade 512+ CCD camera (Photometrics, Tuscon, AZ). This system allowed capture of images at 55 frames/s with a frame resolution of 256 × 256 pixels for these studies.

MCI calcium transient data analysis and code availability. For MCI, the field of view at 40× magnification allowed us to capture ~30–70 OGB-loaded cells per image, and when possible, with multiple regions studied per slice. Manual construction of small oval or round regions of interest (ROI) encompassing the soma was used to analyze the

activity of these cells. The average fluorescence intensities within ROIs were calculated as a function of time and exported as a text file(Takano et al., 2012). Response to the electrical stimulus was quantified with a custom-written Matlab GUI code. Briefly, the average intensity within ROIs over time (calcium transient trace) that had been calculated in Nikon Elements software were imported as a text file in Matlab. Change in fluorescence relative to background fluorescence ($\Delta F/F_0$) was calculated, processed using a Savitzky-Golay smoothing filter, and derivatives of the traces were calculated for each ROI. An initial threshold value for detecting a local maximum in the derivative trace was estimated based on the entire trace for each ROI. With a sliding window, timing for a local maximum of the derivative trace was detected along with the timing for zero-crossing values for each local maximum event. The area under the $\Delta F/F_0$ curve for the event was used as the second threshold to discriminate stimulus response from noise. After determining the stimulus response, the local maximum, onset time, and 90% decay time point was estimated in $\Delta F/F_0$ trace for each ROI. In this algorithm, since the number of events within a trace is unlimited, it is possible to detect multiple peaks in a trace in in response to a slow stimulation rate (~1 Hz) as well as spontaneous activities. The Matlab GUI code also included manual supervision/inspection steps to manually reject incorrectly identified stimulus responses. The code is available upon request. All event and related properties (ROI I.D. number, peak I.D. number, onset time, maximum $\Delta F/F_0$ value, peak timing, 90% decay time, a parameter for an exponential decay fit in decay portion of the trace) were recorded and exported as Excel files for aggregate analysis. Each cell's activity was observed over time and across conditions using an ID number attached to the ROI delineating each cell. Picrotoxin (PTX, 50 μM), a $GABA_A$ receptor antagonist, was applied at the end of experiments to confirm that individual neurons were able to respond to the afferent stimulus. Cells that were inactive in both

control and PTX conditions were excluded from further analysis. Slices in which 70% of cellular ROIs did not activate in the presence of PTX were considered damaged or deafferented and excluded from analysis (< 5% slices).

m- and sIPSC recordings. mIPSCs were recorded in ACSF that, along with DNQX (10 μM) and D-AP-5 (50 μM), included tetrodotoxin (TTX; 1 μM) to block APs, sIPSCs were recorded without TTX. Whole-cell voltage-clamp recording of mIPSCs was conducted using a high-chloride internal pipette solution, which resulted in an inward chloride current with cells clamped at -76 mV (corrected for liquid junction potential in Clampfit). The pipette solution consisted of the following (in mM): 100 $CsCH_3O_3S$, 50 CsCl, 3 KCl, 0.2 BAPTA, 10 HEPES, 1 $MgCl_2$, 2.5 Phosphcreatine-2Na, 2 Mg-ATP, and 0.25 GTP-Tris, titrated to pH 7.2–7.3 with 3 M CsOH (osmolarity 280–290 mOsm). In all experiments, lidocaine N-ethylbromide (QX-314; 5 mM) was added to the pipette solution on the day of the experiment. Synaptic currents were recorded using an Axopatch 200B amplifier (Molecular Devices), filtered at 2 kHz, sampled at 20 kHz, digitized (Digidata 1320A; Molecular Devices), and stored for off- line analysis (using Minianalysis software written in IGOR Pro; Wavemetrics, Lake Oswego, OR) (Hwang and Copenhagen, 1999). Access resistance stability (10–18 MΩ; 80% compensation) was monitored using a 2 mV voltage step applied every 120 s, and data from cells were discarded when >15% change occurred.

Histology and immunocytochemistry. Animals were perfused with 4% paraformaldehyde in phosphate buffered saline. Horizontal hippocampal-entorhinal cortex slices (60 μm) were cut using a vibrating tissue slicer (Vibratome VT1200S, Leica). Slices were blocked for 4 hours from non-specific binding with 5% normal goat serum in PBS with 0.4% Triton-X 100 (Sigma, St. Louis, MO) at 4°. Slices were

incubated in rabbit anti-GFAP polyclonal antibody (Sigma, St. Louis, MO; Cat. #G4546; recommend for human, mouse and rat GFAP) diluted 1:400 in blocking solution for 12 hours at 4°, and washed 3x in PBS with 0.2% Triton-X-100 for 15 minutes. Slices were then incubated in Alexa Fluor 633 conjugated goat anti-rabbit highly cross-adsorbed IgG (H+L) (Thermo Fisher, Carlsbad, CA; Cat. #A21071) and DAPI (Thermo Fisher diluted 1:1000) secondary diluted 1:400 diluted in blocking solution for 1 hour at room temperature , and then washed 3x for 20 minutes. All incubations and washes occurred on a tissue rocker. Slices were mounted on glass slides in SlowFade Gold mounting media (Thermo Fisher). Images were collected using an Olympus FV1000 confocal microscope.

Statistical analysis. N values for experiments were determined based on variance estimates derived from previous similar studies (Cohen et al., 2003; Ortinski et al., 2010; Takano et al., 2012; Yu et al., 2013a). Datasets were tested for normality with a Kolmogorov-Smirnov test to determine appropriate statistical testing methods between groups. Differences in variance between groups were tested with a Brown-Forsythe test. If unequal variances were detected, data were log(value+1) transformed to satisfy statistical testing assumptions of equal variance. For comparisons between 2 groups, significance was tested using either one- or two-way *t* tests, or for non-normally distributed data, a Mann–Whitney *U* test. For multiple group comparisons, statistical significance was tested using either a one- or two-way ANOVA, with *post hoc* Tukey's and Dunnett's tests for multiple-comparisons correction, or for non-normally distributed data, a Kruskal-Wallis test with *post hoc* Dunn's test for multiple-comparisons correction. Center values from normally distributed datasets are expressed as mean ± SEM; center values from non-normally distributed datasets are expressed as median ±

interquartile range. Differences between population distributions were assessed using a Kolmorgorov–Smirnov test. Contingency tables were analyzed with Fisher's exact test. In all statistical testing, p values <0.05 were considered evidence of statistical significance, unless explicitly stated otherwise. Statistical test scores and degrees of freedom (DOF) are reported as score (DOF between groups, DOF between samples), or simply, score (DOF samples) when two groups are compared.

Blinding. Animal selection for naïve or SE groups was random. For MCI studies, experimental blinding was not entirely possible because of obvious behavioral changes in mice following SE. However, time post-SE was blinded where possible. Following collection of MCI images, data analysis was conducted blinded. For whole cell patch recordings and analysis, the experimental investigator was blinded to animal identity.

Chapter 4 Bibliography

Alme CB, Buzzetti RA, Marrone DF, Leutgeb JK, Chawla MK, Schaner MJ, Bohanick JD, Khoboko T, Leutgeb S, Moser EI, Moser M-B, McNaughton BL, Barnes CA (2010) Hippocampal granule cells opt for early retirement. Hippocampus 20:1109–1123.

Ang CW, Carlson GC, Coulter DA (2006) Massive and specific dysregulation of direct cortical input to the hippocampus in temporal lobe epilepsy. J Neurosci 26:11850–11856.

Bakker A, Kirwan CB, Miller M, Stark CEL (2008) Pattern separation in the human hippocampal CA3 and dentate gyrus. Science 319:1640–1642.

Bender R a, Soleymani S V, Brewster AL, Nguyen ST, Beck H, Mathern GW, Baram TZ (2003) Enhanced expression of a specific hyperpolarization-activated cyclic nucleotide-gated cation channel (HCN) in surviving dentate gyrus granule cells of human and experimental epileptic hippocampus. J Neurosci 23:6826–6836.

Buckmaster PS, Dudek FE (1997) Neuron loss, granule cell axon reorganization, and functional changes in the dentate gyrus of epileptic kainate-treated rats. J Comp Neurol 385:385–404.

Buckmaster PS, Yamawaki R, Thind K (2016) More docked vesicles and larger active zones at basket cell-to-granule cell synapses in a rat model of temporal lobe epilepsy. J Neurosci 36:3295–3308.

Buzsáki G (1984) Feed-forward inhibition in the hippocampal formation. Prog Neurobiol 22:131–153.

Chawla MK, Guzowski JF, Ramirez-Amaya V, Lipa P, Hoffman KL, Marriott LK, Worley PF, McNaughton BL, Barnes CA (2005) Sparse, environmentally selective expression of Arc RNA in the upper blade of the rodent fascia dentata by brief spatial experience. Hippocampus 15:579–586.

Cohen AS, Lin DD, Quirk GL, Coulter DA (2003) Dentate granule cell GABA(A) receptors in epileptic hippocampus: enhanced synaptic efficacy and altered pharmacology. Eur J Neurosci 17:1607–1616.

Cossart R, Ikegaya Y, Yuste R (2005) Calcium imaging of cortical networks dynamics. Cell Calcium 37:451–457.

Coulter DA, Carlson GC (2007) Functional regulation of the dentate gyrus by GABA-mediated inhibition. Prog Brain Res 163:235–243.

Coulter DA, Eid T (2012) Astrocytic regulation of glutamate homeostasis in epilepsy. Glia 60:1215–1226.

Dieni C V., Nietz AK, Panichi R, Wadiche JI, Overstreet-Wadiche L (2013) Distinct determinants of sparse activation during granule cell maturation. J Neurosci 33:19131–19142.

Eid T, Thomas MJ, Spencer DD, Rundén-Pran E, Lai JCK, Malthankar G V., Kim JH, Danbolt NC, Ottersen OP, De Lanerolle NC (2004) Loss of glutamine synthetase in the human epileptogenic hippocampus: Possible mechanism for raised extracellular glutamate in mesial temporal lobe epilepsy. Lancet 363:28–37.

Ewell LA, Jones M V (2010) Frequency-tuned distribution of inhibition in the dentate gyrus. J Neurosci 30:12597–12607.

Freund TF, Buzsáki G (1996) Interneurons of the hippocampus. Hippocampus 6:347–470.

Fricke R, Prince D (1984) Electrophysiology of dentate gyrus granule cells. J Neurophysiol 51.

Gibbs JW, Shumate MD, Coulter DA (1997) Differential epilepsy-associated alterations in postsynaptic GABA(A) receptor function in dentate granule and CA1 neurons. J Neurophysiol 77:1924–1938.

Heinemann U, Beck H, Dreier JP, Ficker E, Stabel J, Zhang CL (1992) The dentate gyrus as a regulated gate for the propagation of epileptiform activity. Epilepsy Res Suppl 7:273–280.

Hellier JL, Patrylo PR, Dou P, Nett M, Rose GM, Dudek FE (1999) Assessment of inhibition and epileptiform activity in the septal dentate gyrus of freely behaving rats during the first week after kainate treatment. J Neurosci 19:10053–10064.

Hester MS, Danzer SC (2013) Accumulation of abnormal adult-generated hippocampal granule cells predicts seizure frequency and severity. J Neurosci 33:8926–8936.

Higley MJ, Contreras D (2006) Balanced excitation and inhibition determine spike timing during frequency adaptation. J Neurosci 26:448–457.

Jung MW, McNaughton BL (1993) Spatial selectivity of unit activity in the hippocampal granular layer. Hippocampus 3:165–182.

Kobayashi M, Buckmaster PS (2003) Reduced inhibition of dentate granule cells in a model of temporal lobe epilepsy. J Neurosci 23:2440–2452.

Krook-Magnuson E, Armstrong C, Bui A, Lew S, Oijala M, Soltesz I (2015) In vivo evaluation of the dentate gate theory in epilepsy. J Physiol 593:2379–2388.

Krueppel R, Remy S, Beck H (2011) Dendritic integration in hippocampal dentate granule cells. Neuron 71:512–528.

Leutgeb JK, Leutgeb S, Moser M-B, Moser EI (2007) Pattern separation in the dentate gyrus and CA3 of the hippocampus. Science 315:961–966.

Liang S-L, Carlson GC, Coulter D a (2006) Dynamic regulation of synaptic GABA release by the glutamate-glutamine cycle in hippocampal area CA1. J Neurosci 26:8537–8548.

Lothman EW, Bertram EH, Stringer JL (1991) Functional anatomy of hippocampal seizures. Prog Neurobiol 37:1–82.

Marín-Burgin A, Mongiat LA, Pardi MB, Schinder AF (2012) Unique processing during a

period of high excitation/inhibition balance in adult-born neurons. Science 335:1238–1242.

Masukawa LM, Higashima M, Kim JH, Spencer DD (1989) Epileptiform discharges evoked in hippocampal brain slices from epileptic patients. Brain Res 493:168–174.

Masukawa LM, Wang H, O'Connor MJ, Uruno K (1996) Prolonged field potentials evoked by 1 Hz stimulation in the dentate gyrus of temporal lobe epileptic human brain slices. Brain Res 721:132–139.

Müller A, Kukley M, Stausberg P, Beck H, Müller W, Dietrich D (2005) Endogenous Ca2+ buffer concentration and Ca2+ microdomains in hippocampal neurons. J Neurosci 25:558–565.

Nakashiba T, Buhl DL, McHugh TJ, Tonegawa S (2009) Hippocampal CA3 output is crucial for ripple-associated reactivation and consolidation of memory. Neuron 62:781–787.

Neunuebel JP, Knierim JJ (2012) Spatial firing correlates of physiologically distinct cell types of the rat dentate gyrus. J Neurosci 32:3848–3858.

Ortinski PI, Dong J, Mungenast A, Yue C, Takano H, Watson DJ, Haydon PG, Coulter DA (2010) Selective induction of astrocytic gliosis generates deficits in neuronal inhibition. Nat Neurosci 13:584–591.

Pardi MB, Ogando MB, Schinder AF, Marin-Burgin A (2015) Differential inhibition onto developing and mature granule cells generates high-frequency filters with variable gain. Elife 4:1–17.

Parent JM, Yu TW, Leibowitz RT, Geschwind DH, Sloviter RS, Lowenstein DH (1997) Dentate granule cell neurogenesis is increased by seizures and contributes to aberrant network reorganization in the adult rat hippocampus. J Neurosci 17:3727–3738.

Pathak HR, Weissinger F, Terunuma M, Carlson GC, Hsu F-C, Moss SJ, Coulter DA (2007) Disrupted dentate granule cell chloride regulation enhances synaptic excitability during development of temporal lobe epilepsy. J Neurosci 27:14012–14022.

Patrylo PR, Schweitzer JS, Dudek FE (1999) Abnormal responses to perforant path stimulation in the dentate gyrus of slices from rats with kainate-induced epilepsy and mossy fiber reorganization. Epilepsy Res 36:31–42.

Pinheiro PS, Lanore F, Veran J, Artinian J, Blanchet C, Crépel V, Perrais D, Mulle C (2013) Selective block of postsynaptic kainate receptors reveals their function at hippocampal mossy fiber synapses. Cereb Cortex 23:323–331.

Pouille F, Marin-Burgin A, Adesnik H, Atallah B V, Scanziani M (2009) Input normalization by global feedforward inhibition expands cortical dynamic range. Nat Neurosci 12:1577–1585.

Pouille F, Scanziani M (2001) Enforcement of temporal fidelity in pyramidal cells by somatic feed-forward inhibition. Science 293:1159–1163.

Scharfman HE, Sollas AE, Berger RE, Goodman JH, Pierce JP (2003) Perforant path activation of ectopic granule cells that are born after pilocarpine-induced seizures. Neuroscience 121:1017–1029.

Schmidt-Hieber C, Jonas P, Bischofberger J (2007) Subthreshold dendritic signal processing and coincidence detection in dentate gyrus granule cells. J Neurosci 27:8430–8441.

Scobie KN, Hall BJ, Wilke S a, Klemenhagen KC, Fujii-Kuriyama Y, Ghosh A, Hen R, Sahay A (2009) Krüppel-like factor 9 is necessary for late-phase neuronal maturation in the developing dentate gyrus and during adult hippocampal neurogenesis. J Neurosci 29:9875–9887.

Shao L-R, Dudek FE (2005) Changes in mIPSCs and sIPSCs after kainate treatment: evidence for loss of inhibitory input to dentate granule cells and possible compensatory responses. J Neurophysiol 94:952–960.

Sloviter RS (1987) Decreased hippocampal inhibition and a selective loss of interneurons in experimental epilepsy. Science 235:73–76.

Sloviter RS (1991) Permanently altered hippocampal structure, excitability, and inhibition after experimental status epilepticus in the rat: the “dormant basket cell” hypothesis and its possible relevance to temporal lobe epilepsy. Hippocampus 1:41–66.

Staley KJ, Otis TS, Mody I (1992) Membrane properties of dentate gyrus granule cells: comparison of sharp microelectrode and whole-cell recordings. J Neurophysiol 67:1346–1358.

Sun C, Mtchedlishvili Z, Bertram EH, Erisir A, Kapur J (2007) Selective loss of dentate hilar interneurons contributes to reduced synaptic inhibition of granule cells in an electrical stimulation-based animal model of temporal lobe epilepsy. J Comp Neurol 500:876–893.

Sun C, Sun J, Erisir A, Kapur J (2014) Loss of cholecystokinin-containing terminals in temporal lobe epilepsy. Neurobiol Dis 62:44–55.

Takano H, McCartney M, Ortinski PI, Yue C, Putt ME, Coulter DA (2012) Deterministic and stochastic neuronal contributions to distinct synchronous CA3 network bursts. J Neurosci 32:4743–4754.

Tang FR, Chia SC, Jiang FL, Ma DL, Chen PM, Tang YC (2006) Calcium binding protein containing neurons in the gliotic mouse hippocampus with special reference to their afferents from the medial septum and the entorhinal cortex. Neuroscience 140:1467–1479.

Tauck DL, Nadler J V (1985) Evidence of functional mossy fiber sprouting in hippocampal formation of kainic acid-treated rats. J Neurosci 5:1016–1022.

Thind KK, Yamawaki R, Phanwar I, Zhang G, Wen X, Buckmaster PS (2010) Initial loss but later excess of GABAergic synapses with dentate granule cells in a rat model of temporal lobe epilepsy. J Comp Neurol 518:647–667.

van Praag H, Schinder AF, Christie BR, Toni N, Palmer TD, Gage FH (2002) Functional

neurogenesis in the adult hippocampus. Nature 415:1030–1034.

Williamson A (1994) Electrophysiology of epileptic human neocortical and hippocampal neurons maintained in vitro. Clin Neurosci 2:47–52.

Yu EP, Dengler CG, Frausto SF, Putt ME, Yue C, Takano H, Coulter DA (2013a) Protracted postnatal development of sparse, specific dentate granule cell activation in the mouse hippocampus. J Neurosci 33:2947–2960.

Yu J, Proddutur A, Elgammal FS, Ito T, Santhakumar V (2013b) Status epilepticus enhances tonic GABA currents and depolarizes GABA reversal potential in dentate fast-spiking basket cells. J Neurophysiol 109:1746–1763.

Zhang N, Wei W, Mody I, Houser CR (2007) Altered localization of GABA(A) receptor subunits on dentate granule cell dendrites influences tonic and phasic inhibition in a mouse model of epilepsy. J Neurosci 27:7520–7531.

Zhang W, Yamawaki R, Wen X, Uhl J, Diaz J, Prince DA, Buckmaster PS (2009) Surviving hilar somatostatin interneurons enlarge, sprout axons, and form new synapses with granule cells in a mouse model of temporal lobe epilepsy. J Neurosci 29:14247–14256.

CHAPTER 5: Future directions and conclusions

The DG normally functions as both a sparsifying transformer of cortical inputs in spatial cognitive processes as well as a regulatory checkpoint for these cortical inputs before relay into the hippocampus. In Chapter 3 (Dengler et al., 2017), we describe massive dysregulation in the excitability of this circuit following epileptogenic injury and accompanying epilepsy development in *ex vivo* slice preparations. While other pathways in the hippocampus exhibit heightened excitability with epilepsy development (e.g. direct cortical input to area CA1 via the temporoammonic pathway; Ang et al., 2006), the upward swing observed in DG principle cell excitability is among the most massive phenomena described in the epileptic hippocampus. Substantial changes to the DG's circuit structure accompany this hyperexcitability including the *de novo* sprouting of recurrent mossy fiber collaterals, the death of existing hilar inhibitory neurons and aberrant generation of new neurons, as well as many other perturbations (Reviewed in Chapter 2; Dengler and Coulter, 2016).

Understanding DGC activation *in vivo*

Given these alterations to the DG's activation in slice preparations and the well-documented changes to the circuit's substrate, an important future step is to extend studies of DGC activation *in vivo* to more completely understand how this circuit activates. While electrophysiological recording techniques have been able to access the DG's relatively deep structure and record from DGCs in behaving animals for several decades (Jung and McNaughton, 1993), this approach samples a relatively low number of neurons in the circuit and cannot easily confirm the identity of recorded cells. *In vivo*

MCI approaches, however, are able not only to confirm cellular identity readily via morphological features and fluorescent genetic markers but also inherently allow recording from a relatively large population of neurons while retaining the spatial and temporal properties of their activation. One challenge of applying MCI techniques *in vivo* has been the relatively deep anatomic position of the DG, which sits ventrally beneath both the cortex and area CA1. Recent advances in 2-photon microscopy techniques (Kawakami et al., 2015), microendoscopic approaches (Jung et al., 2004; Levene et al., 2004; Andermann et al., 2013), and subcortical windows (Pilz et al., 2016) have allowed *in vivo* imaging approaches, including functional MCI, to access deep brain structures including the DG. This application of MCI to the DG could be used to more definitively assess how the DG activates *in vivo* and whether pathological activation in entorhinal cortex or epileptic animals produces hyperexcitability in DGCs similar to our results in slice recordings. Further, these MCI techiniques can be used in awake, behaving mice (Dombeck et al., 2010; Danielson et al., 2017) to investigate the coding of spatial information in the epileptic DG. Little is known about how epilepsy alters the spatial receptive fields of DGCs. However, there is evidence that epilepsy corrupts the receptive place fields of CA1 pyramidal cells as well as the performance of hippocampal-dependent cognitive tasks (Liu et al., 2003; Lin et al., 2009; Kleen et al., 2010). Given the DG's inappropriate circuit activation *in vitro*, and its many circuit alterations, similar deficits in the DGC activation are likely to be observed in behaving animals. Future *in vivo* MCI studies in the DG could assess the proportion of DGCs which exhibit spatially modulated firing, the informational content of these cells, and other properties of their spatial receptive fields that may be aberrantly affected by the numerous pathological changes occurring in the DG of animals developing and expressing epilepsy.

Chronic modulation of DGC excitability

The potential significance of the aberrant, pathology-associated changes to the DG's circuit function and its neural substrate are further heightened by several recent studies. Two such studies have examined the temporal sequences of seizure propagation and have demonstrated that that seizures are most often first recorded in hippocampal structures (Toyoda et al., 2013), and that DGCs exhibit heightened activation prior to and early during seizures (Fujita et al., 2014). Another pivotal study used optogenetic techniques to modulate DGC excitability and demonstrated that selective activation of DGCs with channelrhodopsin is sufficient to elicit seizures in healthy control animals, and that such activation exacerbates spontaneous seizures in epileptic mice (Krook-Magnuson et al., 2015). Further, optogenetic hyperpolarization of DGCs stopped spontaneous seizures acutely in these mice. These results clearly support the concept that the DG is a critical node within the hippocampus and provides direct *in vivo* evidence consistent with the dentate "gate" hypothesis. However, they do not address whether the excitability alterations present in the epileptic DG play a causal role in either epileptogenesis, ictogenesis, or the cognitive comorbidities associated with epilepsy.

In light of this uncertainty, several questions are raised. Would restoration of DGC excitability to normal levels be sufficient to reduce the incidence of epilepsy following an epileptogenic injury? Would such a manipulation lower seizure propensity in an already epileptic brain? Conversely, would chronically elevating levels of DGC excitability be ictogenic, or even epileptogenic in an otherwise healthy brain? Recent advances in chemogenetic agents for modulating neural excitability are likely to be of great value in addressing these questions directly. One such system, DREADDs (designer receptors activated exclusively by designer drugs), allows for dose-dependent, tonic, bi-directional modulation of excitability within brain circuits (Alexander et al., 2009; Urban

and Roth, 2015). This approach offers benefits over commonly used optogenetic reagents, which require implantation of light guides and most commonly activate or inhibit neurons in a powerful, "all-or-nothing," time/light dependent manner restricted to brain regions where light penetration occurs, whereas chemogenetic approaches provide a dose-dependent, tonic, widely distributed, and more modulatory approach. DREADD modulation in other non-DG circuits has already shown efficacy in lessening disease severity in several models of epilepsy (Kätzel et al., 2014; Avaliani et al., 2016).

Using such a system, DGC excitability could be enhanced specifically in control animals to test the sufficiency of DGC hyperexcitability in both icto-and epileptogenesis. In epileptogenic and chronically epileptic animals DGC excitability could be lowered to normal levels, to test whether DGC hyperexcitability is necessary for seizure generation and epileptogenesis. Another area where this approach could be implemented is to better understand the role of appropriate DGC excitability in the completion of DG and hippocampal-dependent cognitive functions as well as in the generation of anxiety-like behavior. These functions are compromised in epileptic animals and patients (Jokeit and Ebner, 2002; Liu et al., 2003; Hermann et al., 2006; Kleen et al., 2010; Gu et al., 2015). By increasing DGC excitability in healthy mice, and decreasing it in epileptic mice, we could further understand the necessity and sufficiency of appropriate DGC activation in the completion of the hippocampus's cognitive functions. Further, because proper activation is necessary for the accomplishment of a circuit's cognitive function, it is likely that these manipulations could implicate a causal role in cognitive and affective deficits associated with epilepsy.

DGC excitability as a biomarker

Our finding of massive hyperexcitability in DGCs during epilepsy development provides a rationale for future studies to better understand both how DGCs activate *in vivo* during epileptogenesis and how modulating their excitability modifies epilepsy severity. However, our results also provide potential utility as a biomarker of epileptogenesis and potentially other diseases. Our MCI studies provide a readout of aggregate DG circuit excitability, and as such, could be used to understand better how various therapies affect the DG circuit and, further, how DG circuit activation is altered by disease modifying treatments. While there are currently no cures for temporal lobe epilepsy, one area of great interest has been in epilepsy prevention, or "anti-epileptogenic therapy." The basic premise of anti-epileptogenic strategies is to provide a therapeutic intervention following an epileptogenic injury, which prevents or diminishes the circuit perturbations occurring during the latent period that lead to epilepsy development.

Several lines of research for antiepileptic strategies exist. Among the most successful preclinical investigation of anti-epileptogenic agents is a recent study in which Gu et al. (2015) used a novel peptide that prevents signaling of TrkB receptors through the phospholipase Cγ1 pathway. Following status epilepticus, this therapeutic intervention strongly inhibited the development of epilepsy and also prevented epilepsy-associated anxiety phenotypes. Further successes in anti-epileptogenesis interventional therapy have been shown using anti-inflammatory approaches (reviewed in Terrone et al., (2016), though most of these treatments tend to be disease-modifying, lessening the severity of epilepsy, but exhibit little effect on the likelihood of epilepsy development following injury. Given our results of DGC hyperexcitability in a model of epilepsy, would preventing epilepsy development via anti-epileptogenic therapy also restore normal DGC

activation? Does DGC hyperexcitability predict the development or severity of epilepsy? The answers to these questions would clarify the importance of DGC network dysfunction in epilepsy development.

DGC integration: to fire or not to fire?

One final and very fundamental question about DG physiology is raised by our results, and by many other studies in the field. What makes a DGC activate, or fail to activate, in response to afferent input? While this may seem a simple question, one of the most enigmatic aspects of DG function is the extreme sparseness of activity of its principal cells. Very few DGCs display significant activity, both *in vivo* (Jung and McNaughton, 1993; Chawla et al., 2005; Alme et al., 2010) and *in vitro* (Ewell and Jones, 2010; Yu et al., 2013; Dengler et al., 2017). However, some studies have suggested that the same small fraction of GCs active at any given time appears to be active in many environments (Leutgeb et al., 2007; Alme et al., 2010). As such, some authors have proposed that GCs fall into two populations: active and silent (Aimone et al., 2010; Alme et al., 2010; Lisman, 2011). It is unlikely that these "silent" cells *never* fire, for what would be the evolutionary advantage of maintaining 1 million DGCs in the rodent brain, where 950,000 are merely a nonfunctional, metabolic burden? It is possible that the detected "active cells" are simply more active then their neighboring cells, which are not truly "silent". An alternative possibility is that these "active cells" are only active during certain behavioral epochs and coding switches among different subpopulations of DGCs. The concept of subpopulations of neurons within a circuit having enhanced excitability compared to neighboring cells is not unique to the DG. Yassin et al. (2010) show one such example in the neocortex, where the majority of neurons have extremely low firing rates, and a small, highly active population of cells dominates activity in the network.

The authors use a transgenic mouse expressing a fluorescent immediate-early gene reporter to examine cells with a recent history of elevated activity. These neurons fired at higher rates compared to neurons which did not express the reporter and their heightened excitability was attributed to their receiving increased excitatory and decreased inhibitory drive. Further, these "active" cells had a high likelihood of being inter-connected with each other.

There is no clear mechanism identified to date explaining the relative silence of so many GCs, or what enables the more highly active DGCs to fire. Data presented in the dissertation show that sparse firing is mediated predominately by local inhibition, and in the case of epilepsy development, this sparse activity is corrupted by varying sources of disinhibition. However, these data do not yet explain what makes some DGCs more predisposed to activation. Some studies have indirectly suggested immature abGCs may be more predisposed to activating than their older counterparts (Ramirez-Amaya et al., 2006; Kee et al., 2007; Marín-Burgin et al., 2012). Additional, equally indirect studies have provided evidence that older GCs functionally "retire" and are no longer activated during cognitive tasks (Alme et al., 2010; Sandoval et al., 2011). Some authors modelling DGC network activation have hypothesized that the active pool of DGCs forms because of enhanced long term potentiation in excitable, immature DGCs, and reciprocally, that continual long term depression is a mechanism through which older, less excitable cells become non-functional (Lisman, 2011).

More recent data have suggested the exact opposite: that more mature DGCs are predisposed to activation. In a recent study, Diamantaki et al. (2016) performed *in vivo* juxtacellular recordings of DGCs during spatial navigation tasks in which they fluorescently labeled recorded neurons. They found that the complexity and elaboration of a DGC's dendritic arbor was highly predictive whether a neuron was active or silent *in*

vivo. DGCs with more complex dendritic trees were most likely to activate. Because immature DGCs have smaller, less elaborate dendritic arbors during their development than older DGCs (Espósito et al., 2005; Ge et al., 2006), these data suggest that a subset of mature DGCs are likely to contribute to the DG's active principal cell population. Currently, there is no consensus for explaining what factors contribute to the active and silent populations of DGCs and, further, there is no direct evidence of what specific physiological phenomena differentiate the two. Future patch clamp studies in which active and silent DGCs are identified either molecularly (via immediate early gene reporters) or physiologically (via MCI-targeted recordings) would allow explicit testing of possible mechanisms that contribute to the activate/remain silent decision made by DGCs. These mechanisms are not mutually exclusive, and include: hyper-excitable cell-intrinsic properties, and alterations in local synaptic inhibition or excitation. Such recordings, when coupled with transgenic birth-dating strategies, could more definitively illuminate the mechanisms determining the crucial decision of DGCs to fire or not fire after integrating their inputs: perhaps the most fundamental aspect of circuit function in the nervous system. Understanding these phenomena in the epileptic brain, where DGC's decision to fire is corrupted and biased toward hyperexcitation, would yield critical insights into how epilepsy degrades appropriate circuit activation.

Final Remarks

In this body of work, I have characterized both the development of sparse DGC activation during animal maturation, as well as its corruption during epilepsy development. To best summarize the myriad circuit perturbations occurring in the DG as epilepsy develops, we present an illustration outlining major changes to the DG's circuitry in **Figure 5.1**. Early following epileptogenic injury, the most immediate

compelling circuit disruption is cell death, particularly that of hilar interneurons and mossy cells. In the following days -and out to approximately two weeks after the initial injury - hyperexcitability and disinhibition are evident in the DGCs as assessed by MCI and patch clamp recordings respectively. These phenomena occur concurrently with GABA receptor repression and disrupted chloride regulation and these mechanisms appear to contribute to DGC hyperexcitability early following injury. Also, aberrant neurogenesis occurs from several days out to one month post-injury. Our studies, although indirect, do not implicate disproportionate activation of DGCs born following injury, at least in normotopic abDGCs. However, the activity and circuit contributions of ectopic DGCs were not examined in our studies. Later, DGC excitability exhibits a secondary enhancement at times greater than 2 months following injury. Roughly one month following injury, mossy fiber sprouting (green) becomes evident and this sprouting continues to escalate for months, further enhancing auto-excitatory input between DGCs. Finally, astrocytic gliosis, a phenomenon that appears to be a chronic occurrence following epileptic injury, has several effects on overall hippocampal circuit function, the most interesting of which is the loss of glutamine synthetase which can lead to deficits in presynaptic production of GABA. Our data in Dengler et al. (2017) implicate both astrogliosis-mediated disinhibition and, to a lesser extent, mossy fiber sprouting as contributing mechanisms to the enhanced excitability of DGCs later during chronic epilepsy. Taken together, these data demonstrate a novel, trimodal shift in DGC excitability during epilepsy's development and expression. DGCs transition from a sparsely activating network in healthy animals to a hyperexcitable circuit immediately following SE. Normal activation recovers transiently, and then DG circuit function exhibits a secondary, and likely permanent, collapse towards hyperexcitability as epilepsy manifests. Deficits in local inhibitory functional appear to mediate this

trimodal shift in excitability, though the mechanisms underlying this disinhibition diverge as epilepsy develops.

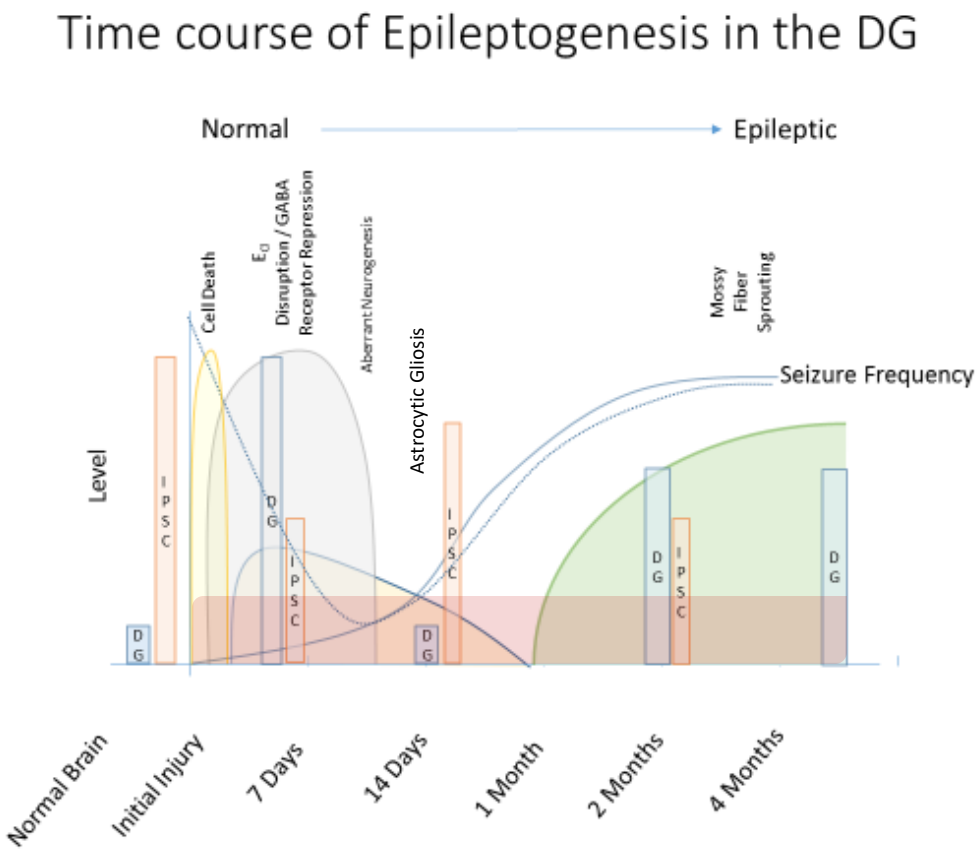

Figure 5.1 Time course of epileptogenesis in the DG. Schematic illustration of the sequence of major pathological circuit alterations in the DG following epileptogenic injury. Blue bars indicate relative degree of proportional DGC firing as assessed by MCI. Red bars indicate relative IPSC amplitudes as assessed by patch recordings. Note that when IPSC amplitudes are reduced, DGC activation is elevated. Yellow indicates occurrence of cell death following injury. Grey indicates time of disruption in chloride regulation and GABA receptor repression. Tan with blue border represents aberrant neurogenesis. Green represents mossy fiber sprouting. Light red represents chronic occurrence of astrocytic gliosis. Blue line indicates seizure frequency, and dotted line accounts for acute, post-SE seizures, occurring immediately following SE in some animals, which are not typically regarded as "epileptic" seizures." Figure C. Dengler, adapted from Rakhade and Jensen, (2009)

In this dissertation, we have characterized a massive enhancement in DGC excitability where inappropriate, pathological circuit function occurs in a circuit critical to normal hippocampal-dependent cognitive functions. This aberrant circuit activation may contribute to seizure propensity, primary and secondary epileptogenic processes, as well as the many cognitive comorbidities associated with epilepsy. Understanding the activation of the DG *in vivo* and how altering its excitability affects seizure propensity and alters cognitive function are critical next steps in understanding the DG's role in both epileptogenesis and cognition. Further work is also required to better understand the utility of DG activation as a biomarker of both epileptogenesis and its prevention. Lastly, investigation of the fundamental physiological parameters that govern DGC activation is crucial to determining how the normal DG functions, and the specific mechanisms which cause its dysfunction. In conclusion, understanding how epilepsy development alters the basic circuit properties of the DG is critical to understanding how a normal brain transforms into an epileptic brain and how epilepsy-associated cognitive comordbidities manifest as a result of this transormation. This understanding is essential to guide the search for new therapies in epilepsy prevention, seizure amelioration, and remediation of comorbidities accompanying epilepsy.

Chapter 5 Bibliography

Aimone JB, Deng W, Gage FH (2010) Put them out to pasture? What are old granule cells good for, anyway…? Hippocampus 20:1124–1125.

Alexander GM, Rogan SC, Abbas AI, Armbruster BN, Pei Y, Allen John A., Nonneman RJ, Hartmann J, Moy SS, Nicolelis MA, McNamara JO, Roth BL (2009) Remote control of neuronal activity in transgenic mice expressing evolved G protein-coupled receptors. Neuron 63:27–39.

Alme CB, Buzzetti RA, Marrone DF, Leutgeb JK, Chawla MK, Schaner MJ, Bohanick JD, Khoboko T, Leutgeb S, Moser EI, Moser M-B, McNaughton BL, Barnes CA (2010) Hippocampal granule cells opt for early retirement. Hippocampus 20:1109–1123.

Andermann ML, Gilfoy NB, Goldey GJ, Sachdev RNS, Wölfel M, McCormick DA, Reid RC, Levene MJ (2013) Chronic cellular imaging of entire cortical columns in awake mice using microprisms. Neuron 80:900–913.

Ang CW, Carlson GC, Coulter DA (2006) Massive and specific dysregulation of direct cortical input to the hippocampus in temporal lobe epilepsy. J Neurosci 26:11850–11856.

Avaliani N, Andersson M, Runegaard AH, Woldbye D, Kokaia M (2016) DREADDs suppress seizure-like activity in a mouse model of pharmacoresistant epileptic brain tissue. Gene Ther 23:1–7.

Chawla MK, Guzowski JF, Ramirez-Amaya V, Lipa P, Hoffman KL, Marriott LK, Worley PF, McNaughton BL, Barnes CA (2005) Sparse, environmentally selective expression of Arc RNA in the upper blade of the rodent fascia dentata by brief spatial experience. Hippocampus 15:579–586.

Danielson NB, Turi GF, Ladow M, Chavlis S, Petrantonakis PC, Poirazi P, Losonczy A (2017) In Vivo Imaging of Dentate Gyrus Mossy Cells in Behaving Mice. Neuron 93:552–559.e4.

Dengler CG, Coulter DA (2016) Normal and epilepsy-associated pathologic function of the dentate gyrus. Prog Brain Res 226:155–178.

Dengler CG, Yue C, Takano H, Coulter DA (2017) Massively augmented hippocampal dentate granule cell activation accompanies epilepsy development. Sci Rep 7:42090.

Diamantaki M, Frey M, Berens P, Preston-Ferrer P, Burgalossi A (2016) Sparse activity of identified dentate granule cells during spatial exploration. Elife 5:1–16.

Dombeck DA, Harvey CD, Tian L, Looger LL, Tank DW (2010) Functional imaging of hippocampal place cells at cellular resolution during virtual navigation. Nat Neurosci 13:1433–1440.

Espósito MS, Piatti VC, Laplagne DA, Morgenstern NA, Ferrari CC, Pitossi FJ, Schinder AF (2005) Neuronal differentiation in the adult hippocampus recapitulates

embryonic development. J Neurosci 25:10074–10086.

Ewell LA, Jones MV (2010) Frequency-tuned distribution of inhibition in the dentate gyrus. J Neurosci 30:12597–12607.

Fujita S, Toyoda I, Thamattoor AK, Buckmaster PS (2014) Preictal activity of subicular, CA1, and dentate gyrus principal neurons in the dorsal hippocampus before spontaneous seizures in a rat model of temporal lobe epilepsy. J Neurosci 34:16671–16687.

Ge S, Goh ELK, Sailor KA, Kitabatake Y, Ming G, Song H (2006) GABA regulates synaptic integration of newly generated neurons in the adult brain. Nature 439:589–593.

Gu B, Huang YZ, He X-P, Joshi RB, Jang W, McNamara JO (2015) A Peptide Uncoupling BDNF Receptor TrkB from Phospholipase Cγ1 Prevents Epilepsy Induced by Status Epilepticus. Neuron 88:484–491.

Hermann BP, Seidenberg M, Dow C, Jones J, Rutecki P, Bhattacharya A, Bell B (2006) Cognitive prognosis in chronic temporal lobe epilepsy. Ann Neurol 60:80–87.

Jokeit H, Ebner A (2002) Effects of chronic epilepsy on intellectual functions. Prog Brain Res 135:455–463.

Jung JC, Mehta AD, Aksay E, Stepnoski R, Schnitzer MJ (2004) In vivo mammalian brain imaging using one- and two-photon fluorescence microendoscopy. J Neurophysiol 92:3121–3133.

Jung MW, McNaughton BL (1993) Spatial selectivity of unit activity in the hippocampal granular layer. Hippocampus 3:165–182.

Kätzel D, Nicholson E, Schorge S, Walker MC, Kullmann DM (2014) Chemical-genetic attenuation of focal neocortical seizures. Nat Commun 5:3847.

Kawakami R, Sawada K, Kusama Y, Fang Y-C, Kanazawa S, Kozawa Y, Sato S, Yokoyama H, Nemoto T (2015) In vivo two-photon imaging of mouse hippocampal neurons in dentate gyrus using a light source based on a high-peak power gain-switched laser diode. Biomed Opt Express 6:891–901.

Kee N, Teixeira CM, Wang AH, Frankland PW (2007) Preferential incorporation of adult-generated granule cells into spatial memory networks in the dentate gyrus. Nat Neurosci 10:355–362.

Kleen JK, Scott RC, Holmes GL, Lenck-Santini PP (2010) Hippocampal interictal spikes disrupt cognition in rats. Ann Neurol 67:250–257.

Krook-Magnuson E, Armstrong C, Bui A, Lew S, Oijala M, Soltesz I (2015) In vivo evaluation of the dentate gate theory in epilepsy. J Physiol 593:2379–2388.

Leutgeb JK, Leutgeb S, Moser M-B, Moser EI (2007) Pattern separation in the dentate gyrus and CA3 of the hippocampus. Science 315:961–966.

Levene MJ, Dombeck DA, Kasischke KA, Molloy RP, Webb WW (2004) In vivo multiphoton microscopy of deep brain tissue. J Neurophysiol 91:1908–1912.

Lin H, Holmes GL, Kubie JL, Muller RU (2009) Recurrent seizures induce a reversible impairment in a spatial hidden goal task. Hippocampus 19:817–827.

Lisman J (2011) Formation of the non-functional and functional pools of granule cells in the dentate gyrus: role of neurogenesis, LTP and LTD. J Physiol 589:1905–1909.

Liu X, Muller RU, Huang L-T, Kubie JL, Rotenberg A, Rivard B, Cilio MR, Holmes GL (2003) Seizure-induced changes in place cell physiology: relationship to spatial memory. J Neurosci 23:11505–11515.

Marín-Burgin A, Mongiat LA, Pardi MB, Schinder AF (2012) Unique processing during a period of high excitation/inhibition balance in adult-born neurons. Science 335:1238–1242.

Pilz G-A, Carta S, Stäuble A, Ayaz A, Jessberger S, Helmchen F (2016) Functional Imaging of Dentate Granule Cells in the Adult Mouse Hippocampus. J Neurosci 36:7407–7414.

Rakhade SN, Jensen FE (2009) Epileptogenesis in the immature brain: emerging mechanisms. Nat Rev Neurol 5:380–391.

Ramirez-Amaya V, Marrone DF, Gage FH, Worley PF, Barnes C a (2006) Integration of new neurons into functional neural networks. J Neurosci 26:12237–12241.

Sandoval CJ, Martínez-Claros M, Bello-Medina PC, Pérez O, Ramírez-Amaya V (2011) When are new hippocampal neurons, born in the adult brain, integrated into the network that processes spatial information? PLoS One 6:e17689.

Terrone G, Pauletti A, Pascente R, Vezzani A (2016) Preventing epileptogenesis: A realistic goal? Pharmacol Res 110:96–100.

Toyoda I, Bower MR, Leyva F, Buckmaster PS (2013) Early activation of ventral hippocampus and subiculum during spontaneous seizures in a rat model of temporal lobe epilepsy. J Neurosci 33:11100–11115.

Urban DJ, Roth BL (2015) DREADDs (Designer Receptors Exclusively Activated by Designer Drugs): Chemogenetic Tools with Therapeutic Utility. Annu Rev Pharmacol Toxicol 55:399–417.

Yassin L, Benedetti BL, Jouhanneau J-S, Wen JA, Poulet JFA, Barth AL (2010) An embedded subnetwork of highly active neurons in the neocortex. Neuron 68:1043–1050.

Yu EP, Dengler CG, Frausto SF, Putt ME, Yue C, Takano H, Coulter DA (2013) Protracted postnatal development of sparse, specific dentate granule cell activation in the mouse hippocampus. J Neurosci 33:2947–2960.